CHAPTER 7

PERMEABILITY

7.1 PERMEABILITY IN THE GASTROINTESTINAL TRACT AND AT THE BLOOD–BRAIN BARRIER

Measured permeability (especially when combined with solubility and charge state) can be viewed as a surrogate property for predicting oral (gastrointestinal) absorption of preclinical drug candidate molecules. This chapter considers the transport of molecules by passive diffusion through phospholipid bilayers. The emphasis is on (1) the current state-of-the-art measurement of permeabilities by the so-called PAMPA method and (2) the theoretical physicochemical models that attempt to rationalize the observed transport properties. Such models are expected to lead to new insights into the in vivo absorption processes. In oral absorption predictions, the established in vitro assay to assess the permeability coefficients is based on Caco-2 cultured-cell confluent monolayers [48,510–515]. We refer to this topic in various places, drawing on the biophysical aspects of the work reported in the literature. We also consider some physicochemical properties of the blood–brain barrier (BBB), insofar as they contrast to those of the gastrointestinal tract (GIT). Our main focus, however, is on results derived from simpler in vitro systems based on artificial membranes.

In order to rationalize membrane permeability and oral absorption in terms of physicochemical drug properties, good experimental data and sound theoretical

Absorption and Drug Development: Solubility, Permeability, and Charge State. By Alex Avdeef
ISBN 0-471-423653. Copyright © 2003 John Wiley & Sons, Inc.

models are needed. Since lipophilicity is such an important concept in ADME (absorption, distribution, metabolism, excretion) predictions, models that address the permeability–lipophilicity relationships are expected to provide important insights. In the simplest models, permeability is linearly related to the membrane–water partition coefficient [Eq. (2.3)], but in practice, linearity is not generally observed over a wide range of lipophilicities. To explain this, different theoretical models for passive membrane diffusion have been described in the literature.

In assays based on synthetic membranes, the nonlinearity may be caused by (1) unstirred water layer; (2) aqueous pores in oily membranes; (3) membrane retention of lipophilic solute; (4) excessive lipophilicity (non-steady-state conditions, long acceptor-side solute desorption times); (5) transmembrane pH gradients; (6) effects of buffers (in the unstirred water layer); (7) precipitation of solute in the donor side; (8) aggregation of solutes in the donor side (slowing diffusion); (9) specific hydrogen bonding, electrostatic, and hydrophobic/lipophilic interactions with membrane constituents; (10) solute charge state (pK_a effects) and membrane surface charge (Gouy–Chapman effects); and (11) the use of inappropriate permeability equations (e.g., neglecting membrane retention of lipophilic drugs).

In vitro systems based on cultured cells are subject to all the above mentioned nonlinear effects, plus those based on the biological nature of the cells. The apical and basolateral membranes have different lipid components, different surface charge domains, and different membrane-bound proteins. Active transporters abound. Some enhance permeability of drugs, others retard it. A very important efflux system, P-gp (where ''P'' denotes permeability), prevents many potentially useful drugs from passing into the cells. P-gp is particularly strongly expressed in the BBB and in cancer cells. The junctions between barrier cells can allow small molecules to permeate through aqueous channels. The tightness of the junctions varies in different parts of the GIT. The junctions are particularly tight in the endothelial cells of the BBB. The GIT naturally has a pH gradient between the apical and basolateral sides of the epithelial cell barrier. Metabolism plays a critical role in limiting bioavailability of drugs.

In penetrating biological barriers, drugs may have simultaneous access to several different mechanisms of transport. To develop an integrated model for the biological processes related to oral absorption is a daunting challenge, since many of these processes are not entirely understood. Most practical efforts have been directed to deriving sufficiently general core models for *passive* membrane transport (both transcellular and paracellular), addressing many of the effects observed in artificial membrane studies, as listed above. Components of the active transport processes, derived from more complex in vitro cultured-cell models, can then be layered on top of the core passive models.

In the bulk of this chapter we will focus on the rapidly emerging new in vitro technology based on the use of immobilized artificial membranes, constructed of phospholipid bilayers supported on lipophilic filters. One objective is to complete the coverage of the components of the transport model explored in Chapter 2, by considering the method for determining the top curve (horizontal line) in the plots

in Fig. 2.2 (i.e., intrinsic permeabilities P_0 of drugs). Also, a new model for gastrointestinal (oral) absorption based on permeability measurements using artificial membranes will be presented.

Approximately 1400 measurements of permeability are presented in tables and figures in this chapter. Most of the data are original, not published previously. Unless otherwise noted, the permeability and membrane retention data are from *p*ION's laboratories, based on the permeation cell design developed at *p*ION. Cells of different designs, employing different filter and phospholipid membrane materials, produce different permeability values for reasons discussed below. Although the analysis of the measurements is the basis of the presentation in this chapter, much of the data can be further mined for useful quantitative structure–property information, and the reader is encouraged to do so. First-person references in this chapter, such as ''our laboratory,'' refer specifically to *p*ION's laboratory, and ''our results'' are those of several colleagues who have contributed to the effort, covering a period of >4 years, as cited in the acknowledgment section. Where possible, comparisons to published permeability results from other laboratories will be made.

The survey of over 50 artificial lipid membrane models (*p*ION) in this chapter reveals a new and very promising in vitro GIT model, based on the use of levels of lecithin membrane components higher than those previously reported, the use of negatively charged phospholipid membrane components, pH gradients, and artificial sink conditions. Also, a novel direction is suggested in the search for an ideal in vitro BBB model, based on the salient differences between the properties of the GIT and the BBB.

We return to using the K_p and K_d symbols to represent the partition coefficient and the apparent partition (distribution) coefficient, respectively. The effective, apparent, membrane, and intrinsic permeability coefficients are denoted P_e, P_a, P_m, and P_0, respectively, and D refers to the diffusivity of molecules.

The coverage of permeability in this book is more comprehensive than that of solubility, lipophilicity, and ionization. This decision was made because permeability is not as thoroughly treated in the pharmaceutical literature as the other topics, and also because much emphasis is placed on the PAMPA in this book, which is indeed a very new technique [547] in need of elaboration.

7.2 HISTORICAL DEVELOPMENTS IN ARTIFICIAL-MEMBRANE PERMEABILITY MEASUREMENT

7.2.1 Lipid Bilayer Concept

The history of the development of the bilayer membrane model is fascinating, and spans at least 300 years, beginning with studies of soap bubbles and oil layers on water [517–519].

In 1672 Robert Hooke observed under a microscope the growth of ''black'' spots on soap bubbles [520]. Three years later Isaac Newton [521], studying the ''images

of the Sun very faintly reflected [off the black patched on the surface of soap bubbles],'' calculated the thickness of the black patches to be equivalent to 95 Å. (Anders Jonas Ångström, 'father of spectroscopy,' who taught at the University of Uppsala, after whom the Å unit is named, did not appear until about 150 years later.)

Ben Franklin, a self-trained scientist of eclectic interests, but better known for his role in American political history, was visiting England in the early 1770s. He published in the Philosophical Transactions of the Royal Society in 1774 [552]:

> At length being at Clapham where there is, on the common, a large pond, which I observed to be one day very rough with the wind, I fetched out a cruet of oil, and dropt a little of it on the water . . . and there the oil, though not more than a tea spoonful, . . . spread amazingly, and extended itself gradually till it reached the lee side, making all that quarter of the pond, perhaps half an acre, as smooth as a looking glass . . . so thin as to produce prismatic colors . . . and beyond them so much thinner as to be invisible.

Franklin mentioned Pliny's account of fisherman pouring oil on troubled waters in ancient times, a practice that survives to the present. (Franklin's experiment was reenacted by the author at the pond on Clapham Common with a teaspoon of olive oil. The spreading oil covered a surface not larger than that of a beach towel–it appears that technique and/or choice of oil is important. The olive oil quickly spread out in circular patterns of brilliant prismatic colors, but then dissolved from sight. Indeed, the pond itself has shrunken considerably over the intervening 230 years.)

More than 100 years later, in 1890, Lord Rayleigh, a professor of natural philosophy at the Royal Institution of London, was conducting a series of quantitative experiments with water and oil, where he carefully measured the area to which a volume of oil would expand. This led him to calculate the thickness of the oil film [517,518]. A year after publishing his work, he was contacted by a German woman named Agnes Pockels, who had done extensive experiments in oil films in her kitchen sink. She developed a device for carefully measuring the exact area of an oil film. Lord Rayleigh helped Agnes Pockels in publishing her results in scientific journals (1891–1894) [517,518].

Franklin's teaspoon of oil (assuming a density 0.9 g/mL and average fatty-acid molecular weight 280 g/mol) would contain 10^{+22} fatty-acid tails. The half-acre pond surface covered by the oil, $\sim$2000 m^2, is about $2 \times 10^{+23}$ $Å^2$. So, each tail would be expected to occupy about 20 $Å^2$, assuming that a single monolayer (25 Å calculated thickness) of oil formed on the surface of the pond.

Pfeffer in 1877 [523] subjected plant cell suspensions to different amounts of salt and observed the cells to shrink under hypertonic conditions and swell in hypotonic conditions. He concluded there was a semipermeable membrane separating the cell interior from the external solution, an invisible (under light microscope) plasma membrane.

Overton in the 1890s at the University of Zürich carried out some 10,000 experiments with more than 500 different chemical compounds [518,524]. He measured

the rate of absorption of the compounds into cells. Also, he measured their olive oil–water partition coefficients, and found that lipophilic compounds readily entered the cell, whereas hydrophilic compounds did not. This lead him to conclude that the cell membrane must be oil-like. The correlation that the greater the lipid solubility of a compound, the greater is the rate of penetration of the plasma membrane became known as *Overton's rule*. Collander confirmed these observations but noted that some small hydrophilic molecules, such as urea and glycerol, could also pass into cells. This could be explained if the plasma membrane contained water-filled pores. Collander and Bärlund concluded that molecular size and lipophilicity are two important properties for membrane uptake [525].

Fricke measured resistance of solutions containing suspensions of red blood cells (RBCs) using a Wheatstone bridge [518]. At low frequencies the impedance of the suspensions of RBC was very high. But at high frequencies, the impedance decreased to a low value. If cells were surrounded by a thin membrane of low dielectric material, of an effective resistance and a capacitance in parallel to the resistor, then current would flow around the cells at low frequencies, and ''through'' the cells (shunting through the capacitor) at high frequencies. Hober in 1910 evaluated the equivalent electrical circuit model and calculated the thickness of the RBC membrane to be 33 Å if the effective dielectric constant were 3 and 110 Å if the effective dielectric constant were 10 [518].

In 1917 Langmuir [526], working in the laboratories of General Electric, devised improved versions of apparatus (now called the Langmuir trough) originally used by Agnes Pockels, to study properties of monolayers of amphiphilic molecules at the air–water interface. The technique allowed him to deduce the dimensions of fatty acids in the monolayer. He proposed that fatty acid molecules form a monolayer on the surface of water by orienting themselves vertically with the hydrophobic hydrocarbon chains pointing away from the water and the lipophilic carboxyl groups in contact with the water.

Gorter and Grendel in 1925 [527], drawing on the work of Langmuir, extracted lipids from RBC ghosts and formed monolayers. They discovered that the area of the monolayer was twice that of the calculated membrane surface of intact RBC, indicating the presence of a ''bilayer.'' This was the birth of the concept of a lipid bilayer as the fundamental structure of cell membranes (Fig. 7.1).

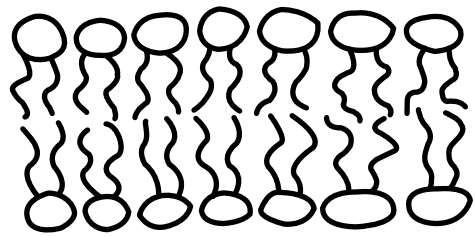

Figure 7.1 Lipid bilayer.

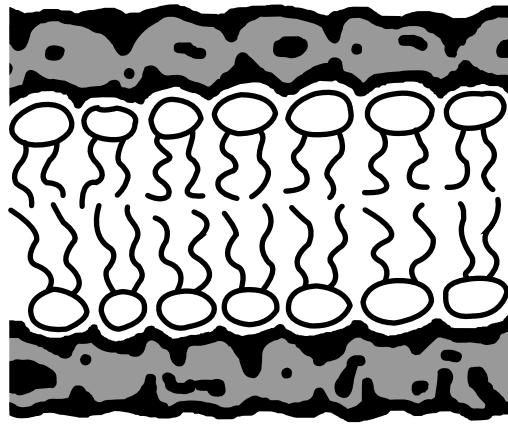

Figure 7.2 Danielli–Davson membrane model. A layer of protein was thought to sandwich a lipid bilayer.

The first membrane model to be widely accepted was that proposed by Danielli and Davson in 1935 [528]. On the basis of the observation that proteins could be adsorbed to oil droplets obtained from mackerel eggs and other research, the two scientists at University College in London proposed the ''sandwich'' of lipids model (Fig. 7.2), where a bilayer is covered on both sides by a layer of protein. The model underwent revisions over the years, as more was learned from electron microscopic and X-ray diffraction studies. It was eventually replaced in the 1970s by the current model of the membrane, known as the fluid mosaic model, proposed by Singer and Nicolson [529,530]. In the new model (Fig. 7.3), the lipid bilayer was retained, but the proteins were proposed to be globular and to freely float within the lipid bilayer, some spanning the entire bilayer.

Mueller, Rudin, Tien, and Wescott in 1961, at the Symposium of the Plasma Membrane [531] described for the first time how to reconstitute a lipid bilayer

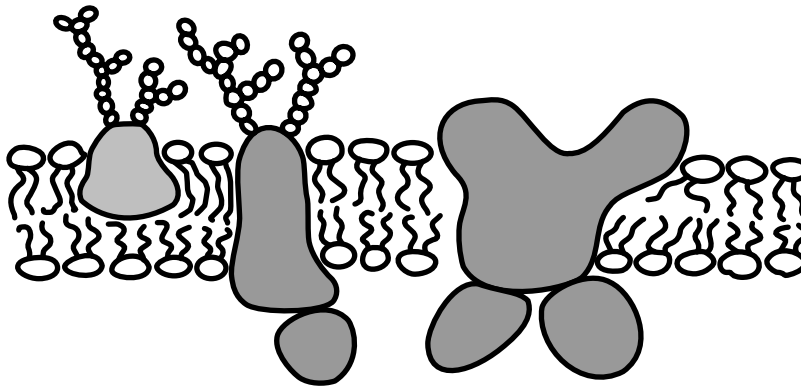

Figure 7.3 Fluid mosaic modern model of a bilayer.

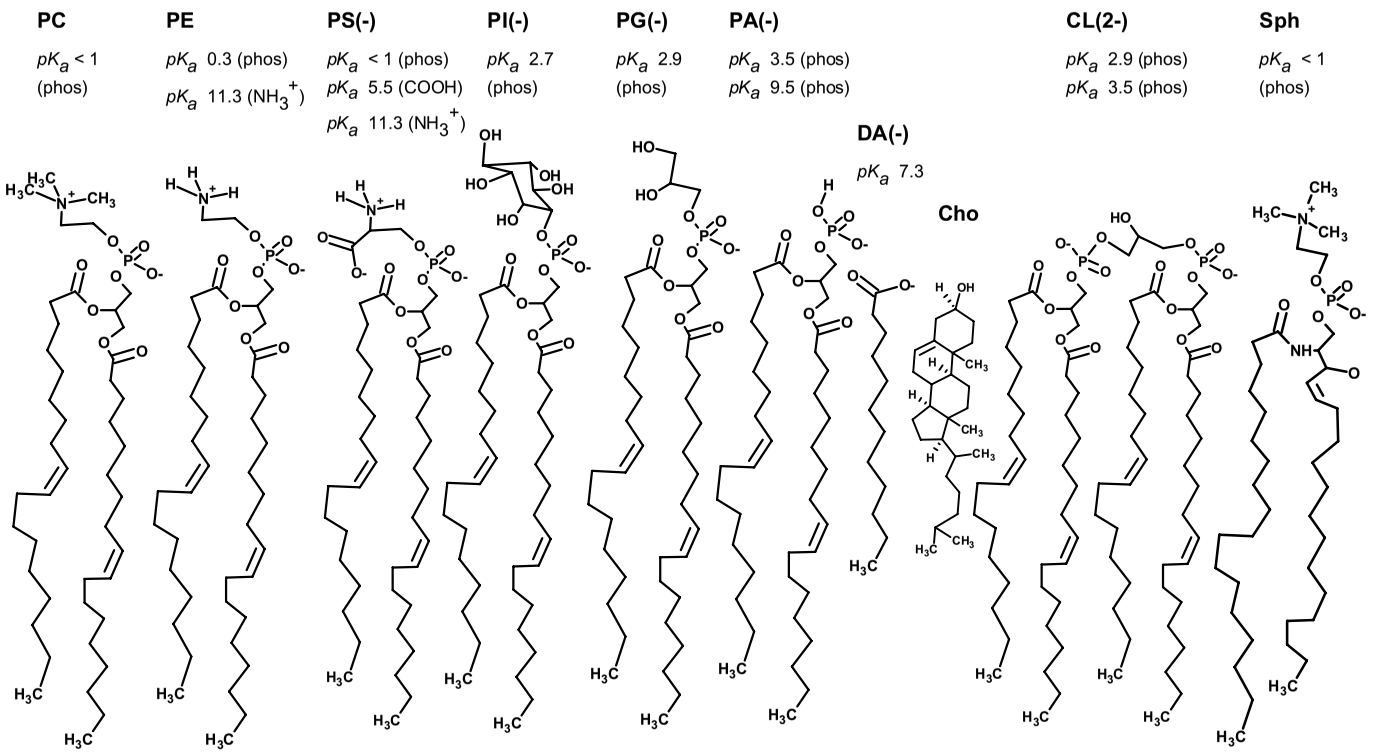

Figure 7.4 Common lipid components of biological membranes. For simplicity, all acyl chains are shown as oleyl residues.

in vitro. It is considered the seminal work on the self-assembly of planar lipid bilayers [516,518,519,531,532]. Their research led them to the conclusion that a soap film in its final stages of thinning has a structure of a single bilayer, with the oily tails of detergent molecules pointing to the side of air, and the polar heads sandwiching a layer of water. Their experimental model drew on three centuries of observations, beginning with the work of Hooke. The membranes prepared by the method of Rudin's group became known as *black lipid membranes* (BLMs). Soon thereafter, vesicles with walls formed of lipid bilayers, called *liposomes*, were described by Bangham [533].

7.2.2 Black Lipid Membranes (BLMs)

Mueller et al. [516,531,532] described in 1961 that when a small quantity of a phospholipid (1-2% wt/vol *n*-alkane or squalene solution) was carefully placed over a small hole (0.5 mm diameter) in a thin sheet of teflon or polyethylene (10–25 μm thick), a thin film gradually forms at the center of the hole, with excess lipid flowing toward the perimeter (forming a ''plateau–Gibbs border''). Eventually, the central film turns optically black as a single (5-nm-thick) bilayer lipid membrane (BLM) forms over the hole. Suitable lipids for the formation of a BLM are mostly isolated from natural sources, including phosphatidylcholine (PC), phosphatidylethanolamine (PE), phosphatidylserine (PS), phosphatidylinositol (PI), and sphingomyelin (Sph). Such membranes have been viewed as useful models of the more complex natural membranes [516,532–544]. Figure 7.4 shows the most common membrane components. Sphingomyelin is an example of a broad class of sphingolipids, which include cerebrosides (carbohydrates attached to the head groups) and gangliosides (found in plasma membrane of nerve cells).

However, a serious drawback in working with BLMs as a model system is that they are extremely fragile (requiring a vibration-damping platform and a Faraday cage during measurements of electrical properties), and tedious to make [536–542]. That notwithstanding, Walter and Gutknecht [537] studied the permeation of a series of simple carboxylic acids across eggPC/decane BLMs. Intrinsic permeability coefficients, P_0, were determined from tracer fluxes. A straight-line relationship was observed between log P_0 and hexadecane–water partition coefficients, log K_p, for all but the smallest carboxylic acid (formic): $\log P_0 = 0.90 \log K_p + 0.87$. Using a similar BLM system, Xiang and Anderson [538] studied the pH-dependent transport of a series of α-methylene-substituted homologs of *p*-toluic acid. They compared the eggPC/decane permeabilities to partition coefficients determined in octanol–, hexadecane–, hexadecene–, and 1,9-decadiene–water systems. The lowest correlation was found from comparisons to the octanol–water scale. With the hexadecane–water system, $\log P_0 = 0.85 \log K_p - 0.64$ (r^2 0.998), and with decadiene–water system, $\log P_0 = 0.99 \log K_p - 0.17$ (r^2 0.996). Corrections for the unstirred water layer were key to these analyses. Figure 7.5 shows the linear correlation between the logarithms of the permeability coefficients and the partition coefficients for the five lipid systems mentioned above.

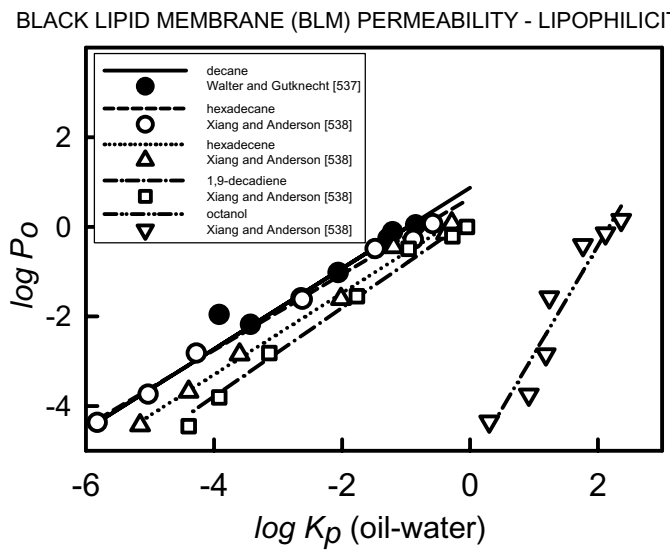

Figure 7.5 Intrinsic permeabilities of ionizable acids versus oil–water partition coefficients.

7.2.3 Microfilters as Supports

Efforts to overcome the limitations of the fragile membranes (as delicate as soap bubbles) have evolved with the use of membrane supports, such as polycarbonate filters (straight-through pores) [543] or other more porous microfilters (sponge-like pore structure) [545–548].

Thompson et al. [543] explored the use of polycarbonate filters, and performed experiments to make the case that just single bilayer membranes formed in each of the straight-through pores. Several possible pore-filling situations were considered: lipid–solvent plug, lipid–solvent plug plus BLM, multilamellar BLM, and unilamellar BLM. The key experiment in support of a single-bilayer disposition involved the use of amphotericin B (Fig. 7.6), which is an amphiphilic polyene zwitterionic molecule, not prone to permeate bilayers, but putatively forming tubular membrane-spanning oligomers if the molecules are first introduced from both sides of a bilayer, as indicated schematically in Fig. 7.6. Once a transmembrane oligomer forms, small ions, such as Na^+ or K^+, are able to permeate through the pore formed. The interpretation of the voltage–current curves measured supported such a single-bilayer membrane structure when polycarbonate microfilters are used as a scaffold support.

Cools and Janssen [545] studied the effect of background salt on the permeability of warfarin through octanol-impregnated membranes (Millipore ultrafiltration filters, VSWP, 0.025-μm pores). At a pH where warfarin was in its ionized form, it was found that increasing background salt increased permeability (Fig. 7.7). This

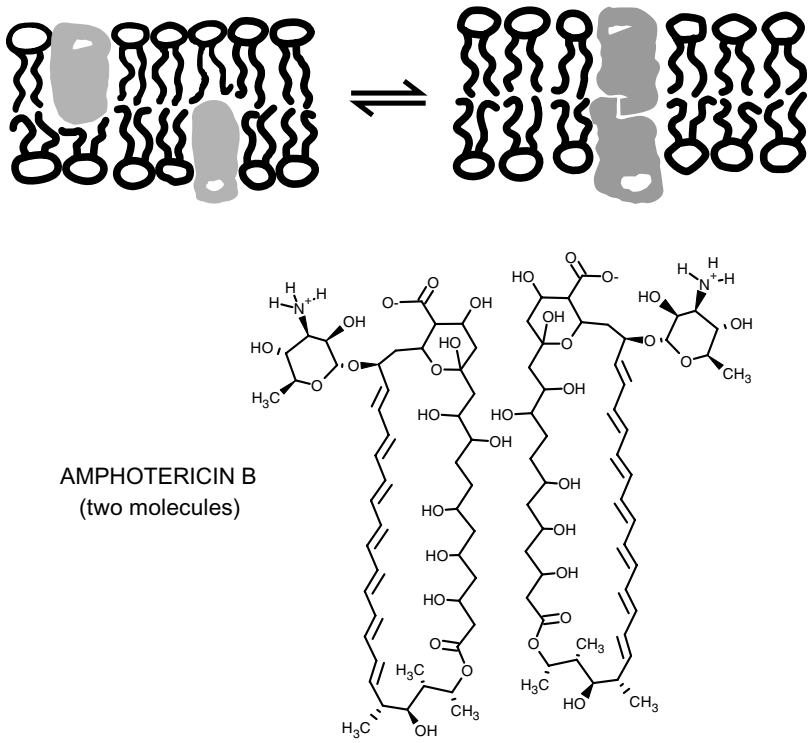

Figure 7.6 Bilayer channel-forming amphotericin B.

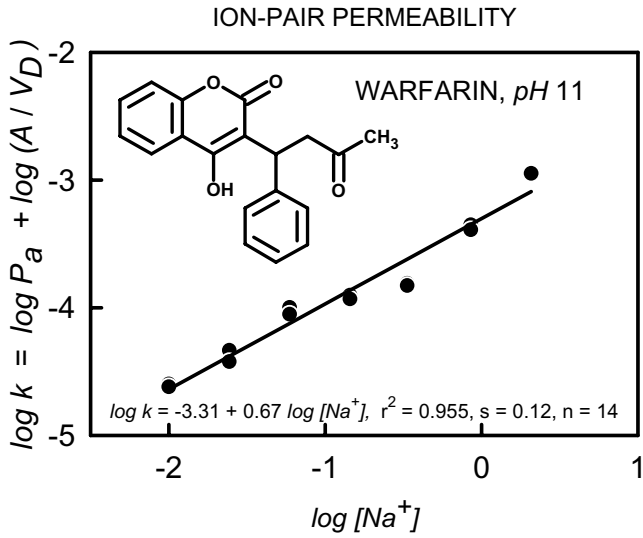

Figure 7.7 Permeation of anionic warfarin (pH 11) through octanol-soaked (impregnated) microfilter as a function of sodium ion concentration.

observation was thought to support an ion pair mechanism of transport of charged drugs across real biological membranes. However, current understanding of the structure of wet octanol (Fig. 2.7), suggests that this isotropic solvent system may not be a suitable model for passive diffusion of *charged* drugs across phospholipid bilayers, since the water clusters in octanol may act as 'shuttles' for the transport of ion pairs. This would not be expected under in vivo conditions.

Camenisch et al. [546] measured the pH 7.4 permeabilities of a diverse group of drugs across octanol-and isopropylmyristate-impregnated artificial membranes (Millipore GVHP mixed cellulose ester filters, 0.22 μm pores), and compared them to permeabilities of the Caco-2 system, and octanol–water apparent partition coefficients, log $K_{d(7.4)}$. The uncharged drug species diffused passively, in accordance with the pH partition hypothesis. (When the GVHP membrane was not impregnated with a lipid, the permeabilities of all the tested drugs were high and largely undifferentiated, indicating only the unstirred water layer resistance.) Over the range of lipophilicities, the curve relating the effective permeability, log P_e, to log $K_{d(7.4)}$ was seen as sigmoidal in shape, and only linear in midrange; between log $K_{d(7.4)} - 2$ and 0, log P_e values correlated with the apparent partition coefficients (Fig. 7.8). However, outside that range, there was no correlation between permeabilities and the octanol–water partition coefficients. At the high end, the permeabilities of very lipophilic molecules were limited by the unstirred water layer. At the other end, very hydrophilic molecules were observed to be more permeable than predicted by octanol, due to an uncertain mechanism.

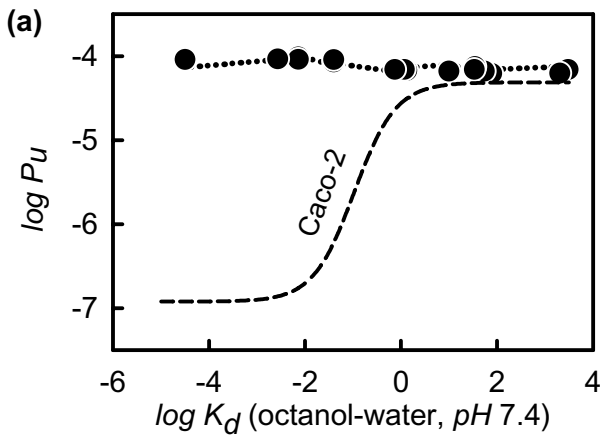

Figure 7.8 Permeation of drugs through oil-soaked microfilters; comparisons to Caco-2 permeabilities (dashed curves) [546]: (a) oil-free (untreated hydrophilic) filters; (b) unstirred water layer permeability versus log MW; (c) octanol-soaked (impregnated) filters; (d) isopropylmyristate-soaked filters.

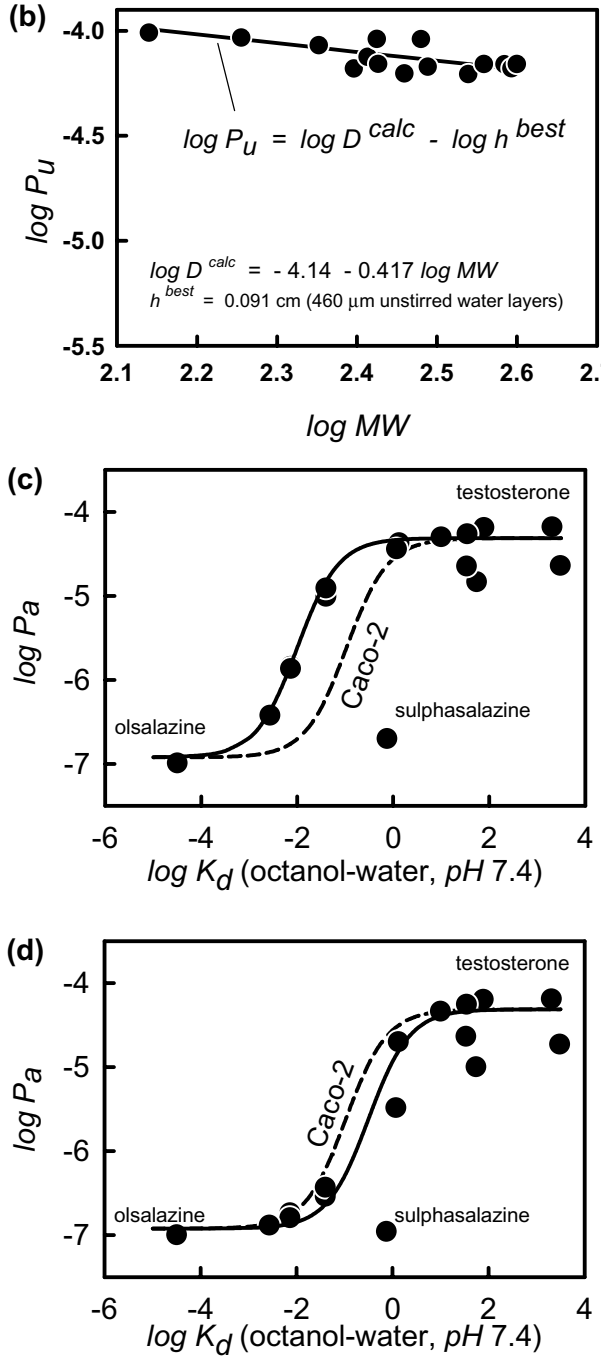

Figure 7.8 (*Continued*)

7.2.4 Octanol-Impregnated Filters with Controlled Water Pores

Ghosh [548] used cellulose nitrate microporous filters (500 μm thick) as scaffold material to deposit octanol into the pores and then under controlled pressure conditions, displace some of the oil in the pores with water, creating a membrane with parallel oil and water pathways. This was thought to serve as a possible model for some of the properties of the outermost layer of skin, the stratum corneum. The relative proportions of the two types of channel could be controlled, and the properties of 5–10% water pore content were studied. Ibuprofen (lipophilic) and antipyrine (hydrophilic) were model drugs used. When the filter was filled entirely with water, the measured permeability of antipyrine was 69 (in 10^{-6} cm/s); when 90% of the pores were filled with octanol, the permeability decreased to 33; 95% octanol content further decreased permeability to 23, and fully octanol-filled filters indicated 0.9 as the permeability.

7.3 PARALLEL ARTIFICIAL-MEMBRANE PERMEABILITY ASSAY (PAMPA)

7.3.1 Egg Lecithin PAMPA Model (Roche Model)

Kansy et al. [547,550] from Hoffmann-La Roche published a widely read study of the permeation of drugs across phospholipid-coated filters, using a technique they coined as ''PAMPA,'' which stands for parallel artificial-membrane permeability assay. Their report could not have come at a better time—just when the paradigm was shifting into screening for biopharmaceutic properties at high speeds, along side the biological screening.

In the commercial version of the PAMPA assay, a ''sandwich'' (Fig. 7.9) is formed from a specially-designed 96-well microtiter plate [*p*ION] and a 96-well microfilter plate [several sources], such that each composite well is divided into two chambers: donor at the bottom and acceptor at the top, separated by a 125-μm-thick microfilter disk (0.45 μm pores, 70% porosity, 0.3 cm^2 cross-sectional area), coated with a 10% wt/vol dodecane solution of egg lecithin (a mixed lipid containing mainly PC, PE, a slight amount of PI, and cholesterol), under conditions that multilamellar bilayers are expected to form inside the filter channels when the system contacts an aqueous buffer solution [543].

The Roche investigators were able to relate their measured fluxes to human absorption values with a hyperbolic curve, much like that indicated in Caco-2

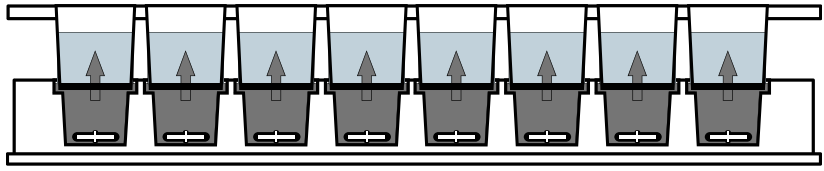

Figure 7.9 Cross section of a *p*ION 96-well microtitre plate PAMPA sandwich assembly.

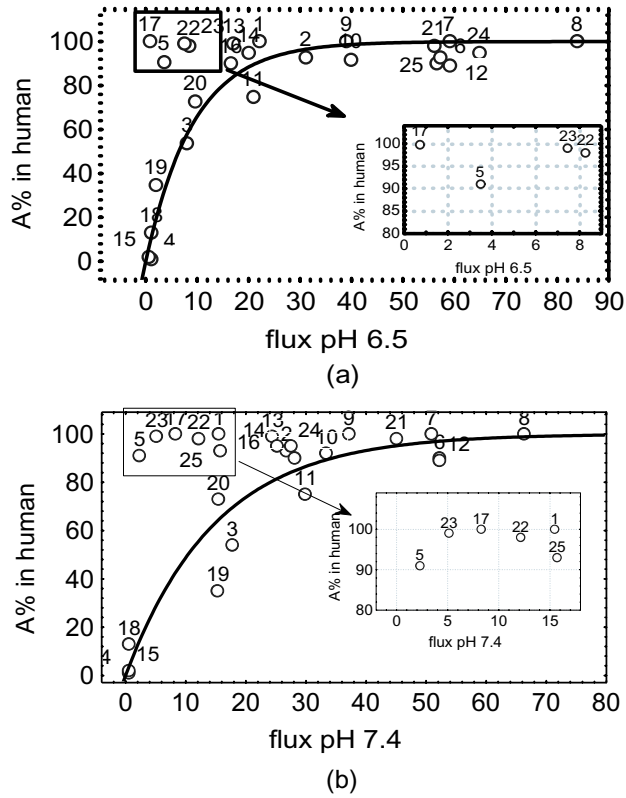

Figure 7.10 Absorption% versus PAMPA flux [547]: (a) pH 6.5; (b) pH 7.4. [Reprinted from Kansy, M.; Senner, F.; Gubernator, K. *J. Med. Chem.,* **41**, 1070–1110 (1998), with permission from the American Chemical Society.]

screening [48,82,91,97,108–110,510–515,551–553]. The outliers in their assays, inset in Fig. 7.10, were molecules known to be actively transported. Since the artificial membranes have no active transport systems and no metabolizing enzymes, the assay would not be expected to model actively transported molecules. What one sees with PAMPA is pure passive diffusion, principally of the uncharged species.

More recently, several publications have emerged, describing PAMPA-like systems. [25–28,509, 554–565] The PAMPA method has attracted a lot of favorable attention, and has spurred the development of a commercial instrument, [25–28,556] and the organization of the first international symposium on PAMPA in 2002 [565].

7.3.2 Hexadecane PAMPA Model (Novartis Model)

Faller and Wohnsland [509,554] developed the PAMPA assay using phospholipid-free hexadecane, supported on 10-μm thick polycarbonate filters(20% porosity,

0.3 cm^2 cross-sectional area), and were able to demonstrate interesting predictions. Their PAMPA method appeared to be a satisfactory substitute for obtaining alkane-water partition coefficients, which are usually very difficult to measure directly, due to the poor solubility of drug molecules in alkanes. They applied the pH-based methods of Walter and Gutknecht [537] to extract the intrinsic permeability coefficients, P_0, of the molecules they studied. A plot of log P_0 vs. hexadecane-water log K_d is a straight line with a slope of 0.86 (r^2 0.96), as shown in Fig. 7.11. Apparently, membrane retention was not measured in the original version of the method. A later measurement in our laboratory, where retention was considered, indicated a slope of 1.00, albeit with a slightly poorer fit (r^2 0.92), as shown by the open circles in Fig. 7.11.

7.3.3 Brush-Border Lipid Membrane (BBLM) PAMPA Model (Chugai Model)

Sugano et al. [561,562] explored the lipid model containing several different phospholipids, closely resembling the mixture found in reconstituted brush border lipids [433,566] and demonstrated dramatically improved property predictions. The best-performing lipid composition consisted of a 3% wt/vol lipid solution in 1,7-octadiene (lipid consisting of 33% wt/wt cholesterol, 27% PC, 27% PE, 7% PS, 7% PI). The donor and acceptor compartments were adjusted in the pH interval between 5.0 and 7.4 [562]. With such a mixture, membrane retention is expected to be extensive when lipophilic drugs are assayed. The use of 1,7-octadiene in the assay was noted to require special safety precautions.

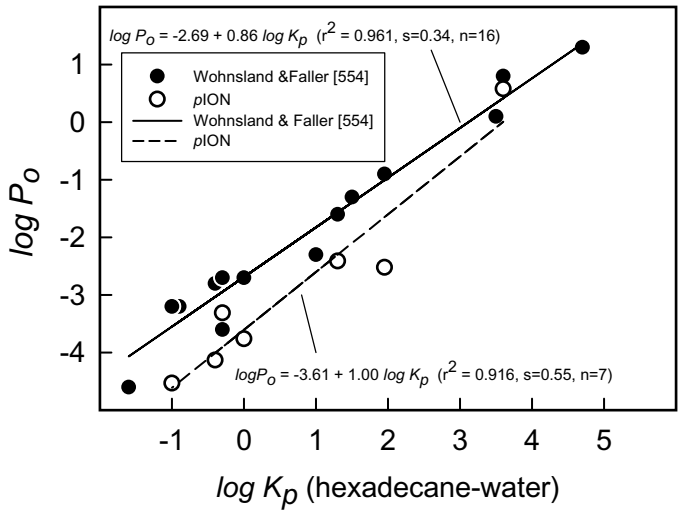

Figure 7.11 Intrinsic permeabilities versus alkane–water partition coefficients for drugs: PAMPA filters soaked with alkane [509].

7.3.4 Hydrophilic Filter Membrane PAMPA Model (Aventis Model)

Zhu et al. [563] found the use of hydrophilic filters (low-protein-binding PVDF) as an advantage in lowering the permeation time to 2 h. Egg lecithin, 1% wt/vol in dodecane, was used as the membrane medium. Over 90 compounds were characterized at pH 5.5 and 7.4. For each molecule, the greater P_e value of the two measured at different pH [509,554] was used to compare to Caco-2 permeabilities reported in the literature. It is noteworthy that many ionizable molecules did not follow the permeability-pH dependency expected from the pH partition hypothesis. It may be that water channels were contributing to the unexpected permeability-pH trends. Solute retention by the membrane was not considered. They tried using the Chugai five-component model, but found difficulties in depositing the lipid mixture on hydrophilic filters. Human intestinal absorption (HIA) values were compared to PAMPA measurements, Caco-2 permeabilities, partition coefficients (log K_p/ log K_d), polar surface area (PSA) and quantitative structure-property relations (QSPRs) developed by Winiwarter et al. [56] It was concluded that PAMPA and Caco-2 measurements best predicted HIA values.

7.3.5 Permeability–Retention–Gradient–Sink PAMPA Models (pION Models)

The system reported by Avdeef and co-workers [25–28,556–560] is an extension of the Roche approach, with several novel features described, including a way to assess membrane retention [25–28,556,557] and a way to quantify the effects of iso-pH [558] and gradient pH [559] conditions applied to ionizable molecules. A highly pure synthetic phospholipid, dioleoylphosphatidylcholine (DOPC), was initially used to coat the filters (2% wt/vol DOPC in dodecane). Other lipid mixtures were subsequently developed, and are described in detail in this chapter.

7.3.6 Structure of Phospholipid Membranes

The structure of the filter-immobilized artificial membranes is not known with certainty. Thompson et al. [543] hypothesized that polycarbonate filters had a single bilayer per pore, based largely on the behavior of amphotericin B in the pore-forming oligomerization reaction. Hennesthal and Steinem [568], using scanning force microscopy, estimated that a single bilayer spans exterior pores of porous alumina. These observations may be incomplete, as there is considerable complexity to the spontaneous process of the formation of BLMs (Section 7.2.1). When 2% phosphatidylcholine (PC)–dodecane solution is suspended in water, where the water exceeds 40 wt%, the lipid solution takes on the inverted hexagonal (H_{II}) structure, where the polar head groups of the PC face water channels in a cylindrical structure [569]. Such structures can alter transport properties, compared to those of normal phases [570]. (It may be possible to model the paracellular transport mechanism, should the presence of aqueous pores be established.) Suspensions

of 2% PC–dodecane have been titrated potentiometrically from pH 10 down to pH 3. Along the way, at about pH 4, the pH electrode stopped functioning and appeared to be choked by a clear gelatinous coating, suggesting that some sort of phase transition had taken place then [Avdeef, unpublished].

7.4 THE CASE FOR THE IDEAL IN VITRO ARTIFICIAL MEMBRANE PERMEABILITY MODEL

7.4.1 Lipid Compositions in Biological Membranes

Different tissues have different lipid compositions. The most common lipid components of membranes are PC and PE. Lipid extracts from brain and lung are also rich in PS; heart tissue is rich in PG, and liver is rich in PI [567]. Human blood cells, as ''ghost'' erythrocytes (with cytoplasm contents removed), are often used as membrane models. These have different compositions between the inner and outer leaflets of the bilayer membrane. Phospholipids account for 46% of the outer leaflet membrane constituents, with PC and Sph about equal in amount. The inner leaflet is richer in phospholipids (55%), with the mix: 19% PE, 12% PS, 7% PC and 5% Sph [567].

Proulx [571] reviewed the published lipid compositions of brush-border membranes (BBM) isolated from epithelial cells from pig, rabbit, mouse, and rat small intestines. Table 7.1 shows the lipid makeup for the rat, averaged from five reported studies [571]. Krämer et al. [572,573] reported Madin–Darby canine kidney (MDCK) and BBB lipid composition profiles, listed in Table 7.1, for comparative purposes. Also shown are typical compositions of soy- and egg-derived lecithin extracts. Sugano's composition [561,562] is an attempt to mimic the BBLM. Table 7.1 lists the anionic-to-zwitterionic lipid weight ratios. On a molar basis, cholesterol accounts for about 50% of the total lipid content (37% on a weight basis) in the BBLM. The cholesterol content in BBLM is higher than that found in kidney epithelial (MDCK) and cultured brain endothelial cells (Table 7.1). (Slightly different BBLM lipid composition was reported by Alcorn et al. [433].) The outer (luminal) leaflet of the BBLM is rich in sphingomyelin, while the inner leaflet (cytosol) is rich in PE and PC. Apical (brush border) and basolateral lipids are different in the epithelium. The basolateral membrane content (not reported by Proulx) is high in PC, whereas the BBM has nearly the same PC as PE content. It appears that the BBB has the highest negative lipid content, and the BBM has the lowest negative lipid content of the three systems listed in the table. Cholesterol content follows the opposite pattern.

7.4.2 Permeability–pH Considerations

The effective permeability of ionizable molecules depends on pH, and the shapes of the permeability–pH profiles can be theoretically predicted when the pK_a of the molecule is known, the pH partition hypothesis are valid, and the resistance of

TABLE 7.1 Lipid Compsitions (%w/w) of Biological Membranes[a]

Lipid[b] [Ref.]	BBM[c] [30]	MDCK[d] [38]	BBB[e] [37]	Sugano BBM Model[f]	Soy "20% Extract" Lecithin[g]	Egg "60% Extract" Lecithin[g]
PC(±)	20	22	18	27	24	73
PE(±)	18	29	23	27	18	11
PS(−)	6	15	14	7	—	—
PI(−)	7	10	6	7	12	1
Sph(±)	7	10	8	—	—	—
FA(−)	—	1	3	—	—	—
PA(−)	—	—	—	—	4	—
LPI(−)	—	—	—	—	—	2
CL(2−)	—	—	2	—	—	—
LPC(±)	—	—	—	—	5	—
CHO + CE	37	10	26	33	—	—
TG	—	1	1	—	37[h]	13[h]
Negative : zwitterionic lipid ratio (exclusive of CHO and TG)	1 : 3.5	1 : 2.3	1 : 1.8	1 : 3.9	1 : 2.9	1 : 28.0

[a]The %w/w values in this table for BBB and MDCK are conversions from the originally reported %mol/mol units.

[b]PC = phosphatidylcholine, PE = phosphatidylethanolamine, PS = phosphatidylserine, PI = phosphatidylinositol, Sph = sphingomyelin, FA = fatty acid, PA = phosphatidic acid, LPI = lyso-PI, CL = cardiolipin, LPC = lyso-PC, CHO = cholesterol, CE = cholesterol ester, TG = triglycerides.

[c]BBM = reconstituted brush-border membrane, rat (average of four studies).

[d]MDCK = Madin–Darby canine kidney cultured epithelial cells [563].

[e]BBB = blood–brain barrier lipid model, RBE4 rat endothelial immortalized cell line.

[f]Refs. 561 and 562.

[g]From Avanti Polar Lipids, Alabaster, AL.

[h]Unspecified neutral lipid, most likely asymmetric triglycerides.

the unstirred water layer (UWL; see Section 7.7.6) may be neglected (as, e.g., in the GIT and the BBB) [536,558,559]. The pH effects of ionizable molecules is illustrated in Fig. 7.12, for a series of weak acids and bases [562]. It is clear that if the 'wrong' pH is used in screening the permeabilities of molecules, highly promising molecules, such as furosemide or ketoprofen (Fig. 7.12), may be characterized as false negatives. The ideal pH to use for in vitro screening ought to reflect the in vivo pH conditions.

Said et al. [78] directly measured the "acid microclimate" on the surface of gastrointestinal tract (GIT) epithelial cells (intact with mucus layer) in rats. The pH on the apical (donor) side of the cells varied from 6.0 to 8.0, while the pH on the basolateral (acceptor) side was 7.4. Furthermore, the pH gradient between

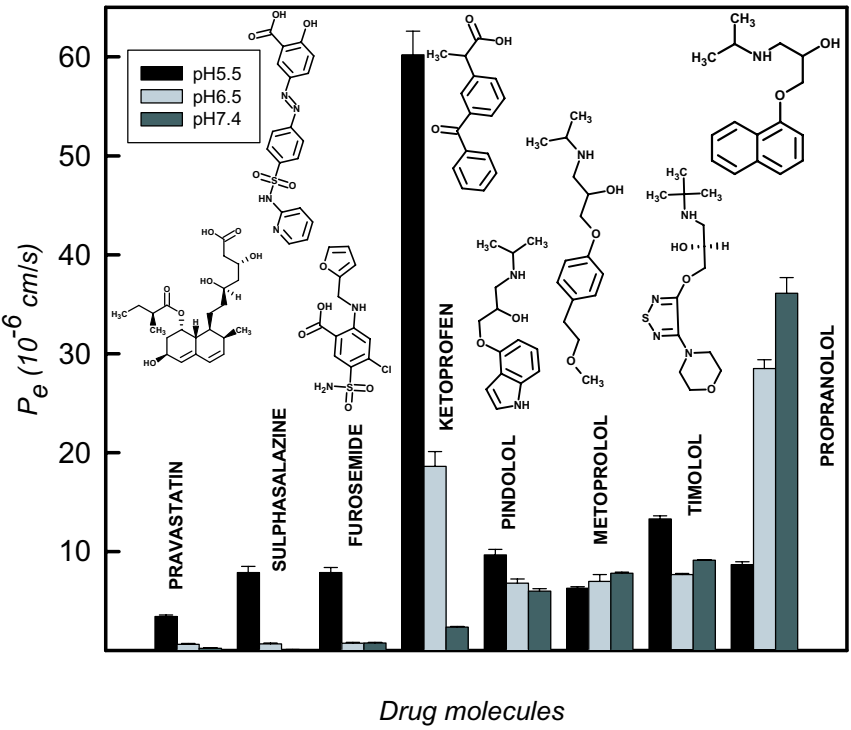

Figure 7.12 Chugai model PAMPA permeabilities as a function of pH for several drug molecules [561].

the donor and acceptor sides varied with position in the GIT, as indicated in Table 7.2. Others have measured microclimate pH as low as 5.2 [73].

Yamashita et al. [82] determined drug permeabilities by performing Caco-2 assays under two pH conditions: pH 6.0_{donor}–$7.4_{acceptor}$ and pH 7.4_{donor}–$7.4_{acceptor}$. These choices adequately span the microclimate range in the GIT. Weak acids were more permeable under the gradient-pH condition, compared to the iso-pH condition. Weak bases behaved in the opposite way. Uncharged molecules showed the same permeabilities under the two conditions. The gradient-pH set of permeability measurements better predicted human absorption than the iso-pH set ($r^2 = 0.85$ vs. 0.50, respectively). The authors may have underestimated some of the permeabilities, by using equations which implied 'iso-pH' conditions (see, Section 7.5).

In designing the ideal screening strategy, it appears important to consider using pH gradients. If the *in vivo* conditions are to be mimicked, at least two effective permeability measurements should be attempted, as suggested by the above mentioned researchers: pH 6.0_{donor}–$7.4_{acceptor}$ (gradient pH) and pH 7.4_{donor}–$7.4_{acceptor}$ (iso-pH), the microclimate pH range spanned in the GIT.

TABLE 7.2 Microclimate pH on the Apical Side of Epithelial Cells in the GIT in Rats

Position in the GIT	Microclimate pH
Stomach	8.0
Proximal duodenum	6.4
Distal duodenum	6.3
Proximal jejunum	6.0
Midjejunum	6.2
Distal jejunum	6.4
Proximal ileum	6.6
Midileum	6.7
Distal ileum	6.9
Proximal colon	6.9
Distal colon	6.9

Source: Refs. 52 and 70.

7.4.3 Role of Serum Proteins

Sawada et al. [574–576] characterized the iso-pH 7.4 MDCK permeabilities of very lipophilic molecules, including chlorpromazine (CPZ) [574]. They included 3% wt/vol bovine serum albumin (BSA) on the apical (donor) side, and 0.1–3% BSA on the basolateral (acceptor) side, and found that plasma protein binding greatly affected the ability of molecules to permeate cellular barriers. They observed cell tissue retention of CPZ ranging within 65–85%, depending on the amount of BSA present in the receiving compartment. They concluded that the rapid rate of disappearance of lipophilic compounds from the donor compartment was controlled by the unstirred water layer (UWL; see Section 7.7.6), a rate that was about the same for most lipophilic compounds; however, the very slow appearance of the compounds in the receiving compartment depended on the rate of desorption from the basolateral side of the membranes, which was strongly influenced by the presence of serum proteins in the receiving compartment. They recommended the use of serum proteins in the receiving compartment, so as to better mimic the in vivo conditions when using cultured cells as in vitro assays.

Yamashita et al. [82] also studied the effect of BSA on transport properties in Caco-2 assays. They observed that the permeability of highly lipophilic molecules could be rate limited by the process of desorption off the cell surface into the receiving solution, due to high membrane retention and very low water solubility. They recommended using serum proteins in the acceptor compartment when lipophilic molecules are assayed (which is a common circumstance in discovery settings).

7.4.4 Effects of Cosolvents, Bile Acids, and Other Surfactants

Figure 7.13 shows some of the structures of common bile acids. In low ionic strength solutions, sodium taurocholate forms tetrameric aggregates, with critical

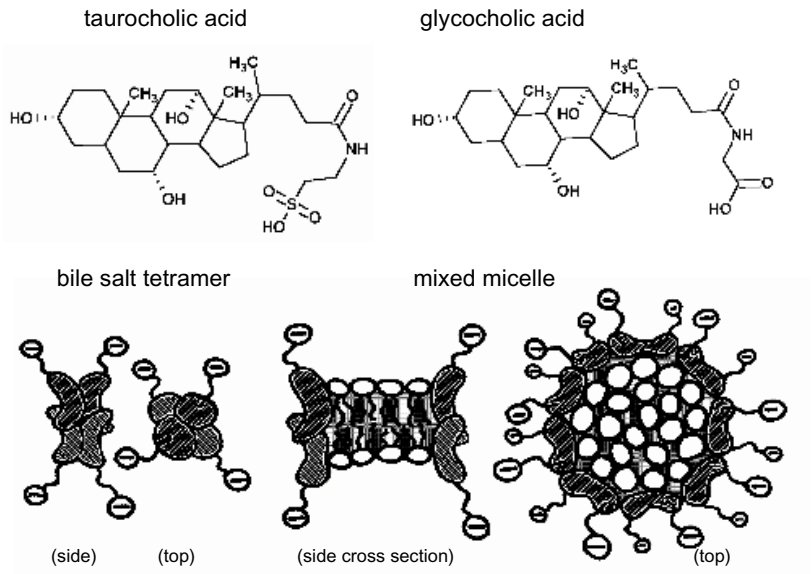

Figure 7.13 Examples of bile salts and aggregate structures formed in aqueous solutions.

micelle concentration (CMC) 10–15 mM. Sodium deoxycholate can have higher levels of aggregation, with lower cmc (4–6 mM) [577]. Mixed micelles form in the GIT, where the edges of small sections of planar bilayer fragments are surrounded by a layer of bile salts (Fig. 7.13).

Yamashita et al. [82] added up to 10 mM taurocholic acid, cholic acid (cmc 2.5 mM), or sodium laurel sulfate (SLS; low ionic strength cmc 8.2 mM) to the donating solutions in Caco-2 assays. The two bile acids did not interfere in the transport of dexamethasone. However, SLS caused the Caco-2 cell junctions to become leakier, even at the sub-CMC 1 mM level. Also, the permeability of dexamethasone decreased at 10 mM SLS.

These general observations have been confirmed in PAMPA measurements in our laboratory, using the 2% DOPC–dodecane lipid. With very lipophilic molecules, glycocholic acid added to the donor solution slightly reduced permeabilities, taurocholic acid increased permeabilities, but SLS arrested membrane transport altogether in several cases (especially cationic, surface-active drugs such as CPZ).

Yamashita et al. [82] tested the effect of PEG400, DMSO, and ethanol, with up to 10% added to solutions in Caco-2 assays. PEG400 caused a dramatic decrease (75%) in the permeability of dexamethasone at 10% cosolvent concentration; DMSO caused a 50% decrease, but ethanol had only a slight decreasing effect.

Sugano et al. [562] also studied the effect of PEG400, DMSO, and ethanol, up to 30%, in their PAMPA assays. In general, water-miscible cosolvents are expected to

decrease the membrane-water partition coefficients. In addition, the decreased dielectric constants of the cosolvent-water solutions should give rise to a higher proportion of the ionizable molecule in the *uncharged* state [25]. These two effects oppose each other. Mostly, increasing levels of cosolvents were observed to lead to decreasing permeabilities. However, ethanol made the weak-acid ketoprofen (pK_a 4.12) more permeable with increasing cosolvent levels, an effect consistent with the increasing pK_a with the decreasing dielectric constant of the cosolvent mixtures (leading to a higher proportion of uncharged species at a given pH). But the same reasoning cannot be used to explain why the weak-base propranolol (pK_a 9.5) decreased in permeability with increasing amounts of ethanol. This may be due to the increased solubility of propranolol in water with the added ethanol in relation to the solubility in the membrane phase. This leads to a lowered membrane/mixed-solvent partition coefficient, hence lowering flux due to a diminished sample concentration gradient in the membrane (Fick's law) [25]. DMSO and PEG400 dramatically reduced permeabilities for several of the molecules studied. Cosolvent use is discussed further in Section 7.7.9.

7.4.5 Ideal Model Summary

The literature survey in this section suggests that the ideal in vitro permeability assay would have pH 6.0 and 7.4 in the donor wells, with pH 7.4 in the acceptor wells. (Such a two-pH combination could differentiate acids from bases and nonionizables by the differences between the two P_e values.) Furthermore, the acceptor side would have 3% wt/vol BSA to maintain a sink condition (or some sink-forming equivalent). The donor side may benefit from having a bile acid (i.e., taurocholic or glycocholic, 5–15 mM), to solubilize the most lipophilic sample molecules. The ideal lipid barrier would have a composition similar to those in Table 7.1, with the membrane possessing substantial negative charge (mainly from PI and PS). Excessive DMSO or other cosolvents use requires further research, due to their multimechanistic effects. *In vitro* assays where permeabilities of lipophilic molecules are diffusion-limited [574–576], the role of the unstirred water layer (UWL; see Section 7.7.6) needs to be accounted, since under *in vivo* conditions, the UWL is nearly absent, especially in the BBB.

7.5 DERIVATION OF MEMBRANE-RETENTION PERMEABILITY EQUATIONS (ONE-POINT MEASUREMENTS, PHYSICAL SINKS, IONIZATION SINKS, BINDING SINKS, DOUBLE SINKS)

The equations used to calculate permeability coefficients depend on the design of the in vitro assay to measure the transport of molecules across membrane barriers. It is important to take into account factors such as pH conditions (e.g., pH gradients), buffer capacity, acceptor sink conditions (physical or chemical), any precipitate of the solute in the donor well, presence of cosolvent in the donor compartment, geometry of the compartments, stirring speeds, filter thickness, porosity, pore size, and tortuosity.

In PAMPA measurements each well is usually a one-point-in-time (single-timepoint) sample. By contrast, in the conventional multitimepoint Caco-2 assay, the acceptor solution is frequently replaced with fresh buffer solution so that the solution in contact with the membrane contains no more than a few percent of the total sample concentration at any time. This condition can be called a ''physically maintained'' sink. Under pseudo–steady state (when a practically linear solute concentration gradient is established in the membrane phase; see Chapter 2), lipophilic molecules will distribute into the cell monolayer in accordance with the effective membrane–buffer partition coefficient, even when the acceptor solution contains nearly zero sample concentration (due to the physical sink). If the physical sink is maintained indefinitely, then eventually, all of the sample will be depleted from both the donor and membrane compartments, as the flux approaches zero (Chapter 2). In conventional Caco-2 data analysis, a very simple equation [Eq. (7.10) or (7.11)] is used to calculate the permeability coefficient. But when combinatorial (i.e., lipophilic) compounds are screened, this equation is often invalid, since a considerable portion of the molecules partitions into the membrane phase during the multitimepoint measurements.

The extra timepoint measurements make the traditional Caco-2 assay too slow for high-throughput applications. Since the PAMPA assay was originally developed for high-throughout uses, there is no continuous replacement of the acceptor compartment solution. Some technical compromises are necessary in order to make the PAMPA method fast. Consequently, care must be exercised, in order for the single-timepoint method to work reliably. If the PAMPA assay is conducted over a long period of time (e.g., $>$20 h), the system reaches a state of equilibrium, where the sample concentration becomes the same in both the donor and acceptor compartments (assuming no pH gradients are used) and it becomes impossible to determine the permeability coefficient. Under such conditions, the membrane will also accumulate some (but sometimes nearly all) of the sample, according to the membrane-buffer partition coefficient. In the commonly practiced PAMPA assays it is best to take the single timepoint at 3–12 h, before the system reaches a state of equilibrium. Since the acceptor compartment is not assumed to be in a sink state, the permeability coefficient equation takes on a more complicated form [Eq. (7.20) or (7.21)] than that used in traditional Caco-2 assays.

For ionizable sample molecules, it is possible to create an effective sink condition in PAMPA by selecting buffers of different pH in the donor and acceptor compartments. For example, consider salicylic acid (pK_a 2.88; see Table 3.1). According to the pH partition hypothesis, only the free acid is expected to permeate lipophilic membranes. If the donor pH < 2 and the acceptor pH is 7.4, then as soon as the free acid reaches the acceptor compartment, the molecule ionizes, and the concentration of the free acid becomes effectively zero, even though the total concentration of the species in the acceptor compartment may be relatively high. This situation may be called an 'ionization-maintained' sink.

Another type of nonphysical sink may be created in a PAMPA assay, when serum protein is placed in the acceptor compartment and the sample molecule

that passes across the membrane then binds strongly to the serum protein. Consider phenazopyridine (pK_a 5.15; see Table 3.1) in a pH 7.4 PAMPA assay, where the acceptor solution contains 3% wt/vol BSA (bovine serum albumin). As soon as the free base reaches the acceptor compartment, it binds to the BSA. The unbound fraction becomes very low, even though the total concentration of the base in the acceptor compartment may be relatively high. This may be called a *binding-maintained* sink.

In this chapter we use the term ''sink'' to mean any process that can significantly lower the concentration of the neutral form of the sample molecule in the acceptor compartment. Under the right conditions, the ionization and the binding sinks serve the same purpose as the physically maintained sink often used in Caco-2 measurements. We will develop several transport models to cover these ''chemical'' sink conditions. When both of the chemical sink conditions (ionization and binding) are imposed, we will use the term ''double sink'' in this chapter.

The chemical sink may be thought of as a method used to increase the volume of distribution of species in the acceptor solution beyond the geometric volume of the receiving compartment. As such, this extension of terminology should be clear to traditional Caco-2 users. The use of the chemical sinks in PAMPA is well suited to automation, and allows the assay to be conducted at high-throughput speeds. As mentioned above, the one-point-in-time (single-timepoint) sampling can lead to errors if not properly executed. We will show that when multitimepoint PAMPA is done (see Fig. 7.15), the equations developed in this chapter for high-speed single-timepoint applications are acceptably good approximations.

7.5.1 Thin-Membrane Model (without Retention)

Perhaps the simplest Fick's law permeation model consists of two aqueous compartments, separated by a very thin, pore-free, oily membrane, where the unstirred water layer may be disregarded and the solute is assumed to be negligibly retained in the membrane. At the start ($t = 0$ s), the sample of concentration $C_D(0)$, in mol/cm^3 units, is placed into the donor compartment, containing a volume (V_D, in cm^3 units) of a buffer solution. The membrane (area A, in cm^2 units) separates the donor compartment from the acceptor compartment. The acceptor compartment also contains a volume of buffer (V_A, in cm^3 units). After a permeation time, t (in seconds), the experiment is stopped. The concentrations in the acceptor and donor compartments, $C_A(t)$ and $C_D(t)$, respectively, are determined.

Two equivalent flux expressions define such a steady-state transport model [41]

$$J(t) = P[C_D(t) - C_A(t)] \tag{7.1}$$

and

$$J(t) = \frac{-V_D}{A}\frac{dC_D(t)}{dt} \tag{7.2}$$

where P denotes either the effective or the apparent permeability, P_e or P_a, depending on the context (see later), in units of cm/s. These expressions may be equated to get the differential equation

$$\frac{dC_D(t)}{dt} = -\left(\frac{A}{V_D}\right)P[C_D(t) - C_A(t)] \tag{7.3}$$

It is useful to factor out $C_A(t)$ and solve the differential equation in terms of just $C_D(t)$. This can be done by taking into account the mass balance, which requires that the total amount of sample be preserved, and be distributed between the donor and the acceptor compartments (disregarding the membrane for now). At $t = 0$, all the solute is in the donor compartment, which amounts to $V_D C_D(0)$ moles. At time t, the sample distributes between two compartments:

$$V_D C_D(0) = V_D C_D(t) + V_A C_A(t) \tag{7.4}$$

This equation may be used to replace $C_A(t)$ in Eq. (7.3) with donor-based terms, to get the simplified differential equation

$$\frac{dC_D(t)}{dt} + aC_D(t) + b = 0 \tag{7.5}$$

where $a = AP/[(V_A V_D)/(V_A + V_D)] = \tau_{eq}^{-1}$, τ_{eq} is the time constant, and $b = APC_D(0)/V_A$. Sometimes, τ_{eq}^{-1} is called the *first-order rate constant*, k [in s^{-1} units (reciprocal seconds)]. The ordinary differential equation may be solved by standard techniques, using integration limits from 0 to t, to obtain an exponential solution, describing the *disappearance* of solute from the donor compartment as a function of time

$$\frac{C_D(t)}{C_D(0)} = \frac{m_D(t)}{m_D(0)} = \frac{V_A}{V_A + V_D}\left[\frac{V_D}{V_A} + \exp(-t/\tau_{eq})\right] \tag{7.6}$$

where $m_D(t)$ refers to the moles of solute remaining in the donor compartment at time t. Note that when $V_A \gg V_D$, Eq. (7.6) approximately equals $\exp(-t/\tau_{eq})$. Furthermore, $\exp(-t/\tau_{eq}) \approx 1 - t/\tau_{eq}$ when t is near zero. Using the mole balance relation [Eq. (7.4)], the exponential expression above [Eq. (7.6)] may be converted into another one, describing the *appearance* of solute in the acceptor compartment.

$$\frac{C_A(t)}{C_D(0)} = \frac{V_D}{V_A + V_D}\left(1 - \exp\frac{-t}{\tau_{eq}}\right) \tag{7.7}$$

In mole fraction units, this is

$$\frac{m_A(t)}{m_D(0)} = \frac{V_A}{V_A + V_D}\left(1 - \exp\frac{-t}{\tau_{eq}}\right) \tag{7.8}$$

Note that when $V_A \gg V_D$, Eq. (7.8) approximately equals $1 - \exp(-t/\tau_{eq})$. Furthermore, $1 - \exp(-t/\tau_{eq}) \approx t/\tau_{eq}$ when t is near zero. Figure 7.14 shows the forms of Eqs. (7.6) and (7.8) under several conditions. When less than ~10% of the compound has been transported, the reverse flux due to $C_A(t)$ term in Eq. (7.1) is nil. This is effectively equivalent to a sink state, as though $V_A \gg V_D$. Under these conditions, Eq. (7.8) can be simplified to

$$\frac{m_A(t)}{m_D(0)} \approx \frac{t}{\tau_{eq}} \approx \frac{APt}{V_D} \tag{7.9}$$

and the apparent permeability coefficient can be deduced from this "one-way flux" equation,

$$P_a = \frac{V_D}{At}\frac{m_A(t)}{m_D(0)} \tag{7.10}$$

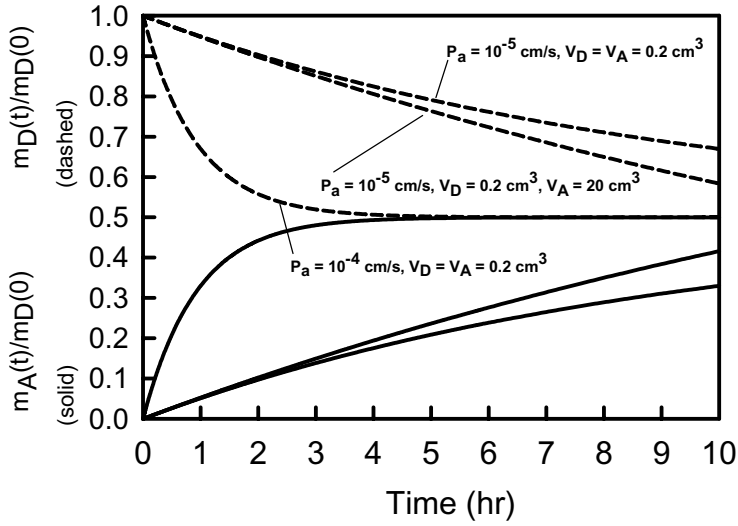

Figure 7.14 Relative concentrations of accetor and donor compartments as a function of time for the thin-membrane model.

We define this permeability as ''apparent,'' to emphasize that there are important but hidden assumptions made in its derivation. This equation is popularly (if not nearly exclusively) used in culture cell in vitro models, such as Caco-2. The sink condition is maintained by periodically moving a detachable donor well to successive acceptor wells over time. At the end of the total permeation time t, the mass of solute is determined in each of the acceptor wells, and the mole sum $m_A(t)$ is used in Eq. (7.10). Another variant of this analysis is based on evaluating the slope in the early part of the appearance curve (e.g., solid curves in Fig. 7.14):

$$P_a = \frac{V_D}{A} \frac{\Delta m_A(t)/\Delta t}{m_D(0)} \tag{7.11}$$

It is important to remember that Eqs. (7.10) and (7.11) are both based on assumptions that (1) sink conditions are maintained, (2) data are taken early in the transport process (to further assure sink condition), and (3) *there is no membrane retention of solute*. In discovery settings where Caco-2 assays are used, the validity of assumption 3 is often untested.

The more general solutions (but still neglecting membrane retention, hence still ''apparent'') are given by ''two-way flux'' in Eqs. 7.12 (disappearance kinetics) and (7.13) (appearance kinetics).

$$P_a = -\frac{2.303\ V_D}{At}\left(\frac{1}{1+r_V}\right)\cdot \log_{10}\left[-r_V + (1+r_V)\cdot\frac{C_D(t)}{C_D(0)}\right] \tag{7.12}$$

$$= -\frac{2.303\ V_D}{At}\left(\frac{1}{1+r_V}\right)\cdot \log_{10}\left[1 - (1+r_V^{-1})\cdot\frac{C_A(t)}{C_D(0)}\right] \tag{7.13}$$

where the aqueous compartment volume ratio, $r_V = V_D/V_A$. Often, $r_V = 1$. From analytical considerations, Eq. (7.13) is better to use than (7.12) when only a small amount of the compound reaches the acceptor wells; analytical errors in the calculated P_a, based on Eq. (7.13), tend to be lower.

Palm et al. [578] derived a two-way flux equation which is equivalent to Eq. (7.13), and applied it to the permeability assessment of alfentanil and cimetidine, two drugs that may be transported by passive diffusion, in part, as charged species. We will discuss this apparent violation of the pH partition hypothesis (Section 7.7.7.1).

7.5.2 Iso-pH Equations with Membrane Retention

The popular permeability equations [(7.10) and (7.11)] derived in the preceding section presume that the solute does not distribute into the membrane to any appreciable extent. This assumption may not be valid in drug discovery research, since most of the compounds synthesized by combinatorial methods are very lipophilic and can substantially accumulate in the membrane. Neglecting this leads to underestimates of permeability coefficients. This section expands the equations to include membrane retention.

7.5.2.1 Without Precipitate in Donor Wells and without Sink Condition in Acceptor Wells

When membrane retention of the solute needs to be considered, one can derive the appropriate permeability equations along the lines described in the preceding section: Eqs. (7.1)–(7.3) apply (with P designated as the effective permeability, P_e). However, the mass balance would need to include the membrane compartment, in addition to the donor and acceptor compartments. At time t, the sample distributes (mol amounts) between three compartments:

$$V_D C_D(0) = V_A C_A(t) + V_D C_D(t) + V_M C_M(t) \tag{7.14}$$

The partition coefficient is needed to determine the moles lost to the membrane, $V_M\ C_M(t)$. If ionizable compounds are considered, then one must decide on the types of partition coefficient to use $-K_p$ (true pH-independent partition coefficient) or K_d (pH-dependent apparent partition coefficient). If the permeability assay is based on the measurement of the *total* concentrations, $C_D(t)$ and $C_A(t)$, summed over all charge-state forms of the molecule, and only the uncharged molecules transport across the membrane to an appreciable extent, it is necessary to consider the apparent partition (distribution) coefficient, K_d, in order to explain the pH dependence of permeability.

The apparent membrane–buffer partition (distribution) coefficient K_d, defined at $t = \infty$, is

$$K_d = \frac{C_M(\infty)}{C_D(\infty)} = \frac{C_M(\infty)}{C_A(\infty)} \tag{7.15}$$

since at equilibrium, $C_D(\infty) = C_A(\infty)$, *in the absence of a pH gradient and other sink conditions*. At equilibrium ($t = \infty$), the mole balance equation [Eq. (7.14)] can be expanded to factor in the partition coefficient, Eq. (7.15):

$$\begin{aligned} V_D C_D(0) &= V_D C_D(\infty) + V_A C_A(\infty) + V_M K_d C_D(\infty) \\ &= V_D C_D(\infty) + V_A C_D(\infty) + V_M K_d C_D(\infty) \\ &= C_D(\infty)(V_D + V_A + V_M K_d) \end{aligned} \tag{7.16}$$

It is practical to make the approximation that $C_M(\infty) \approx C_M(t)$. This is justified if the membrane is saturated with the sample in a short period of time. This lag (steady-state) time may be approximated from Fick's second law as $\tau_{\mathrm{LAG}} = h^2/(\pi^2 D_m)$, where h is the membrane thickness in centimeters and D_m is the sample diffusivity *inside the membrane*, in cm^2/s [40,41]. Mathematically, τ_{LAG} is the time at which Fick's second law has transformed into the limiting situation of Fick's first law. In the PAMPA approximation, the lag time is taken as the time when solute molecules first appear in the acceptor compartment. This is a tradeoff approximation to achieve high-throughput speed in PAMPA. With $\mathrm{h} = 125\ \mu\mathrm{m}$ and $D_m \approx 10^{-7}\ \mathrm{cm}^2/\mathrm{s}$, it should take $\sim$3 min to saturate the lipid membrane with sample. The observed times are of the order of 20 min (see below), short enough for our purposes. Cools

and Janssen [545] reported 10–30-min lag times with octanol-impregnated filters. With thinner BLM membranes, the time to reach steady state under sink conditions was reported to be 3–6 min [537]. Times as short as 50 s have been reported in BLM membranes [84].

From Eq. (7.16), one can deduce $C_D(\infty)$, and apply it in the next step. Before equilibrium is reached, at time $t > \tau_{\mathrm{LAG}}$, the moles of solute in the membrane may be estimated from

$$\begin{aligned} V_M C_M(t) \approx V_M C_M(\infty) &= V_M K_d C_D(\infty) \\ &= \frac{V_D C_D(0) V_M K_d}{V_A + V_D + V_M K_d} \end{aligned} \tag{7.17}$$

At this point, we introduce the *retention fraction* R, which is defined as the mole fraction of solute "lost" to the membrane. Equation (7.16) is used in the steps leading to Eq. (7.18):

$$\begin{aligned} R &= 1 - \frac{m_D(t)}{m_D(0)} - \frac{m_A(t)}{m_D(0)} \\ &= 1 - \frac{C_D(\infty)}{C_D(0)} - \frac{V_A}{V_D} \cdot \frac{C_A(\infty)}{C_D(0)} \\ &= \frac{V_M K_d}{V_A + V_D + V_M K_d} \end{aligned} \tag{7.18}$$

Note that from Eqs. (7.17) and (7.18), $R \approx V_M C_M(t)/V_D C_D(0)$ for $t > \tau_{\mathrm{LAG}}$. The substitution of the apparent partition coefficient with the retention ratio allows us to state the mole balance at time t (provided $t > \tau_{\mathrm{LAG}}$) in a much simplified form:

$$V_A C_A(t) + V_D C_D(t) = V_D C_D(0)(1 - R) \tag{7.19}$$

Given this relationship between $C_A(t)$ and $C_D(t)$, where retention is factored in, we can proceed to convert Eq. (7.3) into Eq. (7.5), where a is the same as before, and b now needs to be multiplied by the partition-related factor, $1 - R$. The so-modified ordinary differential, Eq. (7.5), is solved by standard methods, using integration limits from τ_{LAG} to t (not 0 to t), and the desired effective permeability derived as

$$P_e = -\frac{2.303 V_D}{A(t - \tau_{\mathrm{LAG}})} \left(\frac{1}{1 + r_V}\right) \cdot \log_{10}\left[-r_V + \left(\frac{1 + r_V}{1 - R}\right) \cdot \frac{C_D(t)}{C_D(0)}\right] \tag{7.20}$$

$$= -\frac{2.303 V_D}{A(t - \tau_{\mathrm{LAG}})} \left(\frac{1}{1 + r_V}\right) \cdot \log_{10}\left[1 - \left(\frac{1 + r_V^{-1})}{1 - R}\right) \cdot \frac{C_A(t)}{C_D(0)}\right] \tag{7.21}$$

Note that Eqs. (7.20) and (7.21) are nearly identical to Eqs. (7.12) and (7.13); the differences are the $1 - R$ term (to reflect membrane retention) and the lag

time offset, τ_{LAG} (the time needed to saturate the membrane with solute). These differences warrant the new equations to be denoted with the subscript *e*.

When using the 96-well microtiter plate format, typical metrics are $V_A = 200$–400 μL, $V_D = 200$–400 μL, $A = 0.3$ cm^2, $V_M = 4$–6 μL, h (filter thickness) = 125 μm, 70% porosity (ϵ), t (permeation time) = 3–15 h, $\tau_{LAG} = 0$–60 min. As noted

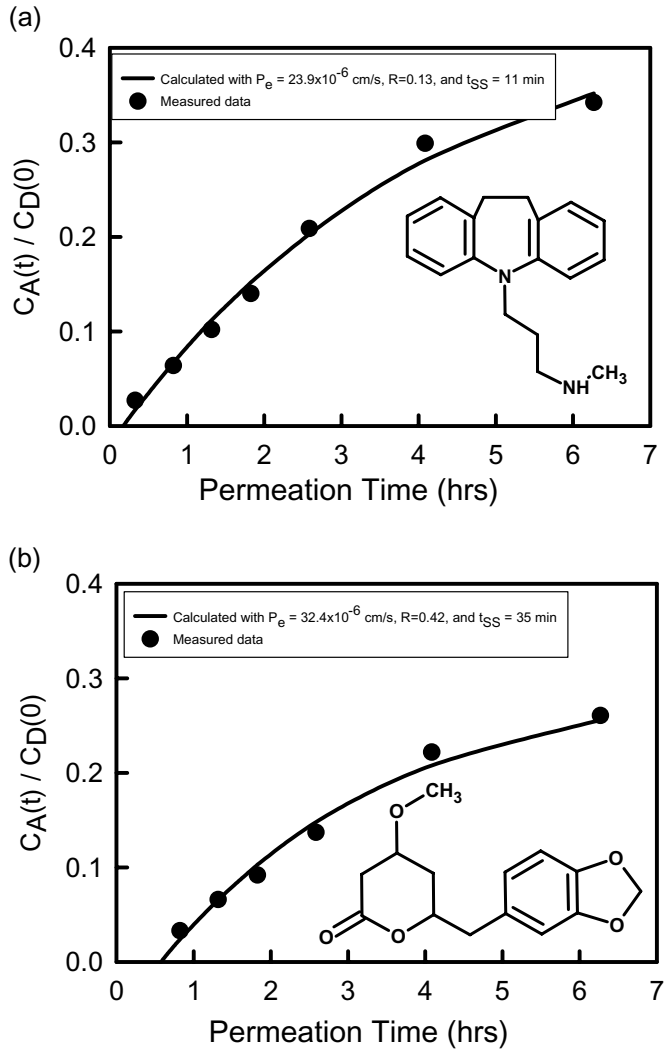

Figure 7.15 Kinetics of transport across a filter-immobilized artificial membrane: (a) desipramine and (b) dihydromethysticin concentrations in acceptor well. [Reprinted from Avdeef, A., in van de Waterbeemd, H.; Lennernäs, H.; Artursson, P. (Eds.). *Drug Bioavailability. Estimation of Solubility, Permeability, Absorption and Bioavailability.* Wiley-VCH: Weinheim, 2003 (in press), with permission from Wiley-VCH Verlag GmbH.]

above, the time constant for the kinetic process is defined as $\tau_{eq} = [(V_A V_D)/(V_A + V_D)]/(AP_e)$. For membranes made with 2% DOPC in dodecane, metoprolol at pH 7.4, has $\tau_{eq} = 4.8 \times 10^{5}$ s or 134 h for the donor concentration to decay to $1/e$ (37%) from the final equilibrium value. For diltiazem, the time constant is 5.3 h. However, for membranes made with 20% soy lecithin in dodecane, under sink conditions created by an anionic surfactant in the acceptor wells, the metoprolol and diltiazem time constants decrease to 3.2 and 2.6 h, respectively, since the permeability coefficients increase in the soy-based membrane under artificially imposed sink conditions (as discussed in a later section).

Figure 7.15 shows the appearance curves of desipramine and dihydromethysticin [556] in the acceptor wells as a function of time. Because some of the material is lost to the membrane, the curves level off asymptotically at acceptor concentration fractions considerably less the 0.5 value expected in the thin-membrane model (Fig. 7.14). The solid curve for desipramine in Fig. 7.15a is a least-squares fit of the data points to Eq. (7.21), with the parameters: P_e 24×10^{-6} cm/s, R 0.13, and τ_{LAG} 11 min. The solid curve for dihydromethisticin in Fig. 7.15b is described by the parameters: P_e 32×10^{-6} cm/s, R 0.42, and τ_{LAG} 35 min.

Ketoprofen, a weak-acid drug, with a pK_a 4.12 (25°C, 0.01 M ionic strength), was selected to illustrate Eqs. (7.20) and (7.21) in a series of simulation calculations, as shown in Fig. 7.16. The membrane–buffer apparent partition coefficients $K_{d(pH)}$ were calculated at various pH values, using the measured constants from

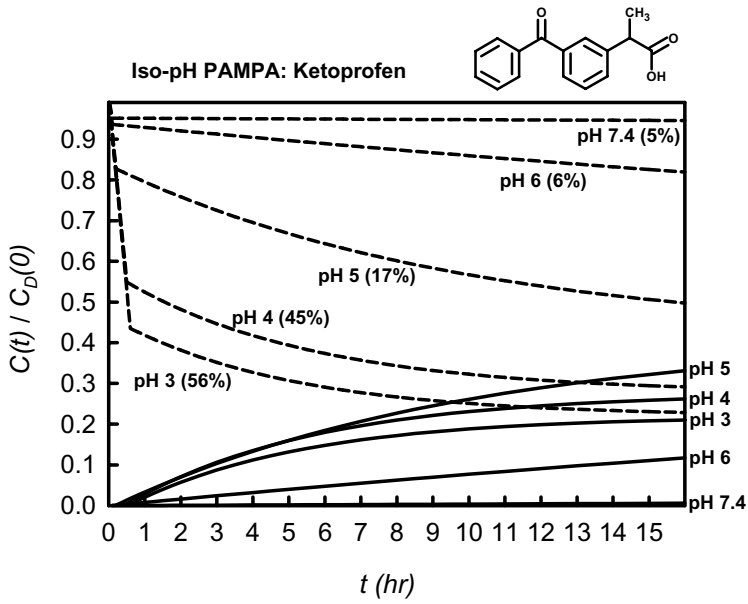

Figure 7.16 Relative concentrations of accetor and donor compartments as a function of time for the iso-pH ketoprofen model.

liposome–water partition studies: the surface ion pair (SIP) constant, log K_p^{SIP} 0.70, corresponding to the partitioning of the anionic form of the drug in bilayers at high pH, and the neutral-species partition coefficient, log K_p^N 2.14, evident at low pH [149]. For example, at pH 7.4, K_d is 5 and at pH 4.3, K_d is 58. Also used for the simulation calculation were the intrinsic permeability coefficient, P_0 1.7×10^{-4} cm/s, corresponding to the transport property of the uncharged form of ketoprofen, and the unstirred water layer permeability coefficient, P_u 2.2×10^{-5} cm/s. (These two types of permeability are described later in this chapter.)

At pH 3, ketoprofen is mostly in an uncharged state in solution. The dashed curve in Fig. 7.16 corresponding to pH 3 shows a rapid decline of the sample in the donor well in the first half-hour; this corresponds to the membrane loading up with the drug, to the extent of 56%. The corresponding appearance of the sample in the acceptor well is shown by the solid line at pH 3. The solid curve remains at zero for $t < \tau_{\mathrm{LAG}}$. After the lag period, the acceptor curve starts to rise slowly, mirroring in shape the donor curve, which decreases slowly with time. The two curves nearly meet at 16 h, at a concentration ratio near 0.22, far below the value of 0.5, the expected value had the membrane retention not taken a portion of the material out of the aqueous solutions.

7.5.2.2 Sink Condition in Acceptor Wells

In Section 7.7.5.4, we discuss the effects of additives in the acceptor wells that create a sink condition, by strongly binding lipophilic molecules that permeate across the membrane. As a result of the binding in the acceptor compartment, the transported molecule has a reduced "active" (unbound) concentration in the acceptor compartment, $c_A(t)$, denoted by the lowercase letter c. The permeability equations in the preceding section, which describe the nonsink process, are inappropriate for this condition. In the present case, we assume that the reverse transport is effectively nil; that is, $C_A(t)$ in Eq. (7.1) may be taken as $c_A(t) \approx 0$. As a result, the permeability equation is greatly simplified:

$$P_a = -\frac{2.303\, V_D}{A(t - \tau_{\mathrm{LAG}})} \cdot \log_{10}\left[\frac{1}{1-R} \cdot \frac{C_D(t)}{C_D(0)}\right] \tag{7.22}$$

Note that we call this the "apparent" permeability, since there is a hidden assumption (unbound concentration is zero).

7.5.2.3 Precipitated Sample in the Donor Compartment

When very insoluble samples are used, sometimes precipitate forms in the donor wells, and the solutions remain saturated during the entire permeation assay. Equations (7.20) and (7.21) would not appropriately represent the kinetics. One needs to consider the following modified flux equations [see, Eqs. (7.1) and (7.2)]

$$J(t) = P_e(S - C_A(t)) \tag{7.23}$$

and

$$J(t) = \frac{V_A}{A}\frac{dC_A(t)}{dt} \tag{7.24}$$

The donor concentration becomes constant in time, represented by the solubility, $S = C_D(0) = C_D(t)$. Reverse flux can still occur, but as soon as the sample reaches the donor compartment, it would be expected to precipitate. Furthermore, the concentration in the acceptor compartment would not be expected to exceed the solubility limit: $C_A(t) \leq S$. After equating the two flux expressions, and solving the differential equation, we have the saturated-donor permeability equation

$$P_e = -\frac{2.303\,V_A}{A(t-\tau_{\text{LAG}})} \cdot \log_{10}\left[1 - \frac{C_A(t)}{S}\right] \tag{7.25}$$

Ordinarily it is not possible to determine the membrane retention of solute under the circumstances of a saturated solution, so no R terms appear in the special equation [Eq. (7.25)], nor is it important to do so, since the concentration gradient across the membrane is uniquely specified by S and $C_A(t)$. The permeability coefficient is "effective" in this case.

7.5.3 Gradient pH Equations with Membrane Retention: Single and Double Sinks

When the pH is different on the two sides of the membrane, the transport of ionizable molecules can be dramatically altered. In effect, sink conditions can be created by pH gradients. Assay improvements can be achieved using such gradients between the donor and acceptor compartments of the permeation cell. A three-compartment diffusion differential equation can be derived that takes into account gradient pH conditions and membrane retention of the drug molecule (which clearly still exists—albeit lessened—in spite of the sink condition created). As before, one begins with two flux equations

$$J(t) = P_e^{(D\rightarrow A)}C_D(t) - P_e^{(A\rightarrow D)}C_A(t) \tag{7.26}$$

and

$$J(t) = -\left(\frac{V_D}{A}\right)\frac{dC_D(t)}{dt} \tag{7.27}$$

It is important to note that two different permeability coefficients need to be considered, one denoted by the superscript $(D\rightarrow A)$, associated with donor (e.g., pH_D

5.0, 6.5, or 7.4)-to-acceptor (pH_A 7.4) transport, and the other denoted by the superscript ($A \rightarrow D$), corresponding to the reverse-direction transport. The two equivalent flux relationships can be reduced to an ordinary differential equation in $C_D(t)$, following a route similar to that in Section 7.5.2.1.

The gradient pH (2-P_e) model developed here implies that some backflux ($A \rightarrow D$) is possible. As far as we know, reported literature studies generally considered backflux to be nil under gradient pH conditions. That is, either Eq. (7.10) or (7.11) were used to interpret the membrane transport under a pH gradient conditions. If it can be assumed that $C_A(t)$ in Eq. (7.26) represents a fully charged (i.e., impermeable) form of the solute, then its contribution to backflux may be neglected, and an effective sink condition would prevail; that is, the concentration of the *uncharged* form of the solute, $c_A(t)$, is used in place of $C_A(t)$, where $c_A(t) \approx 0$. Under such circumstances, the generic sink equation, Eq. (7.22), may be used to determine an apparent permeability coefficient, P_a—"apparent" so as to draw attention to hidden assumptions (i.e., no reverse flux). However, valid use of Eq. (7.22) is restricted to strictly maintained sink conditions and presumes the absence of membrane retention of solute. This is a rather impractical constraint in high-throughput applications, where molecules with potentially diverse transport properties may be assayed at the same time.

A more general analysis requires the use of two effective permeability coefficients, one for each pH, each of which would be valid in the respective iso-pH conditions. Since fewer limiting assumptions are made, the more general method may be more suitable for high-throughput applications. We continue to derive the appropriate new model.

The donor–acceptor membrane mass balance is

$$\text{mol}_{\text{TOT}} = V_D C_D(0) = V_A C_A(\infty) + V_D C_D(\infty) + V_M C_M(\infty) \tag{7.28}$$

Each side of the barrier has a different membrane–buffer apparent partition coefficient K_d, defined at $t = \infty$ as

$$K_{d(A)} = \frac{C_M(\infty)}{C_A(\infty)} \tag{7.29}$$

and

$$K_{d(D)} = \frac{C_M(\infty)}{C_D(\infty)} \tag{7.30}$$

The moles lost to the membrane are derived from Eqs. (7.28)–(7.30):

$$\text{mol}_M = C_M(\infty) V_M = \frac{V_M V_D C_D(0)}{V_A / K_{d(A)} + V_D / K_{d(D)} + V_M} \tag{7.31}$$

The membrane retention fraction R may be defined as membrane-bound moles of sample, divided by the total moles of sample in the system:

$$R = \frac{\text{mol}_M}{\text{mol}_{\text{TOT}}} = \frac{V_M}{V_A/K_{d(A)} + V_D/K_{d(D)} + V_M} \tag{7.32}$$

The membrane saturates with solute early in the transport process. So, for $t \gg 20$ min, we may assume that $C_M(\infty) \approx C_M(t)$ is reasonably accurate. With this assumption, the acceptor concentration may be expressed in terms of the donor concentration as

$$C_A(t) = \frac{V_D}{V_A[C_D(0)(1-R) - C_D(t)]} \tag{7.33}$$

A differential equation as a function of $C_D(t)$ only, similar to Eq. (7.5), can be derived, where the specific constants $a = A(P_e^{(A\to D)}/V_A + P_e^{(D\to A)}/V_D)$ and $b = C_D(0)(1-R)AP_e^{(A\to D)}/V_A$. The solution to the ordinary differential equation is

$$P_e = -\frac{2.303\,V_D}{A(t-\tau_{SS})}\left(\frac{1}{1+r_a}\right)\cdot\log_{10}\left[-r_a + \left(\frac{1+r_a}{1-R}\right)\cdot\frac{C_D(t)}{C_D(0)}\right] \tag{7.34}$$

where

$$r_a = \left(\frac{V_D}{V_A}\right)\frac{P_e^{(A\to D)}}{P_e^{(D\to A)}} = \frac{r_V P_e^{(A\to D)}}{P_e^{(D\to A)}} \tag{7.35}$$

is the sink asymmetry ratio (gradient-pH-induced). When the aqueous solution conditions are identical in the two chambers of the permeation cell (apart from the sample), $r_a = r_V$, and Eq. (7.34) becomes equivalent to Eq. (7.20). This presumes that the system is free of serum proteins or surfactants in the acceptor well. We discuss such assay extensions later.

7.5.3.1 Single Sink: Eq. (7.34) in the Absence of Serum Protein or Sink in Acceptor Wells

In general, Eq. (7.34) has two unknowns: $P_e^{(A\to D)}$ and $P_e^{(D\to A)}$. In serum protein-free assays, the following method is used to solve Eq. (7.34). At least two assays are done: one as gradient pH (e.g., pH 5.0_{donor}–7.4_{acceptor}) and the other as iso-pH (e.g., pH 7.4_{donor}–7.4_{acceptor}), with one pH common to the two assays. For iso-pH, $P_e^{(A\to D)} = P_e^{(D\to A)}$. This case can be solved directly using Eq. (7.20). Then, iteratively, Eq. (7.34) is solved for $P_e^{(D\to A)}$. Initially r_a is assumed to be r_V, but with each iteration, the r_a estimate is improved by using the calculated $P_e^{(D\to A)}$ and the $P_e^{(A\to D)}$ taken from the iso-pH case. The process continues until self-consistency is reached within the accuracy required.

In iso-pH serum protein- and surfactant-free solutions, the concentration of the sample in the acceptor wells cannot exceed that in the donor wells. With gradient-pH conditions, this limitation is lifted. At very long times, the concentrations in the donor and acceptor chambers reach equilibrium values, depending on the pH gradient

$$\frac{C_D(\infty)}{C_A(\infty)} = \frac{P_e^{(A\to D)}}{P_e^{(D\to A)}} \tag{7.36}$$

or in terms of mole ratios

$$\frac{m_D(\infty)}{m_A(\infty)} = r_a \tag{7.37}$$

This limiting ratio can be predicted for any gradient-pH combination, provided the pK_a values of the molecule, the unstirred water layer (UWL) P_u, and the intrinsic P_0 permeabilities were known [25]. (The topic of the UWL are discussed in greater detail in Section 7.7.6.) In gradient pH assays, it is sometimes observed that nearly all the samples move to the acceptor side, due to the sink conditions created, sometimes limiting the determination of concentrations. Shorter permeation times solve the problem, a welcome prospect in a high-throughput application. A 3–4-h period suffices, which is a considerable reduction over the original 15 h permeation time [547,550]. Shorter times would lead to greater uncertainties in the calculated permeability, since the approximate lag time τ_{LAG} can be as long as one hour for the most lipophilic molecules.

7.5.3.2 Double Sink: Eq. (7.34) in the Presence of Serum Protein or Sink in Acceptor Wells

If serum protein or surfactant is added to the acceptor wells, then, in general, $P_e^{(A\to D)}$ and $P_e^{(D\to A)}$ are not the same, even under iso-pH conditions. The acceptor-to-donor permeability needs to be solved by performing a separate iso-pH assay, where the serum protein or surfactant is added to the *donor* side, instead of the acceptor side. The value of P_e is determined, using Eq. (7.20), and used in gradient-pH cases in place of $P_e^{(A\to D)}$, as described in the preceding section. The gradient-pH calculation procedure is iterative as well.

Figure 7.17 shows the asymmetry ratios of a series of compounds (acids, bases, and neutrals) determined at iso-pH 7.4, under the influence of sink conditions created not by pH, but by anionic surfactant added to the acceptor wells (discuss later in the chapter). The membrane barrier was constructed from 20% soy lecithin in dodecane. All molecules show an upward dependence on lipophilicity, as estimated by octanol–water apparent partition coefficients, log $K_{d(7.4)}$. The bases are extensively cationic at pH 7.4, as well as being lipophilic, and so display the highest responses to the sink condition. They are driven to interact with the surfactant by both hydrophobic and electrostatic forces. The anionic acids are largely indifferent

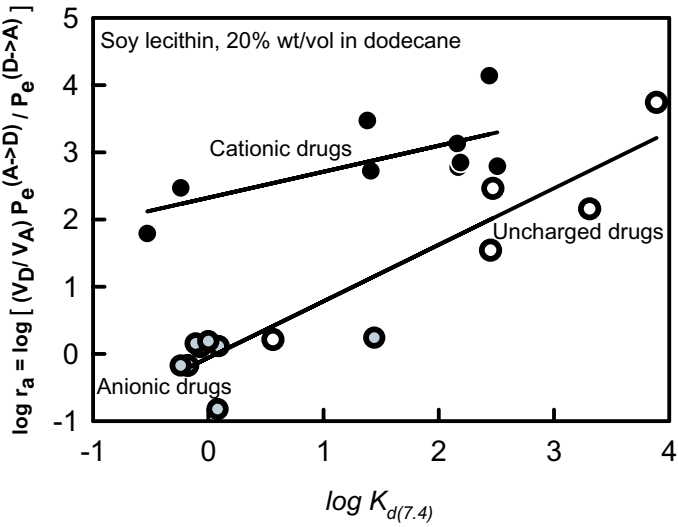

Figure 7.17 Surfactant-induced sink asymmetry ratio versus octanol–water apparent partition coefficient at pH 7.4.

to the presence of the anionic surfactant in the acceptor wells, with a slight suggestion of repulsion in one case (Fig. 7.17).

For ionizable lipophilic molecules, the right pH gradients can drive the solute in the acceptor compartment to the charged (impermeable) form; the uncharged fraction is then further diminished in concentration by binding to the serum protein or surfactant, in the double-sink assay.

7.5.3.3 Simulation Examples

Ketoprofen was selected to illustrate the properties of the gradient-pH permeability equation, Eq. (7.34), in a series of simulation calculations, as shown in Fig. 7.18. The membrane-buffer apparent partition coefficients, $K_{d(\mathrm{pH})}$, were calculated at various pH values, using the approach described in Section 7.5.2.1. The pH in the acceptor well was pH_A 7.4 in all cases, while that in the donor wells was pH_D 3–7.4. It is interesting to compare the transport properties of ketoprofen under iso-pH (Fig. 7.16) and gradient pH (Fig. 7.18) conditions. Under gradient pH conditions, at pH_D 3, ketoprofen is mostly in an uncharged state in solution. The dashed curve in Fig. 7.18 corresponding to pH_D 3 shows a rapid but not extensive decline of the sample in the donor well in the first few minutes; this corresponds to the membrane loading up with the drug, to the extent of only 9%, compared to 56% for iso-pH 3 conditions. The corresponding appearance of the sample in the acceptor well is shown by the solid line corresponding to pH_D 3, pH_A 7.4. After a short lag period, the acceptor curve starts to rise rapidly, mirroring in shape the donor curve, which decreases with time. The two curves cross at 7 h, whereas in the

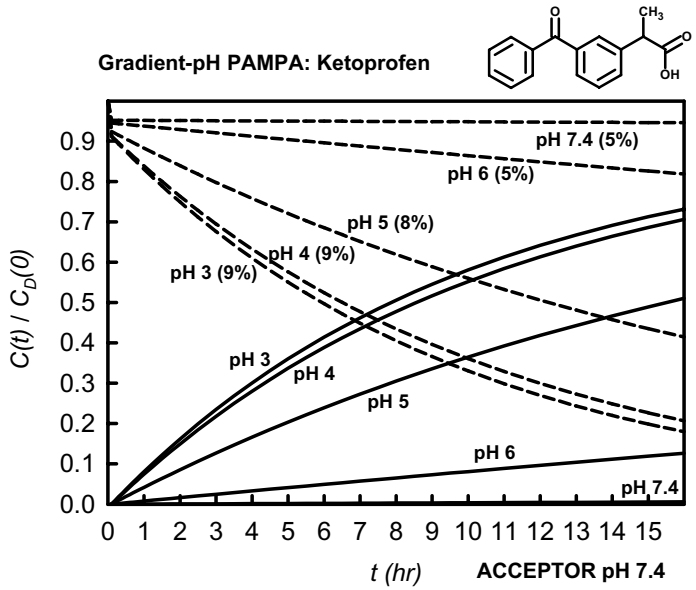

Figure 7.18 Relative concentrations of accetor and donor compartments as a function of time for the gradient–pH ketoprofen model.

iso-pH case, 16 h shows only near meeting. Also, the gradient pH curves cross slightly below the 0.5 concentration ratio, since membrane retention is only 9%.

7.5.3.4 Gradient pH Summary

The benefits of an assay designed under gradient pH conditions are (1) less retention and thus more analytical sensitivity, (2) shorter permeation times and thus higher throughput possible, and (3) more realistic modeling of the in vivo pH gradients found in the intestinal tract and thus better modeling. Time savings with increased sensitivity are important additions to an assay designed for high-throughput applications. A double-sink condition created by the combination of a pH gradient and serum protein (or an appropriate surfactant) in the acceptor compartment is an important component of the biophysical GIT transport model. In contrast, a no-sink condition may be more suitable for a BBB transport model. This is discussed in greater detail later.

7.6 PERMEABILITY–LIPOPHILICITY RELATIONS

7.6.1 Nonlinearity

In the introductory discussion in Chapter 2, it was indicated that the effective permeability P_e linearly depends on the apparent membrane–water partition

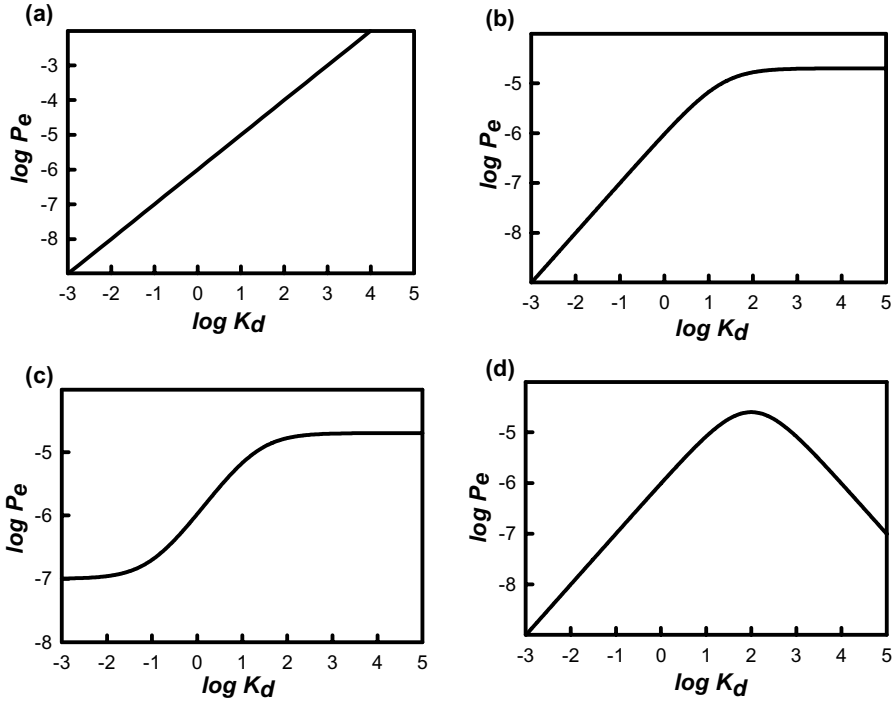

Figure 7.19 Permeability–lipophilicity relations: (a) linear; (b) hyperbolic; (c) sigmoidal; (d) bilinear.

coefficient, K_d [Eq. (2.3)]. The simple model system considered there assumed the membrane barrier to be a structureless homogeneous oil, free of aqueous pores, and also assumed the aqueous solutions on both sides of the barrier to be well mixed by convection, free of the UWL (Section 7.7.6) effect. A log P_e/log K_d plot would be a straight line. Real membrane barriers are, of course, much more complicated. Studies of permeabilities of various artificial membranes and culture-cell monolayers indicate a variety of permeability–lipophilicity relations (Fig. 7.19). These relationships have been the subject of two reviews [49,54]. Figure 7.19 shows linear [579], hyperbolic [580–582], sigmoidal [552,583,584], and bilinear [23,581,585,586] permeability–lipophilicity relations.

Early efforts to explain the nonlinearity were based on drug distribution (equilibrium) or transport (kinetic) in multicompartment systems [21,22]. In this regard, the 1979 review by Kubinyi is highly recommended reading [23]. He analyzed the transport problem using both kinetic and equilibrium models. Let us consider the simple three-compartment equilibrium model first. Imagine an organism reduced to just three phases: water (compartment 1), lipid (compartment 2), and receptor (compartment 3). The corresponding volumes are v_1, v_2, and v_3, respectively, and $v_1 \gg v_2 \gg v_3$. If all of the drug is added to the aqueous phase at time 0, concentration $C_1(0)$, then at equilibrium, the mass balance (see Section 7.5) would be

$v_1C_1(0) = v_1C_1(\infty) + v_2C_2(\infty) + v_3C_3(\infty)$. Two partition coefficients need to be defined: $K_{p2} = C_2(\infty)/C_1(\infty)$ and $K_{p3} = C_3(\infty)/C_1(\infty)$. With these, the mass balance may be rewritten as $v_1C_1(0) = v_1C_1(\infty) + v_2K_{p2}C_1(\infty) + v_3K_{p3}C_1(\infty) = C_1(\infty)(v_1 + v_2K_{p2} + v_3K_{p3})$. If the organic : aqueous volume ratios are r_2 and r_3, then the equilibrium concentrations in the three phases can be stated as

$$C_1(\infty) = \frac{C_1(0)}{(1 + r_2K_{p2} + r_3K_{p3})} \tag{7.38}$$

$$C_2(\infty) = \frac{C_1(0)K_{p2}}{(1 + r_2K_{p2} + r_3K_{p3})} \tag{7.39}$$

$$C_3(\infty) = \frac{C_1(0)K_{p3}}{(1 + r_2K_{p2} + r_3K_{p3})} \tag{7.40}$$

Further reduction is possible. To a good approximation, partition coefficients from different organic solvents may be interrelated by the so-called Collander equation [364,587]: $\log K_{p3} = a \log K_{p2} + c$, or $K_{p3} = 10^c K_{p2}^a$, where a and c are constants. Equations (7.38)–(7.40) can be expressed in log forms as a function of just one partition coefficient (i.e., $K_p = K_{p2}$):

$$\text{Water :} \quad \log \frac{C_1(\infty)}{C_1(0)} = -\log(1 + r_2K_p + r_3 10^c K_p^a) \tag{7.41}$$

$$\text{Lipid :} \quad \log \frac{C_2(\infty)}{C_1(0)} = \log K_p - \log(1 + r_2K_p + r_3 10^c K_p^a) \tag{7.42}$$

$$\text{Receptor :} \quad \log \frac{C_3(\infty)}{C_1(0)} = a \log K_p - \log(1 + r_2K_p + r_3 10^c K_p^a) + c \tag{7.43}$$

Figure 7.20 is a sample plot of relative equilibrium concentrations, Eqs. (7.41)–(7.43). In the example, the three phases were picked to be water, octanol, and phosphatidylcholine-based liposomes (vesicles consisting of a phospholipid bilayer), with the volumes $v_1 = 1$ mL (water), $v_2 = 50$ μL (octanol), and $v_3 = 10$ μL (liposomes). The Collander equation was deduced from Fig. 5.6: $\log K_{p,\text{liposome}} = 0.41 \log K_{p,\text{oct}} + 2.04$. Figure 7.20 suggests that when very hydrophilic molecules (with $\log K_{p,\text{oct}} < -6$) are placed into this three-phase mixture, most of them distribute into the water phase (solid curve), with only minor liposome phase occupation (dashed-dotted curve), but virtually no octanol phase occupation (dashed curve). In the example, molecules with $\log K_{p,\text{oct}}$ of -4 to $+3$, mostly reside in the liposome fraction, schematically modeling the lipophilic property of a hypothetical receptor site, reaching maximum occupancy for compounds with $\log K_{p,\text{oct}}$ at about $+1.5$. Very lipophilic molecules, with $\log K_{p,\text{oct}} > 5$ preferentially concentrate in the (more lipophilic) octanol compartment, becoming unavailable to the receptor region.

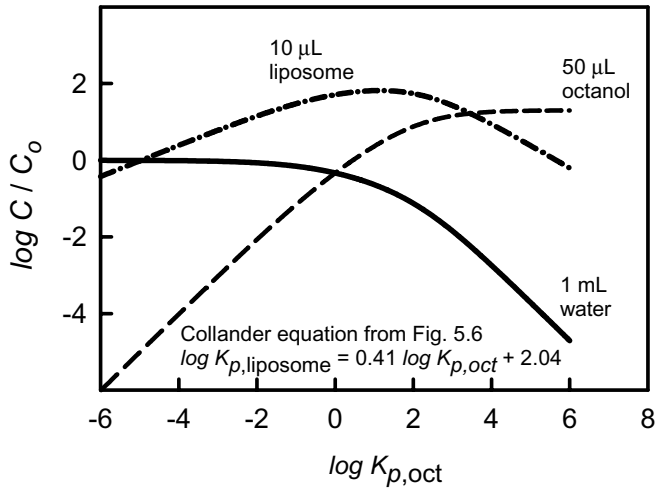

Figure 7.20 Three-compartment equilibrium distribution model (after Kubinyi [23]).

Kubinyi [23] showed that the bilinear equation (7.43) can be approximated by a general form

$$\log C = a \ \log \ K_p + c - b \ \log \ (rK_p + 1) \tag{7.44}$$

where a, b, c, r are empirical coefficients, determined by regression analysis, and C is the concentration in the intermediate phase. Equation (7.44) was used to calculate the curve in Fig. 7.19d.

Our present topic is the relationship between *permeability* and lipophilicity (kinetics), whereas we just considered a *concentration* and lipophilicity model (thermodynamics). Kubinyi demonstrated, using numerous examples taken from the literature, that the kinetics model, where the thermodynamic partition coefficient is treated as a ratio of two reaction rates (forward and reverse), is equivalent to the equilibrium model [23]. The liposome curve shape in Fig. 7.20 (dashed-dotted line) can also be the shape of a permeability-lipophilicity relation, as in Fig. 7.19d.

This relationship was further clarified by van de Waterbeemd in the ''two-step distribution'' model [588–590]. Later, the model was expanded by van de Waterbeemd and colleagues to include the effects of ionization of molecules, with the use of log K_d, in place of log K_p, as well as the effects of aqueous pores [49,54].

7.7 PAMPA: 50+ MODEL LIPID SYSTEMS DEMONSTRATED WITH 32 STRUCTURALLY UNRELATED DRUG MOLECULES

In the rest of the chapter, we describe over 50 specific PAMPA lipid models developed at *p*ION, identified in Table 7.3. The lipid models are assigned a two

TABLE 7.3 PAMPA Lipid Models

Lipid Type	Composition	pH_{DON}/pH_{ACC}	Model Number	
			No Sink	Sink
Neutral	2% DOPC[a]	7.4	1.0	1.1
	2% DOPC + 0.5% Cho	7.4	1A.0	—[d]
	Olive oil	7.4	2.0	—
	Octanol	7.4	3.0	—
	Dodecane	7.4	4.0	—
2-Component anionic[b]	2% DOPC + 0.6% DA	7.4	5.0	5.1
	2% DOPC + 1.1% DA	7.4	6.0	6.1
	2% DOPC + 0.6% PA	7.4	7.0	7.1
	2% DOPC + 1.1% PA	7.4	8.0	8.1
	2% DOPC + 0.6% PG	7.4	9.0	9.1
	2% DOPC + 1.1% PG	7.4	10.0	10.1
5-Component, anionic[c]	0.8% PC + 0.8% PE + 0.2% PS + 0.2% PI + 1.0% Cho	7.4	11.0	—[d]
Lecithin extracts[e] (anionic)	10% egg (Avanti)	7.4	12.0	12.1
	10% egg (Avanti) + 0.5% Cho	7.4	13.0	—[d]
	10% egg (Sigma)	7.4	14.0	14.1
	10% egg (Sigma) + 0.5% Cho	7.4	15.0	15.1
	10% soy	7.4	16.0	16.1
	20% soy	7.4	17.0	17.1
	20% soy + 0.5% Cho	7.4	18.0	18.1
	35% soy	7.4	19.0	19.1
	50% soy	7.4	—	20.1
	68% soy	7.4	21.0	—
	74% soy	7.4	—	22.1
Sink asymmetry	20% soy	7.4	—	23.2
Iso-pH	20% soy	6.5 / 6.5	—	24.1
	20% soy	5.0 / 5.0	—	25.1
Gradient–pH (corr UWL)	20% soy	6.5 / 7.4	—	26.1
	20% soy	6.0 / 7.4	—	27.1
	20% soy	5.5 / 7.4	—	28.1
	20% soy	5.0 / 7.4	—	29.1
	20% soy	4.5 / 7.4	—	30.1

[a] 20 mg DOPC + 1 mL dodecane.

[b] 20 mg DOPC + 6 (or 11) mg negative lipid (DA = dodecylcarboxylic acid, PA = phosphatidic acid, PG = phosphatidylglycerol) + 1 mL dodecane.

[c] Based on Sugano's formula, but using dodecane in place of 1,7-octadiene.

[d] Acceptor well solutions turn turbid in the presence of surfactant sink.

[e] Egg lecithin was "60% extract" grade. The products from Avanti and Sigma behaved differently. Soy lecithin was "20% extract" grade, from Avanti. The model number digit after the decimal point indicates 0 = no sink in system, 1 = sink in acceptor, 2 = sink in donor.

part serial number (Table 7.3). The first index is simply a serial designation and the second index indicates whether an artificial sink condition is in effect in the assay (0 = no, 1 = yes). Special cases (e.g., cosolvent, cyclodextrin, bile salt, or mixed-micelle assays) will employ other values of the second index. We have selected 32 unrelated drug molecules, whose structures are shown in Fig. 7.21, to illustrate the properties of the PAMPA lipid models.

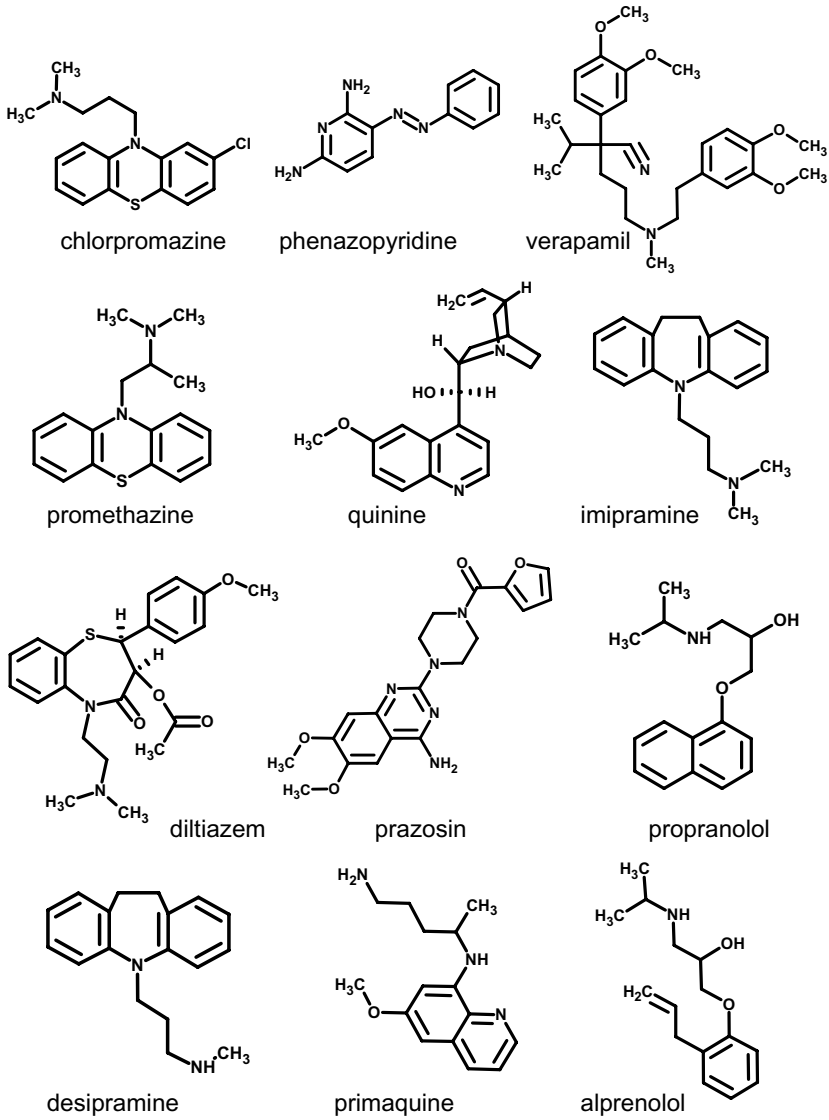

Figure 7.21 Structures of probe drugs used in the PAMPA models.

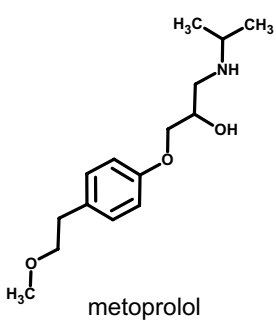

metoprolol

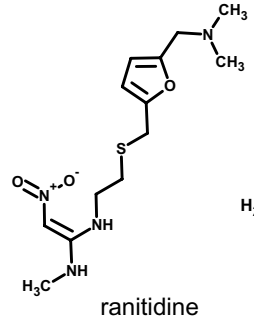

ranitidine

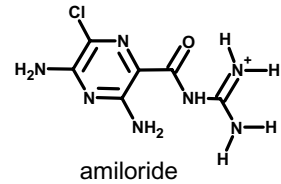

amiloride

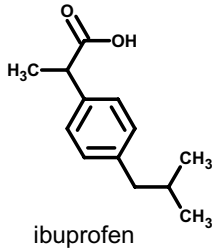

ibuprofen

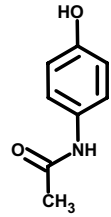

acetaminophen

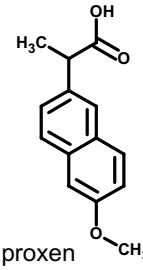

naproxen

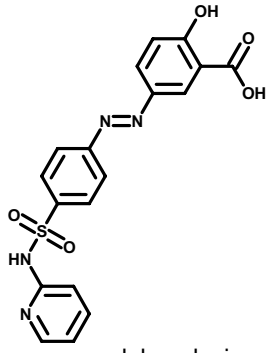

sulphasalazine

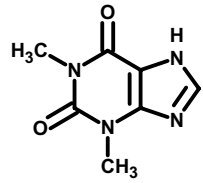

theophylline

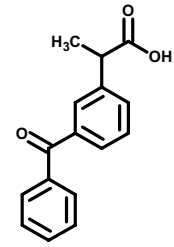

ketoprofen

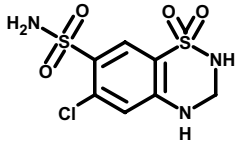

hydrochlorothiazide

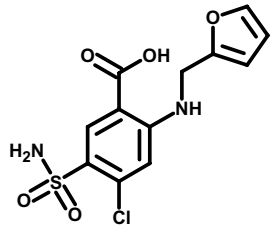

furosemide

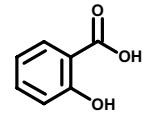

salicylic acid

Figure 7.21 (*Continued*)

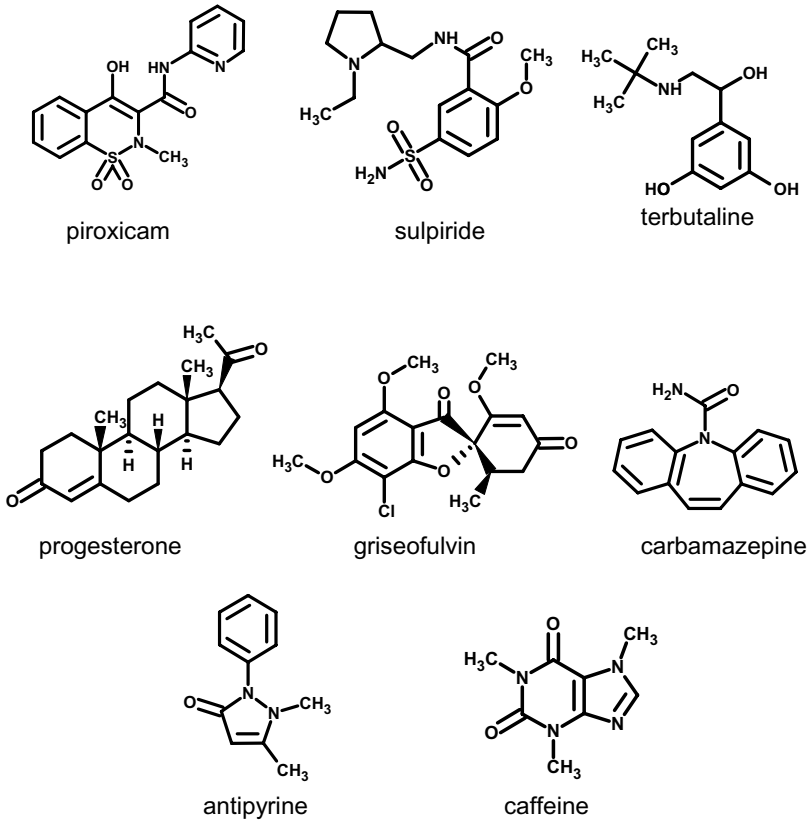

Figure 7.21 (*Continued*)

Table 7.4 summarizes the key pharmacokinetic (PK) and physicochemical properties of the selected probe molecules, consisting of bases, acids, and neutral species.

7.7.1 Neutral Lipid Models at pH 7.4

Four neutral lipid models were explored at pH 7.4: (1) 2% wt/vol DOPC in dodecane, (2) olive oil, (3) octanol, and (4) dodecane. Table 7.5 lists the effective permeabilities P_e, standard deviations (SDs), and membrane retentions of the 32 probe molecules (Table 7.4). The units of P_e and SD are 10^{-6} cm/s. Retentions are expressed as mole percentages. Figure 7.22a is a plot of log P_e versus log K_d (octanol–water apparent partition coefficients, pH 7.4) for filters loaded with 2% wt/vol DOPC in dodecane (model 1.0, filled-circle symbols) and with phospholipid-free dodecane (model 4.0, open-circle symbols). The dashed line in the plot was calculated assuming a UWL permeability (see Section 7.7.6) P_u, 16×10^{-6} cm/s (a typical value in an unstirred 96-well microtiter plate assay), and P_e of 0.8×10^{-6} cm/s

TABLE 7.4 Pharmacokinetic and Physicochemical Properties of Selected Probe Drugs[a]

Sample	% HIA	$P_e(10^{-4}\,cm/s)$	$\log K_{d(7.4)}$	$\log K_p$	pK_{a1}	pK_{a2}	pK_{a3}	Charge Profile	f_u(pH 7.4)	Type
Chlorpromazine	100	—	3.45	5.40	9.24	—	—	$+ > o$	0.01	Base
Phenazopyridine	—	—	3.31	3.31	5.15	—	—	$+ > o$	0.99	Base
Verapamil	95	6.7	2.51	4.44	9.07	—	—	$+ > o$	0.02	Base
Promethazine	80	—	2.44	4.05	9.00	—	—	$+ > o$	0.02	Base
Quinine	80	—	2.19	3.50	4.09	8.55	—	$\ddagger > + > o$	0.07	Base
Imipramine	99	—	2.17	4.39	9.51	—	—	$+ > o$	0.008	Base
Diltiazem	99	—	2.16	2.89	8.02	—	—	$+ > o$	0.19	Base
Prazosin	50	—	2.00	2.18	7.11	—	—	$+ > o$	0.66	Base
Propranolol	99	2.9	1.41	3.48	9.53	—	—	$+ > o$	0.007	Base
Desipramine	95	4.4	1.38	3.79	10.16	—	—	$+ > o$	0.002	Base
Primaquine	100	—	1.17	3.00	3.55	10.03	—	$\ddagger > + > o$	0.002	Base
Alprenolol	93	—	0.86	2.99	9.51	—	—	$+ > o$	0.008	Base
Metoprolol	95	1.3	−0.24	1.95	9.56	—	—	$+ > o$	0.007	Base
Ranitidine	50	0.43	−0.53	1.28	1.96	8.31	—	$\ddagger > + > o$	0.11	Base
Amiloride	50	—	−0.60	−0.26	8.65	—	—	$+ > \pm$	0.000	Base
Ibuprofen	80	—	1.44	4.13	4.59	—	—	$o > -$	0.002	Acid
Acetaminophen	100	—	0.34	0.34	9.78	—	—	$o > -$	1.00	Acid
Naproxen	99	8.3	0.09	3.24	4.32	—	—	$o > -$	0.001	Acid
Sulfasalazine	13	—	0.08	3.61	2.80	8.25	10.96	$o > - >=>\equiv$	0.000	Acid
Theophylline	98	—	0.00	0.00	8.70	—	—	$o > -$	0.95	Acid

TABLE 7.4 (*Continued*)

Sample	% HIA	$P_e(10^{-4}\,\mathrm{cm/s})$	$\log K_{d(7.4)}$	$\log K_p$	pK_{a1}	pK_{a2}	pK_{a3}	Charge Profile	f_u(pH 7.4)	Type
Ketoprofen	100	8.4	−0.11	3.16	4.12	—	—	$o > -$	0.001	Acid
Hydrochlorothiazide	67	0.04	−0.18	−0.03	8.91	10.25	—	$o > - >=$	0.97	Acid
Furosemide	61	0.05	−0.24	2.56	3.67	10.93	—	$o > - >=$	0.000	Acid
Salicyclic Acid	100	—	−1.68	2.19	3.02	—	—	$o > -$	0.000	Acid
Piroxicam	100	7.8	0.00	1.98	2.33	5.22	—	$+ > o > -$	0.007	Amphorphous
Sulpiride	35	—	−1.15	1.31	9.12	10.14	—	$+ > o > -$	0.05	Amphorphous
Terbutaline	60	0.3	−1.35	−0.08	8.67	10.12	11.32	$+ > \pm > - >=$	0.02	Zwitterionic
Progesterone	91	—	3.89	3.89	—	—	—	o	1.00	Neutral
Griseofulvin	28	—	2.18	2.18	—	—	—	o	1.00	Neutral
Carbamazepine	100	4.3	2.45	2.45	—	—	—	o	1.00	Neutral
Antipyrine	100	4.5	0.56	0.56	—	—	—	o	1.00	Neutral
Caffeine	100	—	−0.07	−0.07	—	—	—	o	1.00	Neutral

[a] %HIA human intestinal absorption fraction, oral dose administration; P_e is human jejunal permeability [56]; $\log K_{d(7.4)}$ apparent octanol–water partition coefficient; $\log K_p$ octanol–water partition coefficient; pK_a are ionization constants, at 0.01 M ionic strength; charge profile: the order in which charges on molecules change as pH is raised by 2–10. For example, for terbutaline at pH < 8.67 (pK_{a1}), the main species in solution is a cation (+); for pH 8.67–10.12, a zwitterion exists (±); between pH 10.12 and 11.32, an anion forms (−); and for pH > 11.32, the dianion predominates (=). The symbol > denotes transition in charge state when pH is increased. The fraction of the molecule in the uncharged form at pH 7.4 is represented by f_u.

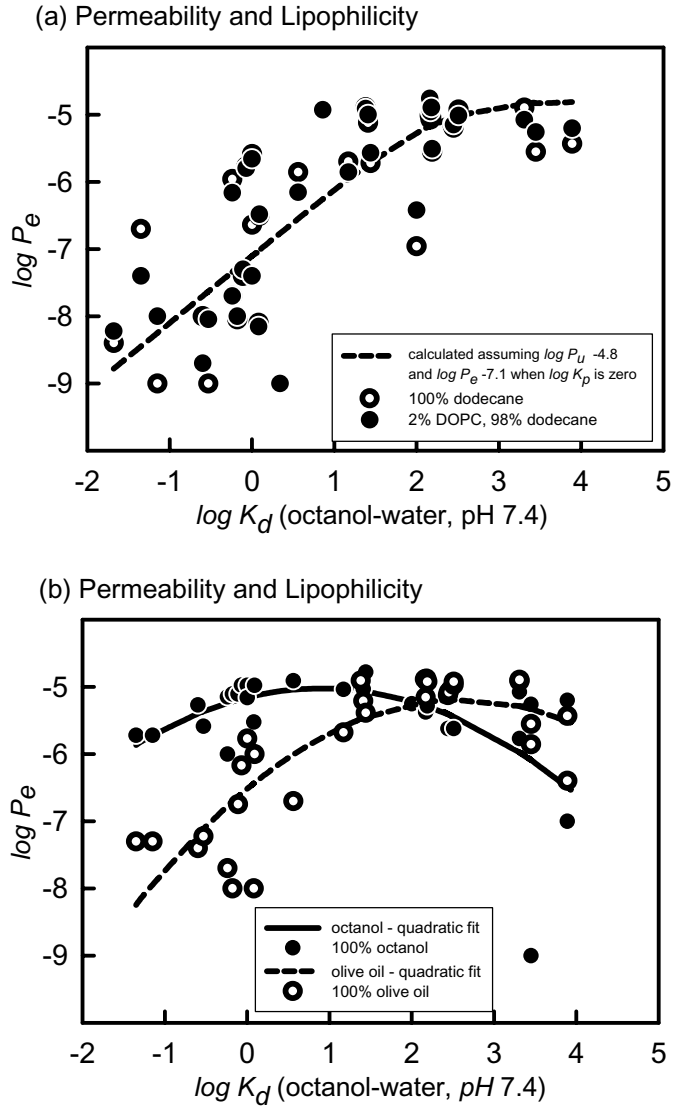

Figure 7.22 Lipophilic nature of membrane retention, log(%R) versus octanol–water apparent partition coefficient, pH 7.4, neutral lipid models.

corresponding to where log K_d is zero (approximately equal to the P_e of metoprolol in 2% DOPC). Although the scatter of points is considerable, the pattern of the relationship between log P_e and log K_d best resembles the hyperbolic plot in Fig. 7.19b, with diffusion-limited (UWL) permeabilities for log $K_d > 2$ and membrane-limited permeabilities for log $K_d < 1$. (We discuss the UWL further Section 7.7.6.)

TABLE 7.5 Neutral Lipid PAMPA Models, pH 7.4[a]

Sample	2%DOPC (Model 1.0) P_e (SD)	%R	Olive Oil (Model 2.0) P_e(SD)	%R	Octanol (Model 3.0) P_e (SD)	%R	Dodecane (Model 4.0) P_e (SD)	%R
Chlorpromazine	5.5 (0.4)	85	1.4 (0.2)	82	0.000 (0.005)	90	2.8 (1.2)	89
Phenazopyridine	8.4 (1.1)	70	12.2 (2.5)	80	1.7 (0.2)	87	12.7 (1.6)	23
Verapamil	9.7 (1.0)	39	10.7 (2.8)	55	2.4 (0.3)	72	11.9 (1.0)	28
Promethazine	7.3 (0.7)	70	7.5	73	2.4 (0.2)	82	6.8 (1.4)	67
Quinine	3.1 (0.6)	1	11.9 (0.8)	21	5.2 (0.2)	63	2.8 (0.2)	10
Imipramine	11.1 (0.8)	56	7.0 (0.8)	75	4.2 (0.1)	76	8.5 (3.0)	55
Diltiazem	17.4 (1.8)	21	13.0 (2.6)	26	5.4 (1.2)	50	9.7 (0.1)	10
Prazosin	0.38 (0.07)	15	—	—	5.6 (0.2)	52	0.11 (0.03)	10
Propranolol	10.0 (0.5)	18	6.2 (0.9)	18	9.3 (0.2)	33	7.6 (0.1)	11
Desipramine	12.3 (0.4)	40	12.4 (1.8)	24	9.8 (0.6)	42	12.9 (1.1)	9
Primaquine	1.4 (0.1)	70	2.1	21	9.2 (0.1)	22	2.0 (0.1)	6
Alprenolol	11.8 (0.3)	16	—	—	—	—	—	—
Metoprolol	0.69 (0.04)	11	—	—	7.1 (0.1)	16	1.1 (0.1)	4
Ranitidine	0.009 (0.004)	2	0.06 (0.06)	0	2.6 (0.1)	13	0.000 (0.005)	2
Amiloride	0.002 (0.005)	0	0.04 (0.01)	2	5.4 (0.4)	14	0.01 (0.01)	2

Ibuprofen	2.7 (0.5)	38	4.1 (0.03)	11	16.6 (8.3)	34	1.9 (0.5)	0
Acetaminophen	0.001(0.005)	1	—	—	—	—	—	—
Naproxen	0.33 (0.03)	4	1.0 (0.1)	2	10.5 (0.7)	14	0.31 (0.12)	4
Sulfasalazine	0.007 (0.004)	1	0.01 (0.01)	0	3.0 (0.1)	11	0.008 (0.005)	3
Theophylline	0.04 (0.01)	1	—	—	10.5 (0.1)	12	0.23 (0.05)	1
Ketoprofen	0.05 (0.01)	4	0.18 (0.17)	2	7.8 (0.2)	13	0.04 (0.04)	1
Hydrochlorothiazide	0.01 (0.01)	1	0.01 (0.01)	3	7.8 (0.1)	14	0.009 (0.005)	1
Furosemide	0.02 (0.01)	1	0.02 (0.01)	2	1.0 (0.1)	12	0.02 (0.04)	0
Salicyclic acid	0.006 (0.004)	1	—	—	—	—	0.004 (0.006)	7
Piroxicam	2.2 (0.1)	3	1.7 (0.2)	4	6.9 (0.1)	18	2.6 (0.2)	1
Sulpiride	0.01 (0.01)	1	0.05 (0.05)	0	1.9 (0.1)	11	0.000 (0.005)	0
Terbutaline	0.04 (0.01)	6	0.05 (0.04)	2	1.9 (0.2)	14	0.20 (0.17)	0
Progesterone	6.3 (0.5)	84	0.4 (0.6)	83	0.1 (0.1)	91	3.7 (0.7)	82
Griseofulvin	12.8 (1.2)	18	13.2 (3.1)	9	6.5 (0.6)	62	9.2 (0.4)	10
Carbamazepine	7.1 (0.3)	10	8.3 (0.1)	7	9.4 (0.2)	40	6.4 (0.3)	6
Antipyrine	0.7 (0.1)	13	0.2 (0.2)	5	12.3 (0.9)	15	1.4 (0.1)	4
Caffeine	1.6 (0.1)	2	0.68 (0.08)	1	10.6 (0.2)	13	1.7 (0.1)	1

[a] All P_e and SD(P_e) are in units of 10^{-6} cm/s.

Figure 7.22b is a similar plot for the other two lipids considered: olive oil (unfilled symbols) and octanol (filled symbols). Both lipids can be described by a bilinear relationship, patterned after the case in Fig. 7.19d [Eq. (7.44)]. Octanol shows a declining log P_e relationship for very lipophilic molecules (log $K_d > 2$). The probe set of 32 molecules does not have examples of very hydrophilic molecules, with log $K_d < -2$, so the expected hydrophilic ascending part of the solid curve in Fig. 7.22b is not fully shown. Nevertheless, the shape of the plot is very similar to that reported by Camenisch et al. [546], shown in Fig. 7.8c. The UWL in the latter study (stirred solutions) is estimated to be ~ 460 μm (Fig. 7.8b), whereas the corresponding value in unstirred 96-well microtiter late assay is about 2300 μm. For this reason, the high point in Fig. 7.22b is $\sim 16 \times 10^{-6}$ cm/s, whereas it is $\sim 70 \times 10^{-6}$ cm/s in Fig. 7.8c.

Kansy et al. [550] reported the permeability–lipophilicity relationship for about 120 molecules based on the 10% wt/vol egg lecithin plus 0.5% wt/vol cholesterol in dodecane membrane lipid (model 15.0 in Table 7.3), shown in Fig. 7.23. The vertical axis is proportional to *apparent* permeability [see Eq. (7.9)]. For log $K_d > 1.5$, P_a *decreases* with increasing log K_d. In terms of characteristic permeability–lipophilicity plots of Fig. 7.19, the Kansy result in Fig. 7.23 resembles the bilinear case in Fig. (7.19d). Some of the P_a values may be underestimated for the most lipophilic molecules because membrane retention was not considered in the analysis.

7.7.1.1 DOPC

The 2% DOPC in dodecane (model 1.0, Table 7.3) was the first PAMPA model explored by the *p*ION group [25–28,556–558]. The lipid is commercially available in a highly purified preparation (in flame-sealed ampules packed under nitrogen), and is most like that used in the original BLM experiments [516,518,519, 523,532,542]. The lipid is completely charge neutral. It shows relatively low membrane retention for most molecules in Table 7.5, with the exception of chlorpromazine, phenazopyridine, primaquine, and progesterone. Our experience has been that as long as $R < 90\%$, most drug molecules have sufficient UV absorptivity to be adequately characterized when the initial concentrations are ~ 50 μm (a typical concentration in high-throughput applications). Lipid systems based on 10% or higher lecithin content can show very high membrane retention, in some cases preventing the assessment of permeability by UV spectrophotometry.

A few molecules have unexpectedly low permeability in 2% DOPC, not consistent with their octanol–water partition coefficients. Notably, metoprolol has a P_e value ~ 10 times lower in 2% DOPC, compared to 10% egg lecithin. Also, prazosin P_e appears to be significantly lower in DOPC, compared to other lipids.

The quality of the data collected from 2% DOPC membranes is unmatched by any other system we have explored. It's not uncommon to see interplate reproducibility <5% and intraplate even better than that (1–3% SD). As will be seen later, lipid model 1.0 does not predict GIT absorption as well as some of the newer *p*ION models. However, this may not be the case when BBB models are explored in detail.

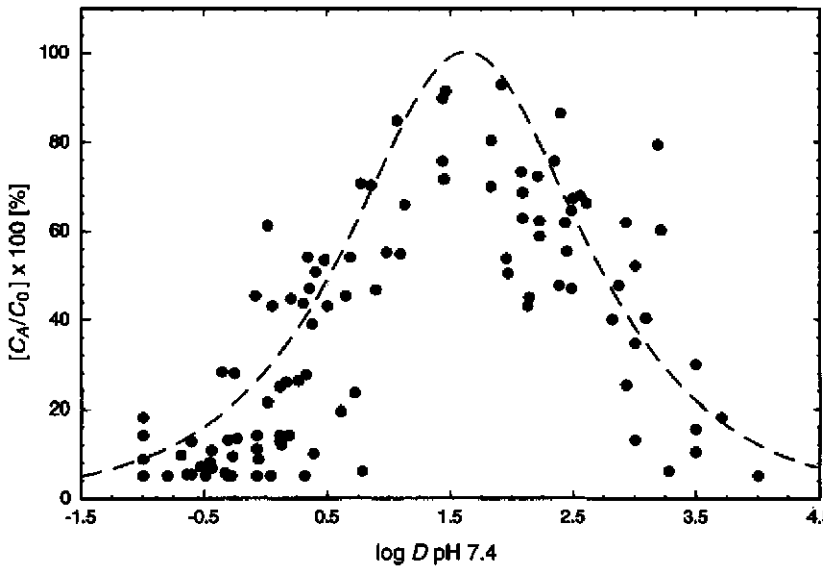

Figure 7.23 Relative acceptor compartment concentrations versus octanol–water apparent partition coefficients [550]. [Reprinted from Kansy, M.; Fischer, H.; Kratzat, K.; Senner, F.; Wagner, B.; Parrilla, I., in Testa, B.; van de Waterbeemd, H.; Folkers, G.; Guy, R. (Eds.). *Pharmacokinetic Optimization in Drug Research*, Verlag Helvetica Chimica Acta: Zürich and Wiley-VCH, Weinheim, 2001, pp. 447–464, with permission from Verlag Helvetica Chimica Acta AG.]

7.7.1.2 Olive Oil

Olive oil was the ''original'' model lipid for partition studies, and was used by Overton in his pioneering research [518,524]. It fell out of favor since the 1960s, over concerns about standardizing olive oil from different sources. At that time, octanol replaced olive oil as the standard for partition coefficient measurements. However, from time to time, literature articles on the use of olive oil appear. For example, Poulin et al. [264] were able to demonstrate that partition coefficients based on olive oil–water better predict the in vivo adipose-tissue distribution of drugs, compared to those from octanol–water. The correlation between in vivo log $K_{P\,(\text{adipose tissue–plasma})}$ and log $K_{P\,(\text{olive oil–water})}$ was 0.98 (r^2), compared to 0.11 (r^2) in the case of octanol. Adipose tissue is white fat, composed mostly of triglycerides. The improved predictive performance of olive oil may be due to its triglyceride content.

It was thus interesting for us to examine the permeability and membrane retention properties of olive oil. As Table 7.5 shows, most of the P_e values for olive oil are less than or equal to those of 2% DOPC, with notable exceptions; for instance, quinine is 4 times more permeable and progesterone is 16 times less permeable in olive oil than in DOPC. Both lipids show progesterone retention to be >80%, but quinine retention in olive oil is substantially greater than in DOPC.

7.7.1.3 Octanol

Octanol permeability is important to explore, since it is the principal basis for the lipophilicity scale in pharmaceutical research. Most interesting to us, in this light, is to address the question of ion pair partitioning and its meaning in the prediction of absorption of charged drugs. It has been discussed in the literature that quaternary ammonium drugs, when matched with lipophilic anions, show considerably increased octanol–water partition coefficients [291]. It has been hypothesized that with the right counterion, even charged drugs could be partly absorbed in the GIT. Given the structure of wet octanol, it could be argued that the 25 mol% water in octanol may be an environment that can support highly charged species, if lipophilic counterions are added. Unexpectedly high partition coefficients can be measured for ion pair forming drugs. But does this mean that ion pair transport takes place in vivo? This was addressed by the *p*ION group by comparing permeability coefficients derived from DOPC and octanol lipid membrane models. For molecules showing very low permeabilities in DOPC (model 1.0) and very high permeabilities in octanol-impregnated membranes (Model 3.0), one could hypothesize that the water clusters in wet octanol act like ''ion pair shuttles,'' an interesting effect, but perhaps with uncertain physiological interpretation [560].

Figure 7.22b shows that hydrophilic molecules, those with $\log K_d < 1$, are much more permeable in octanol than in olive oil. The same may be said in comparison to 2% DOPC and dodecane. Octanol appears to enhance the permeability of hydrophilic molecules, compared to that of DOPC, dodecane, and olive oil. This is dramatically evident in Fig. 7.7, and is confirmed in Figs. 7.8c and 7.22b. The mechanism is not precisely known, but it is reasonable to suspect a ''shuttle'' service may be provided by the water clusters in octanol-based PAMPA (perhaps like an inverted micelle equivalent of endocytosis). Thus, it appears that charged molecules can be substantially permeable in the octanol PAMPA. However, do charged molecules permeate phospholipid bilayers to any appreciable extent? We will return to this question later, and will cite evidence at least for a partial answer.

Membrane retention of lipophilic molecules is significantly increased in octanol, compared to 2% DOPC. Chlorpromazine and progesterone show $R >$ 90% in octanol. Phenazopyridine, verapamil, promethazine, and imipramine show $R > 70\%$.

7.7.1.4 Dodecane

Dodecane-coated filters were studied to determine what role hydrogen-bonding and electrostatic effects play in the 2% DOPC system. Measuring the differences between P_e deduced from 2% DOPC in dodecane and 0% DOPC in dodecane might indicate the extent of H-bonding and/or electrostatic interactions for specific probe molecules. Table 7.5 indicates that some molecules are retarded by the presence of DOPC (e.g., phenazopyridine, verapamil, metoprolol, theophylline, terbutaline, antipyrine), while most molecules are accelerated by DOPC (e.g., chlorpromazine, imipramine, diltiazem, prazosin, progesterone). The quantitative structure–permeability relationships for a much larger set of drug-like molecules are currently investigated in our laboratory (see Section 7.7.8).

It is also quite interesting that lipid model 4.0 may be used to obtain alkane partition coefficients at high-throughput speeds, as suggested by Faller and Wohnsland [509,554]. It is also interesting to note that since our P_e are corrected for membrane retention, the slope in Fig. 7.11 corresponding to the dashed line (our data) is 1.0, whereas the data not corrected for retention (solid line) show a lesser slope. This may not matter if the objective is to obtain alkane–water log K_p values at high speeds.

7.7.2 Membrane Retention (under Iso-pH and in the Absence of Sink Condition)

The membrane retention R is often stated as a mole percentage of the sample lost to the membrane. Its value can at times be very high, as high as 85% for chlorpromazine and 70% for phenazopyridine, with membranes made of 2% DOPC dissolved in dodecane. Regression analysis of log $\%R$ versus log $K_{d(7.4)}$, the octanol–water apparent partition coefficient, produces r^2 0.59. For DOPC-free dodecane, such analysis yields a higher r^2 (0.67). Olive oil and octanol further improve, with r^2 of 0.80 and 0.90, respectively. As far as $\%R$ representing lipophilicity as indicated by octanol–water partition coefficients is concerned, the order of ''octanol-likeness'' is octanol > olive oil > dodecane > DOPC in dodecane. Figure 7.24 shows the log $\%R$/log K_d plot for octanol-impregnated membranes, at pH 7.4. It's clear that retention is due to the lipophilicity of molecules.

Culture-cell assays are also subject to sample retention by the monolayer. Sawada et al. [574] studied the transport of chlorpromazine across MDCK cell

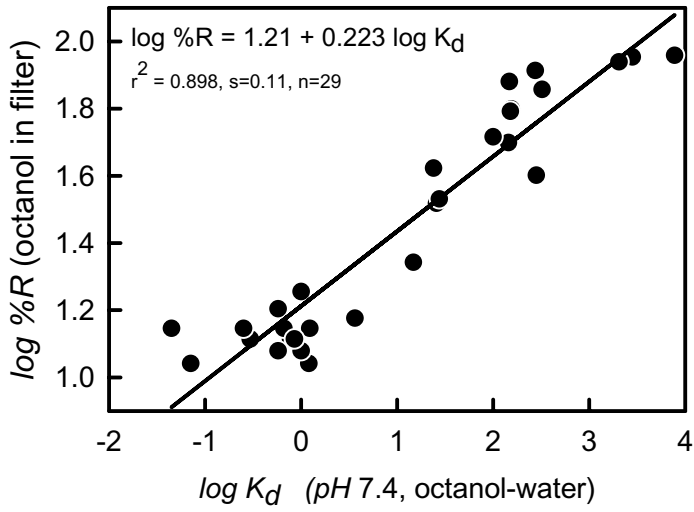

Figure 7.24 Membrane retention in octanol-soaked filters versus octanol–water apparent partition coefficients.

monolayers in the presence of various levels of serum proteins, and observed 65–85% retentions of the drug molecule by the MDCK cells. Wils et al. [591] reported retentions as high as 44% in Caco-2 cells. In a later publication, Sawada et al. [575] cited values as high as 89% for a homologous series of lipophilic molecules. Krishna et al. [551] more recently reported Caco-2 permeability results for lipophilic molecules, including progesterone and propranolol. They found retentions as high as 54%. It is undoubtedly a common phenomenon with research compounds, which are often very lipophilic. Yet in most reported assays, the effect is ignored, it appears. Ho et al. [514] derived an equation [similar to Eq. (7.22)] to describe the phenomenon in cultured cells, but its application in cultured-cell assays is scarce so far.

Retention may be a good predictor of the PK volume of distribution, of protein binding [264,592] or possibly even of conditions suitable for P-gp binding and extrusion of drugs. Apparently, these themes have not yet been adequately explored.

It is curious that the log of the expression for R, Eq. (7.18), produces a ''Kubinyi-like'' bilinear equation

$$\log R = \log K_d - \log(rK_d + 1) + \log r \tag{7.45}$$

where the oil–water volume ratio, $r = V_M/(V_A + V_D)$. Its form is essentially that of Eq. (7.44). When 2% DOPC in dodecane is used for the PAMPA membrane lipid, V_M could be taken as the volume of dodecane (4–6 μL) or the volume of DOPC

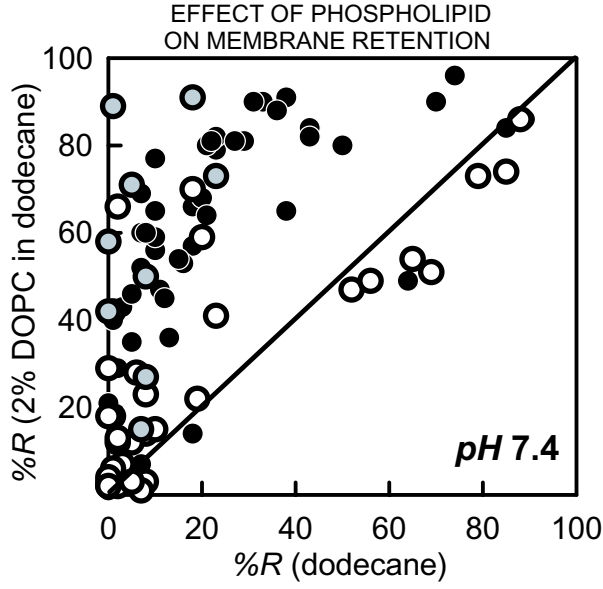

Figure 7.25 Membrane retention in 2%DOPC/dodecane-soaked filters versus dodecane-soaked filters.

(0.08–0.12 μL). The choice rests on the presumed structure of the membrane lipids (and where the drug preferentially partitions), which is not absolutely certain at present (see Section 7.3.6). It may be best to treat r as an empirical parameter, determined by regression against some lipophilicity model.

Figure 7.25 is a plot of $\%R$ (2%DOPC in dodecane) versus $\%R$ (100% dodecane). It shows that even 2% DOPC in dodecane can influence membrane retention to a considerable extent, compared to retentions observed in the absence of DOPC. Many molecules show retentions exceeding 70% in DOPC, under conditions where the retentions in dodecane are below 10%. However, it cannot be assumed that retention is always very low in dodecane, since several points in Fig. 7.25 are below the diagonal line, with values as high as 90% (chlorpromazine).

7.7.3 Two-Component Anionic Lipid Models with Sink Condition in the Acceptor Compartment

The use of simple single-component neutral lipids has played a valuable role in development of the PAMPA technique. Since it was an early objective of such work to predict GIT absorption, it became necessary to test the effect of phospholipid mixtures, where variable amounts of negative lipid could be introduced. Table 7.1 indicates that brush-border membrane (BBM) lipid mixture contains one negative phospholipid for every 3.5 zwitterionic lipids, and the blood–brain barrier (BBB) lipid has even a higher negative lipid content. The simplest model to simulate the BBM mixture could consist of two components: DOPC plus a negatively charged phospholipid: for example, phosphatidylserine, phosphatidylinositol, phosphatidylglycerol, phosphatidic acid, or cardiolipin (see Fig. 7.4). Even a fatty acid, such as dodecylcarboxylic acid (DA), could play the role of introducing negative charge to the mixture. Our design criterion was to begin with 2% DOPC and add the additional negatively charged lipid in the proportion consistent with BBM (0.6% added lipid) or BBB (1.1% added lipid) negative-zwitterionic proportions (Table 7.1).

Since there would be increased overall lipid concentration in the dodecane solution, we decided to create a sink condition in the acceptor wells, to lower the membrane retention. We discovered that the pH 7.4 buffer saturated with sodium laurel sulfate serves as an excellent artificial sink-forming medium. Since the new PAMPA membranes would possess substantial negative charge, the negatively charged micellar system was not expected to act as an aggressive detergent to the two-component artificial membrane infused in the microfilter.

Six two-component models were tested under sink conditions (models 5.1–10.1 in Table 7.3), employing three negatively charged lipids (dodecylcarboxylic acid, phosphatidic acid, and phosphatidylglycerol). These models were also tested in the absence of the sink condition (models 5.0–10.0 in Table 7.3).

Tables 7.6–7.8 list the P_e, SD, and $\%R$ of the 32 probe molecules in the thirteen new PAMPA lipid models, one of which is 2% DOPC assayed under sink conditions (model 1.1). The latter model served as a benchmark for assessing the effects of negative membrane charge.

TABLE 7.6 Two-Component Anionic Lipid PAMPA Models (with Sink), pH 7.4[a]

Sample	2%DOPC (Model 1.1) P_e(SD)	%R	+0.6%DA (Model 5.1) P_e(SD)	%R	+1.1%DA (Model 6.1) P_e(SD)	%R	+0.6%PA (Model 7.1) P_e(SD)	%R	+1.1%PA (Model 8.1) P_e(SD)	%R
Chlorpromazine	21.3 (0.3)	16	31.4 (1.2)	30	35.5 (6.7)	31	31.2 (0.5)	27	34.3 (7.2)	31
Phenazopyridine	31.4 (1.6)	26	27.0 (1.6)	30	23.9 (2.8)	31	23.2 (1.3)	36	21.6 (1.1)	42
Verapamil	37.4 (4.2)	17	40.8 (0.9)	29	25.1 (1.9)	25	24.9 (2.1)	21	34.6 (3.8)	31
Promethazine	31.5 (1.7)	12	44.4 (7.4)	24	28.5 (0.6)	24	40.1 (4.3)	18	37.3 (2.0)	20
Quinine	2.7 (0.1)	13	27.7 (2.5)	38	30.7 (3.2)	31	19.1 (1.3)	27	24.7 (2.0)	33
Imipramine	22.2 (0.7)	21	29.9 (0.8)	33	26.8 (0.6)	32	25.0 (0.6)	32	29.0 (1.2)	32
Diltiazem	33.9 (8.7)	13	35.4 (9.1)	12	31.9 (5.8)	16	29.4 (1.3)	16	31.4 (1.4)	20
Prazosin	—	—	13.3 (1.5)	17	10.1 (0.7)	14	4.2 (0.4)	17	16.2 (0.6)	17
Propranolol	14.3 (0.1)	16	39.2 (1.0)	28	27.3 (2.6)	30	29.9 (1.5)	29	36.2 (1.3)	27
Desipramine	25.1 (6.3)	22	33.9 (6.8)	38	26.7 (4.6)	42	22.8 (3.1)	32	40.0 (7.0)	33
Primaquine	1.4 (0.1)	10	22.8 (0.4)	23	22.9 (0.3)	25	18.5 (3.0)	27	22.7 (0.7)	27
Metoprolol	0.41 (0.03)	3	5.8 (0.4)	16	8.7 (0.5)	17	4.7 (0.8)	13	16.9 (1.1)	18
Ranitidine	0.01 (0.02)	0	0.01 (0.02)	3	0.02 (0.03)	4	(nd)	1	0.02 (0.02)	4
Amiloride	(nd)	1	1.6 (0.3)	8	4.7 (0.1)	13	0.01 (0.02)	2	(nd)	1

Ibuprofen	2.4 (0.1)	7	11.9 (4.3)	14	10.1 (2.4)	28	3.8 (0.5)	10	(nd)	27
Naproxen	0.3 (0.1)	1	0.7 (0.1)	4	1.8 (0.6)	6	0.8 (0.2)	1	0.9 (0.5)	2
Sulfasalazine	0.03 (0.05)	3	(nd)	2	0.04 (0.06)	1	(nd)	3	(nd)	2
Theophylline	—	—	0.2 (0.1)	3	0.4 (0.4)	4	0.04 (0.06)	4	0.4 (0.3)	3
Ketoprofen	0.2 (0.2)	2	0.6 (0.2)	6	0.6 (0.1)	4	0.3 (0.1)	2	0.3 (0.1)	4
Hydrochlorothiazide	0.001 (0.005)	1	0.001 (0.005)	2	(nd)	3	0.002 (0.005)	1	0.01 (0.01)	2
Furosemide	0.04 (0.01)	1	(nd)	3	0.06 (0.08)	5	(nd)	1	0.1 (0.1)	2
Piroxicam	2.0 (0.1)	3	3.3 (0.1)	5	3.5 (0.1)	6	2.3 (0.1)	4	2.6 (0.1)	4
Sulpiride	0.1 (0.2)	1	(nd)	3	0.5 (0.1)	3	(nd)	2	0.03 (0.07)	4
Terbutaline	0.1 (0.1)	0	(nd)	4	0.1 (0.2)	7	0.1 (0.2)	3	0.5 (0.6)	4
Progesterone	22.7 (1.1)	34	30.3 (3.3)	44	21.2 (0.6)	32	35.7 (0.5)	34	29.2 (2.0)	37
Griseofulvin	18.2 (1.0)	10	19.4 (0.3)	17	18.9 (1.9)	24	19.4 (1.3)	21	21.2 (1.5)	22
Carbamazepine	6.4 (0.2)	13	17.3 (0.3)	9	18.0 (1.4)	19	9.4 (1.0)	12	13.7 (0.6)	15
Antipyrine	0.6 (0.12)	4	0.6 (0.1)	5	1.0 (0.3)	6	0.7 (0.4)	6	0.6 (0.2)	3
Caffeine	1.2 (0.1)	4	1.3 (0.2)	5	1.4 (0.2)	6	1.3 (0.1)	4	1.5 (0.1)	3

[a] All P_e and SD(P_e) are in units of 10^{-6} cm/s; (nd) = compound not detected in the acceptor compartment.

TABLE 7.7 Two-Component Anionic Lipid PAMPA Models (Only PG with Sink), pH 7.4[a]

Sample	+0.6%PG (Model 9.1) P_e(SD)	%R	+1.1%PG (Model 10.1) P_e(SD)	%R	+0.6%PA (Model 7.0) P_e(SD)	%R
Chlorpromazine	16.2 (2.1)	51	5.1 (1.6)	73	1.3 (1.5)	80
Phenazopyridine	17.2 (1.2)	53	5.4 (0.4)	56	3.6 (0.1)	56
Verapamil	21.1 (3.3)	37	8.4 (0.7)	53	4.8 (1.7)	56
Promethazine	35.4 (1.3)	45	13.1 (2.2)	62	(nd)	63
Quinine	2.4 (0.2)	38	5.2 (1.4)	60	7.2 (0.7)	54
Imipramine	24.3 (2.9)	49	7.6 (0.1)	60	1.8 (1.0)	56
Diltiazem	18.2 (3.7)	36	8.9 (2.8)	55	14.8 (0.1)	50
Prazosin	1.0 (0.5)	39	1.0 (0.2)	53	4.9 (1.2)	16
Propranolol	8.0 (0.6)	50	3.4 (1.4)	66	2.7 (0.2)	47
Desipramine	9.0 (2.0)	56	0.4 (0.6)	66	3.4 (2.9)	72
Primaquine	1.1 (0.2)	43	0.2 (0.2)	59	2.0 (0.3)	43
Alprenolol	—	—	—	—	7.9 (2.8)	42
Metoprolol	(nd)	22	(nd)	42	6.0 (0.8)	10
Ranitidine	(nd)	1	(nd)	2	0.1 (0.1)	1
Amiloride	0.03 (0.03)	2	(nd)	5	(nd)	0
Ibuprofen	18.9 (1.3)	0	(nd)	24	(nd)	28
Naproxen	(nd)	2	(nd)	4	2.2 (0.8)	0
Sulfasalazine	(nd)	1	0.004 (0.007)	2	0.03 (0.05)	3
Theophylline	(nd)	2	(nd)	3	(nd)	0
Ketoprofen	0.36 (0.04)	1	0.03 (0.04)	9	1.1 (0.6)	1
Hydrochlorothiazide	0.007 (0.007)	1	(nd)	3	0.04 (0.01)	0
Furosemide	(nd)	0	0.05 (0.08)	3	(nd)	0
Piroxicam	2.0 (0.2)	2	2.0 (0.1)	3	2.3 (0.1)	1
Sulpiride	(nd)	1	0.4 (0.3)	4	—	—
Terbutaline	(nd)	2	(nd)	3	(nd)	1
Progesterone	35.2 (2.2)	46	33.2 (0.9)	42	1.6 (0.1)	55
Griseofulvin	18.5 (2.7)	20	17.7 (1.5)	21	18.3 (0.9)	25
Carbamazepine	8.5 (0.7)	11	9.7 (0.5)	13	10.4 (1.4)	10
Antipyrine	1.1 (0.4)	3	0.7 (0.2)	5	1.4 (0.4)	1
Caffeine	1.5 (0.1)	4	2.1 (0.1)	4	2.1 (0.1)	0

[a]All P_e and SD(P_e) are in units of 10^{-6} cm/s; (nd) = compound not detected in the acceptor compartment.

TABLE 7.8 Two-Component Anionic Lipid PAMPA Models (without Sink), pH 7.4[a]

Sample	+0.6% DA (Model 5.0) P_e(SD)	%R	+1.1% DA (Model 6.0) P_e(SD)	%R	+1.1% PA (Model 8.0) P_e(SD)	%R	+0.6% PG (Model 9.0) P_e(SD)	%R	+1.1% PG (Model 10.0) P_e(SD)	%R
Chlorpromazine	0.6 (0.1)	59	0.2 (0.2)	60	0.28 (0.03)	62	0.4 (0.2)	64	0.3 (0.1)	68
Phenazopyridine	4.6 (0.3)	47	5.1 (0.2)	48	2.8 (0.1)	52	3.7 (0.1)	41	2.9 (0.1)	49
Verapamil	2.9 (1.3)	53	4.6 (0.4)	58	1.4 (0.2)	58	0.7 (0.3)	57	0.6 (0.6)	68
Promethazine	0.8 (0.3)	61	1.5 (0.3)	68	0.01 (0.01)	62	0.9 (0.4)	59	0.6 (0.3)	69
Quinine	6.0 (0.6)	37	7.4 (0.2)	47	3.4 (0.5)	53	0.5 (0.1)	28	0.2 (0.2)	51
Imipramine	2.3 (0.3)	53	2.7 (0.2)	59	2.0 (0.2)	51	2.5 (0.2)	37	0.8 (0.1)	46
Diltiazem	7.7 (0.3)	35	8.1 (1.0)	38	5.1 (0.4)	48	1.2 (0.2)	49	0.3 (0.4)	62
Prazosin	6.2 (0.4)	15	7.7 (0.5)	17	5.6 (1.3)	19	0.04 (0.01)	15	(nd)	36
Propranolol	4.6 (0.2)	47	6.9 (0.5)	57	1.9 (0.1)	50	0.9 (0.1)	34	0.4 (0.1)	53
Desipramine	2.8 (0.5)	54	2.1 (0.7)	61	1.2 (0.1)	55	2.3 (0.4)	40	1.6 (0.2)	58
Primaquine	7.7 (0.3)	45	5.2 (0.6)	48	1.4 (0.2)	48	(nd)	39	0.4 (0.2)	51
Alprenolol	7.8 (0.3)	34	7.9 (0.6)	40	4.1 (0.8)	46	2.2 (2.0)	33	1.2 (0.1)	51
Metoprolol	5.2 (0.3)	13	10.0 (0.8)	10	4.7 (0.5)	15	0.3 (0.4)	14	0.05 (0.09)	22
Ranitidine	0.12 (0.01)	3	0.3 (0.1)	8	0.08 (0.05)	2	0.02 (0.03)	0	(nd)	0
Amiloride	4.5 (0.5)	10	6.9 (0.1)	12	(nd)	1	(nd)	0	(nd)	0

TABLE 7.8 (*Continued*)

Sample	+0.6% DA (Model 5.0) P_e(SD)	%R	+1.1% DA (Model 6.0) P_e(SD)	%R	+1.1% PA (Model 8.0) P_e(SD)	%R	+0.6% PG (Model 9.0) P_e(SD)	%R	+1.1% PG (Model 10.0) P_e(SD)	%R
Ibuprofen	5.0 (5.4)	8	19.1 (3.3)	14	7.6 (2.3)	2	0.5 (0.8)	0	—	—
Naproxen	2.0 (0.2)	2	2.8 (0.2)	6	0.3 (0.2)	16	0.4 (0.2)	0	—	—
Theophylline	(nd)	4	0.8 (0.3)	7	(nd)	3	(nd)	0	(nd)	0
Ketoprofen	0.75 (0.09)	1	0.93 (0.08)	5	0.7 (0.1)	1	0.3 (0.1)	0	0.3 (0.1)	0
Hydrochlorothiazide	0.02 (0.02)	2	0.04 (0.04)	4	0.008 (0.007)	1	0.03 (0.01)	0	(nd)	1
Furosemide	0.04 (0.03)	2	0.05 (0.02)	7	0.01 (0.02)	1	0.03 (0.02)	0	0.03 (0.01)	0
Piroxicam	3.3 (0.1)	3	3.3 (0.1)	8	2.5 (0.1)	2	1.8 (0.1)	0	1.5 (0.1)	0
Sulpiride	0.3 (0.5)	3	0.7 (0.2)	7	0.06 (0.08)	2	0.1 (0.1)	0	0.2 (0.1)	0
Terbutaline	(nd)	4	0.1 (0.2)	10	0.02 (0.04)	1	0.06 (0.06)	0	0.02 (0.04)	1
Progesterone	2.3 (0.5)	57	3.0 (0.3)	64	3.5 (0.3)	61	3.9 (0.8)	66	3.5 (1.0)	66
Griseofulvin	8.5 (0.1)	20	9.0 (0.2)	18	7.2 (1.6)	29	6.9 (0.6)	20	8.1 (0.3)	24
Carbamazepine	11.7 (0.8)	9	13.5 (1.4)	11	8.0 (0.4)	10	5.9 (0.1)	4	5.6 (0.4)	6
Antipyrine	1.0 (0.1)	2	1.3 (0.1)	7	1.1 (0.2)	6	1.3 (0.2)	1	1.0 (0.1)	3
Caffeine	1.7 (0.1)	2	1.9 (0.1)	8	1.7 (0.2)	4	1.9 (0.1)	0	1.6 (0.2)	0

[a]All P_e and SD(P_e) are in units of 10^{-6} cm/s; (nd) = compound not detected in the acceptor compartment.

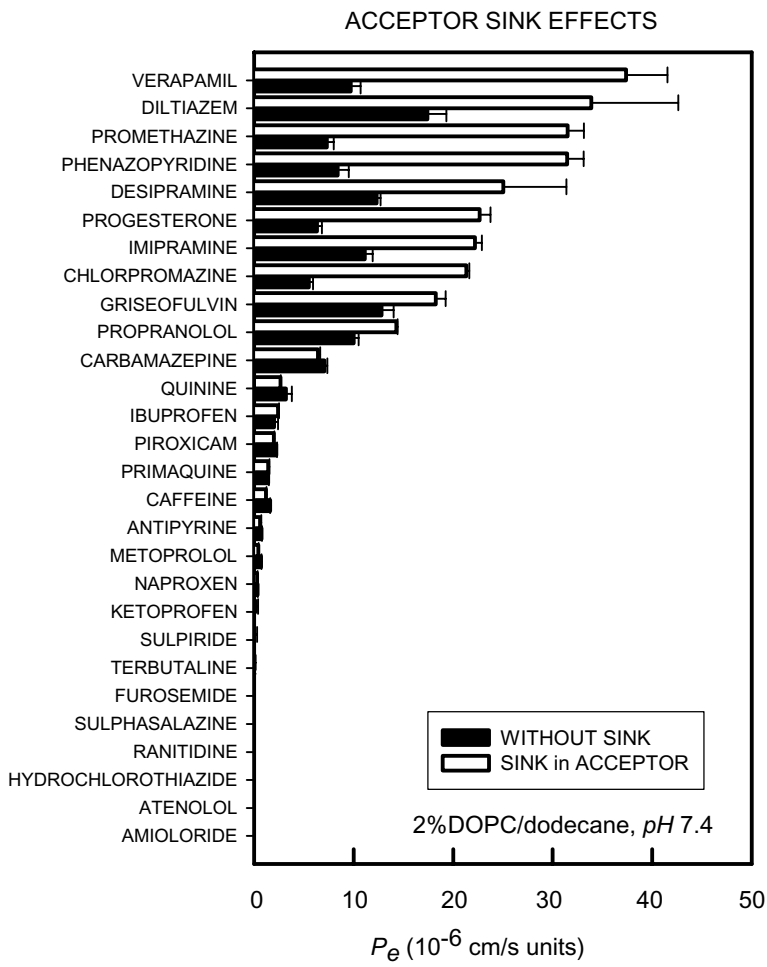

Figure 7.26 Permeabilities with and without sink, 2% DOPC model.

7.7.3.1 DOPC under Sink Conditions

Figure 7.26 shows the effect of the sink condition on the effective permeabilities in the 2% DOPC system (model 1.1). Just about all of the lipophilic bases showed a two- to three-fold increase in P_e. The simplest interpretation of this is that when lipophilic molecules reach the acceptor wells, they are bound to the surfactant, and the concentration of the unbound (membrane-permeating) form of the drug greatly diminishes. Hence, the reverse flux, based on the unbound portion of the concentration $C_A(t)$ in Eq. (7.1), is nil. Thus, half of the UWL resistance effectively disappears, leading to a doubling of P_e for the diffusion-limited molecules. The topic of the UWL is discussed in greater detail in Section 7.7.6. The binding of the positively charged lipophilic molecules by the negatively charged micelles is

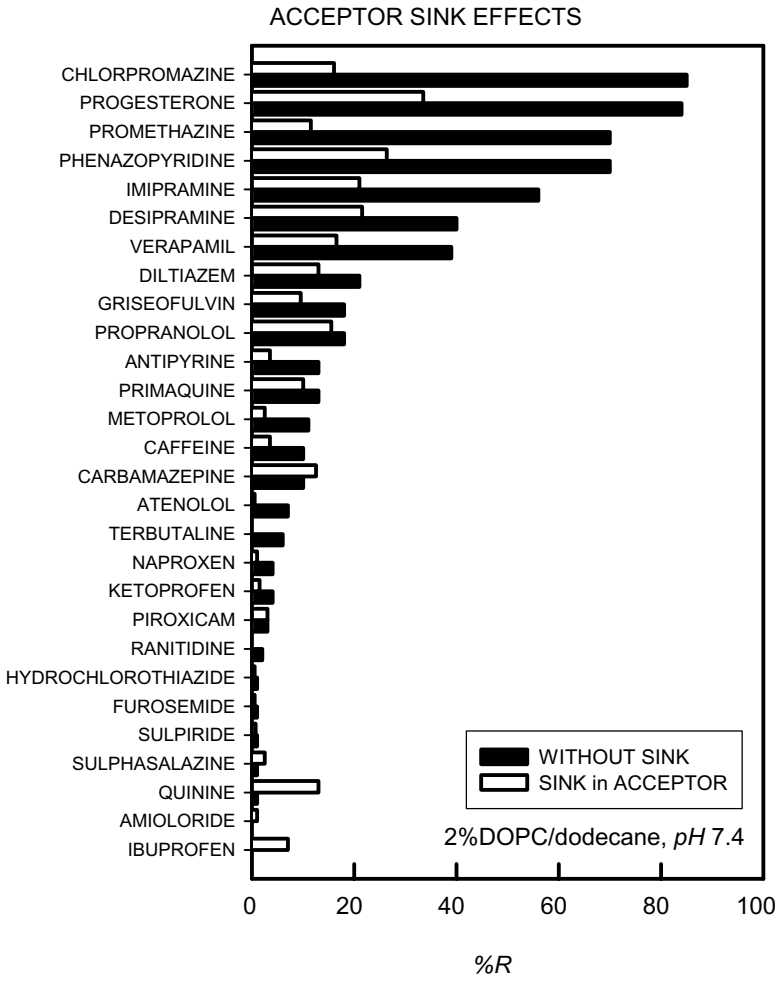

Figure 7.27 Membrane retentions with and without sink, 2% DOPC model.

expected to have a strong electrostatic component, as well as a hydrophobic component.

Furthermore, the membrane retentions of the lipophilic probe molecules are dramatically decreased in the presence of the sink condition in the acceptor wells, as shown in Fig. 7.27. All molecules show $R < 35\%$, with progesterone and phenazopyridine showing the highest values, 34% and 26%, respectively.

The combination of increased P_e and decreased $\%R$ allowed the permeation time to be lowered to 4 h, in comparison to the originally specified time of 15 h [547,550], a considerable improvement for high-throughput applications. The quality of the measurements of the low-permeability molecules did not substantially improve with sink conditions or the reduced assay times.

7.7.3.2 DOPC with Dodecylcarboxylic Acid under Sink Conditions

The free fatty acid model 5.1 shows dramatic differences in permeabilities over the neutral-charge model 1.1. For example, quinine, metoprolol, and primaquine are 10, 14, and 16 times more permeable, respectively, in the charged (0.6% wt/vol in dodecane) lipid system. The most remarkable enhancement is that of amiloride. In the DOPC system, no detectable amount of amiloride permeates; however, P_e is 1.6×10^{-6}cm/s when 0.6% DA is added to the dodecane. It is thought that a very strong ion-pair complex forms between the positively-charged amiloride (Fig. 7.21) and the negative-charge dodecylcarboxylate group, through strong electrostatic and hydrogen bonding, perhaps forming an eight-membered ring $-(-C{=}N^{+}-H \cdots {}^{-}O-C{=}O \cdots H-N-)-$. Uncharged carboxylic acids are known to form dimeric units of a similar sort when dissolved in oil [538].

The increase of negative charge from 0.6% to 1.1% wt/vol in dodecane (modeling the expected increase between BBM and BBB lipid compositions; see Table 7.1) shows further increases to the permeabilities of the dramatically affected molecules, especially amiloride, which becomes effectively more permeable than piroxicam.

Most of the weak-acid probe molecules (ibuprofen, naproxen, ketoprofen, piroxicam) show significant increase in permeabilities with models 5.1 and 6.1, compared to model 1.1. This is surprising, considering that most of the weak-acid probes are negatively charged themselves, and would be expected to be less permeable, due to electrostatic repulsions. Apparently, the increased membrane–water partitioning of weak acids in the two-component lipid models overcomes the expected negative charge repulsions between the ionized acids and the charged membrane components, and leads to increased permeability. Also, membrane surface negative charge is expected to lower the surface pH, thus increasing interfacial f_u (Table 7.4), leading to higher permeabilities of ionizable acids [457].

7.7.3.3 DOPC with Phosphatidic Acid under Sink Conditions

The PA systems (models 6.1 and 7.1) seem to show some of the general patterns of changes seen above, but to a lesser extent. Amiloride permeates in its usual way (poorly). The weak-acid probes are more permeable in the PA models, compared to neutral DOPC, but to a lesser extent than in DA. As a predictor of GIT absorption, the phosphatidic acid system appears to be the best. (The rankings of all the investigated lipid systems are discussed in Section 7.8.3.) Figure 7.28a shows the effect of PA on the permeabilities of the weak-base probe molecules. Dramatic and systematic increases are seen in all the membrane-limited permeabilities (left side of the bar graph). When the permeabilities reach the UWL limit of model 1.1, then no substantial effects due to increasing amounts of PA are seen (right side of the bar graph). So, most of the charged bases are elevated to be nearly diffusion-limited in their permeabilities, when PA is part of the membrane constituents.

Figure 7.28b shows that membrane retention is very systematically increased for almost all of the weak bases. This is a general pattern for bases with any of the negatively charged membrane models, and is probably best explained by the increased electrostatic attractions between the drugs and the membranes. Still, all retentions are below 50%, due to the offsetting sink condition created in the acceptor wells.

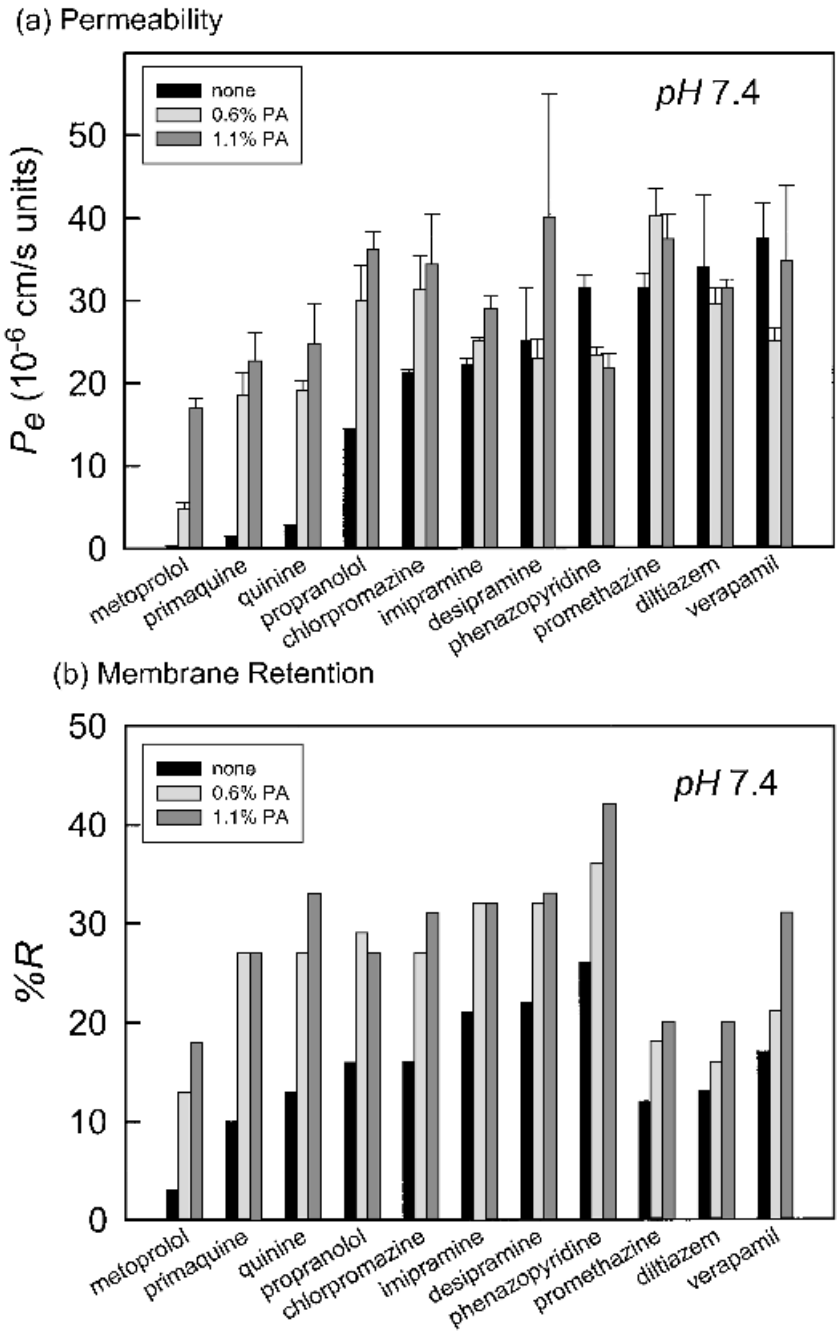

Figure 7.28 (a) Permeability (with 2% DOPC +0.0 − 1.1% PA/sink in acceptor) and (b) membrane retentions as a function of phosphatidic acid in 2% DOPC/dodecane lipid membranes at pH 7.4 for a series of weak bases.

7.7.3.4 DOPC with Phosphatidylglycerol under Sink Conditions

The PG models 9.1 and 10.1 show similar trends as indicated by PA, but the effects are somewhat muted. The increase in PG from 0.6% to 1.1% causes the permeabilities of weak bases to decrease and membrane retentions to increase, with many bases showing $R > 60\%$. Many molecules were not detected in the acceptor compartments by UV spectrophotometry after 4 h permeation times (Table 7.7). These properties of the PG system make it less attractive for high-throughput applications than the other two-component models.

7.7.3.5 DOPC with Negative Lipids without Sink

The two-component lipid models were also characterized in the absence of sink conditions (Table 7.8). Comparisons between models 7.0 (Table 7.7) and 1.0 (Table 7.5) suggest that negative charge in the absence of sink causes the permeabilities of many of the bases to decrease. Exceptions are quinine, prazosin, primaquine, ranitidine, and especially metoprolol. The inclusion of 0.6% PA causes P_e of metoprolol to increase nearly 10-fold, to a value twice that of propranolol, a more lipophilic molecule than metoprolol (based on the octanol-water scale). Naproxen and ketoprofen become notably more permeable in the two-component system. Surprisingly, the neutral progesterone becomes significantly less permeable in this system.

With the noted exceptions above, the other negative-lipid combinations (Table 7.8) show consistently lower permeabilities compared to neutral DOPC. Surprisingly, the retentions are not concomitantly higher than in the neutral DOPC lipid.

7.7.4 Five-Component Anionic Lipid Model (Chugai Model)

The interesting five-component BBM model (11.0 in Table 7.3) proposed by Sugano et al. [561,562] was tested by us (Table 7.9). A small modification was made to the original composition: 1,7-octadiene was replaced by dodecane, due to safety concerns over the use of the octadiene in an unprotected laboratory setting [561]. The permeabilities in the dodecane-modified Chugai model were considerably lower than those shown in *p*ION model 1.0 (and those reported by Sugano's group). This may be due to the lessened ''fluidity'' of the membrane mixture when the octadiene is replaced by dodecane. Retention is quite considerable in the modified Chugai model, with chlorpromazine and progesterone showing R 95% and 87%, respectively. As discussed later, the Sugano model actually has a good GIT absorption prediction property, about as good as that of model 7.1 (which contains only two lipid components).

The Chugai model was unstable in the presence of a sink-forming surfactant in the acceptor wells, and no further efforts were devoted to the untenable model 11.1. The 1% wt/vol cholesterol in dodecane may have interacted with the sink-forming micelles.

TABLE 7.9 Five-Component Anionic Lipid PAMPA Model (without Sink), pH 7.4[a]

Sample	2%DOPC (Model 1.0) P_e(SD)	%R	2%DOPC +0.5% Cho (Model 1A.0) P_e(SD)	%R	Sugano[b] (Model 11.0) P_e(SD)	%R
Chlorpromazine	5.5 (0.4)	85	6.4 (1.0)	93	6.3 (0.2)	95
Phenazopyridine	8.4 (1.1)	70	7.9 (0.1)	71	6.9 (0.1)	79
Verapamil	9.7 (1.0)	39	7.6 (0.1)	31	6.3 (1.2)	46
Promethazine	7.3 (0.7)	70	6.8 (0.1)	70	6.7 (0.3)	76
Quinine	3.1 (0.6)	1	5.1 (0.1)	10	6.4 (0.1)	22
Imipramine	11.1 (0.8)	56	7.4 (0.1)	53	7.4 (0.2)	64
Diltiazem	17.4 (1.8)	21	7.6 (0.3)	17	7.4 (0.6)	31
Prazosin	0.4 (0.1)	15	3.6 (0.1)	9	5.4 (0.4)	33
Propranolol	10.0 (0.5)	18	6.9 (0.1)	18	7.2 (0.1)	34
Desipramine	12.3 (0.4)	40	7.5 (0.1)	39	7.1 (0.8)	55
Primaquine	1.4 (0.1)	70	5.0 (0.2)	18	6.5 (0.1)	28
Alprenolol	11.8 (0.3)	16	—	—	—	—
Metoprolol	0.69 (0.04)	11	2.0 (0.7)	7	3.8 (0.1)	17
Ranitidine	0.009 (0.004)	2	0.04 (0.01)	0	(nd)	2
Amiloride	0.002 (0.005)	0	(nd)	0	(nd)	0
Ibuprofen	2.7 (0.5)	38	4.8 (1.6)	27	9.8 (2.3)	43
Acetaminophen	0.001 (0.005)	1	—	—	—	—
Naproxen	0.33 (0.03)	4	0.7 (0.1)	2	0.85 (0.01)	2
Sulfasalazine	0.007 (0.004)	1	(nd)	3	(nd)	0
Theophylline	0.04 (0.01)	1	0.18 (0.05)	2	0.28 (0.02)	1
Ketoprofen	0.05 (0.01)	4	0.16 (0.04)	3	0.19 (0.02)	1
Hydrochlorothiazide	0.01 (0.01)	1	(nd)	1	(nd)	0
Furosemide	0.02 (0.01)	1	0.002 (0.005)	0	(nd)	1
Salicyclic acid	0.006 (0.004)	1	—	—	—	—
Piroxicam	2.2 (0.1)	3	2.5 (0.1)	2	2.8 (0.1)	3
Sulpiride	0.01 (0.01)	1	0.01 (0.01)	2	(nd)	1
Terbutaline	0.04 (0.01)	6	0.02 (0.03)	2	(nd)	5
Progesterone	6.3 (0.5)	84	6.2 (0.2)	87	5.5 (0.3)	87
Griseofulvin	12.8 (1.2)	18	7.5 (0.1)	20	7.6 (0.1)	16
Carbamazepine	7.1 (0.3)	10	6.4 (0.1)	6	6.8 (0.3)	7
Antipyrine	0.73 (0.05)	13	0.8 (0.1)	5	0.91 (0.08)	7
Caffeine	1.6 (0.1)	2	1.6 (0.1)	2	1.6 (0.1)	3

[a]All P_e and SD(P_e) are in units of 10^{-6} cm/s; (nd) = compound not detected in the acceptor compartment.
[b]Five-lipid formula as reported by Sugano, except 1,7-octadiene was substituted with dodecane.

DOPC (model 1.0) and DOPC + 0.5% cholesterol (model 1A.0) results are listed in Table 7.9 for comparison with the Chugai model. It is quite surprising that the complex mixture of components in the Chugai model is very closely approximated by the cholesterol-DOPC system (model 1A.0), as shown in Fig. 7.29.

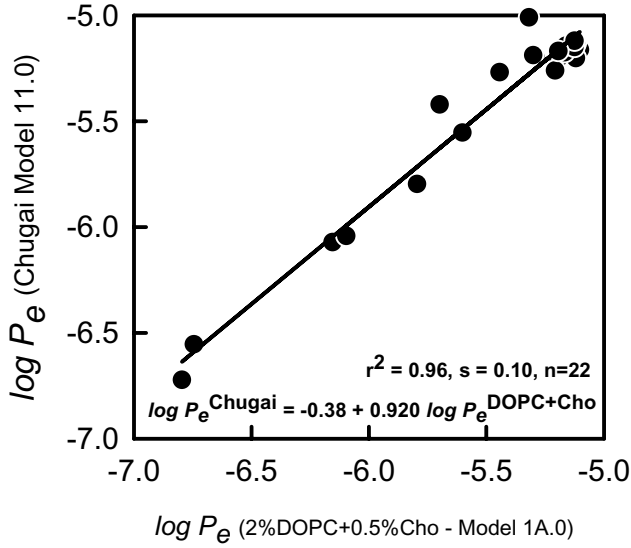

Figure 7.29 Modified Chugai model compared to 2% DOPC + 0.5% cholesterol model.

7.7.5 Lipid Models Based on Lecithin Extracts from Egg and Soy

Hydrogen bonding and electrostatic interactions between the sample molecules and the phospholipid bilayer membranes are thought to play a key role in the transport of such solute molecules. When dilute 2% phospholipid in alkane is used in the artificial membrane [25,556], the effect of hydrogen bonding and electrostatic effects may be underestimated. We thus explored the effects of higher phospholipid content in alkane solutions. Egg and soy lecithins were selected for this purpose, since multicomponent mixtures such as model 11.0 are very costly, even at levels of 2% wt/vol in dodecane. The costs of components in 74% wt/vol (see below) levels would have been prohibitive.

7.7.5.1 Egg Lecithin from Different Sources

Egg lecithins from two sources were considered: Avanti Polar Lipids (Alabaster, AL) and Sigma-Aldrich (St. Louis, MO). The ''60% lecithin total extract'' grade from Avanti and the ''60% lecithin'' grade from Sigma-Aldrich were tested. Apparently, different procedures are used to extract the lipids from egg yolk, since the permeability properties of the lecithins from the two sources are significantly different. The Avanti catalog identifies their procedure as a chloroform–methanol extraction. The extract is partitioned against deionized water, and the chloroform phase is concentrated. This extraction procedure is expected to remove proteins and polar (e.g., phenolic) substituents. The Avanti principal lipid components are listed in Table 7.1. The Sigma-Aldrich composition was not available.

TABLE 7.10 Egg Lecithin 10% wt/vol in Dodecane PAMPA Models, pH 7.4[a]

Sample	Avanti (Model 12.0), No Sink P_e(SD)	%R	Avanti (Model 12.1), Sink P_e(SD)	%R	Avanti +0.5%Cho (Model 13.0) No Sink P_e(SD)	%R
Chlorpromazine	—	—	—	—	1.5 (0.1)	83
Phenazopyridine	6.1 (0.4)	91	20.3 (2.9)	44	3.0 (0.5)	84
Verapamil	10.7 (3.0)	73	23.4 (1.1)	20	5.8 (0.5)	58
Promethazine	2.5 (0.5)	85	31.2 (1.2)	17	1.9 (0.8)	82
Quinine	9.2 (2.5)	61	9.9 (4.5)	31	7.3 (0.6)	48
Imipramine	7.0 (1.5)	83	31.8 (4.7)	23	4.0 (0.7)	76
Diltiazem	11.1 (1.5)	50	27.6 (2.5)	12	9.7 (0.8)	46
Prazosin	8.8 (3.2)	28	3.8 (0.5)	20	—	—
Propranolol	5.7 (1.1)	73	16.1 (3.5)	24	5.2 (0.4)	64
Desipramine	5.5 (0.8)	89	21.8 (2.1)	30	7.8 (0.9)	61
Primaquine	—	—	—	—	5.7 (1.8)	62
Alprenolol	12.5 (6.3)	65	23.1 (3.7)	27	—	—
Metoprolol	17.8 (9.7)	71	23.4 (4.9)	19	6.6 (0.5)	18
Ranitidine	0.2 (0.1)	8	0.2 (0.2)	7	0.3 (0.1)	8
Amiloride	0.006 (0.005)	15	(nd)	7	0.03 (0.03)	11
Ibuprofen	7.8	58	10.3 (2.4)	16	4.9 (0.2)	14
Acetaminophen	0.9 (0.3)	0	(nd)	3	—	—
Naproxen	1.4 (0.1)	12	0.9 (0.1)	4	1.6 (0.1)	2
Sulfasalazine	0.002 (0.003)	2	0.01 (0.02)	3	0.003 (0.005)	4
Theophylline	0.3 (0.1)	6	0.4 (0.1)	5	—	—
Ketoprofen	0.5 (0.1)	12	0.6 (0.1)	1	0.5 (0.1)	5
Hydrochlorothiazide	0.01 (0.01)	24	0.1 (0.1)	4	0.005 (0.005)	4
Furosemide	0.01 (0.01)	19	0.06 (0.05)	4	0.03 (0.01)	8
Salicyclic acid	0.04 (0.03)	15	0.9 (0.8)	3	—	—
Piroxicam	2.6 (0.2)	15	2.7 (0.2)	6	2.5 (0.1)	7
Sulpiride	0.2 (0.1)	5	0.04 (0.07)	5	0.17 (0.03)	2
Terbutaline	0.2 (0.1)	11	0.1 (0.2)	6	(nd)	3
Progesterone	2.8 (0.8)	93	29.8 (2.8)	22	2.6 (0.5)	82
Griseofulvin	10.5 (0.5)	42	19.0 (0.5)	15	11.4 (0.6)	18
Carbamazepine	8.6 (0.2)	19	10.7 (0.5)	19	10.8 (1.6)	16
Antipyrine	1.3 (0.1)	27	1.9 (0.5)	3	1.4 (0.1)	5
Caffeine	1.9 (0.1)	6	2.2 (0.3)	5	2.1 (0.4)	8

[a]All P_e and SD(P_e) are in units of 10^{-6} cm/s; (nd) = compound not detected in the acceptor compartment.

Kansy et al. [547,550] used 10% wt/vol egg lecithin in dodecane. Cholesterol was added as well. We also chose to use 10% egg lecithin (“60% grade”) in our laboratory. Tables 7.10 and 7.11 list the results of the various 10% egg lecithin models tested at *p*ION. Some of the models were used in conjunction with a sink

TABLE 7.11 Egg Lecithin 10% wt/vol in Dodecane PAMPA Models, pH 7.4[a]

Sample	Sigma (Model 14.0), No Sink P_e(SD)	%R	Sigma (Model 14.1), Sink P_e(SD)	%R	Sigma +0.5%Cho (Model 15.0), No Sink P_e(SD)	%R	Sigma +0.5%Cho (Model 15.1), Sink P_e(SD)	%R
Chlorpromazine	1.2	84	31.9 (6.1)	41	0.7 (0.3)	86	32.1 (8.6)	31
Phenazopyridine	2.7 (0.1)	84	17.4 (1.5)	55	3.1 (0.3)	86	18.8 (1.7)	50
Verapamil	3.1 (0.5)	69	25.4 (5.8)	33	1.8 (1.2)	83	28.4 (3.1)	23
Promethazine	2.2 (0.3)	84	35.3 (0.5)	35	1.3 (0.4)	89	36.4 (3.5)	22
Quinine	4.6 (0.7)	52	9.6 (0.5)	48	4.0 (0.7)	59	12.8 (0.6)	39
Imipramine	2.5	74	34.3 (1.0)	40	3.8 (0.3)	75	35.3 (6.3)	34
Diltiazem	7.1 (3.0)	50	31.3 (4.9)	18	3.8 (0.2)	64	33.2 (3.8)	8
Prazosin	5.3 (0.5)	34	11.8 (0.3)	21	4.4 (0.4)	38	16.9 (1.1)	16
Propranolol	4.1 (1.6)	65	21.2 (0.8)	43	3.5 (0.3)	70	22.3 (0.5)	34
Desipramine	3.9 (0.7)	78	24.3 (7.5)	49	2.7 (0.3)	80	29.2 (8.6)	30
Primaquine	4.4 (0.7)	65	22.8 (1.2)	36	4.4 (0.8)	81	30.0 (0.9)	26
Alprenolol	—	—	—	—	5.5 (0.2)	65	—	—
Metoprolol	4.0	26	4.3 (0.4)	22	3.7 (0.1)	26	8.0 (0.9)	12
Ranitidine	0.3	2	(nd)	9	0.1 (0.1)	7	(nd)	11
Amiloride	(nd)	5	(nd)	4	0.02 (0.03)	3	(nd)	3
Ibuprofen	(nd)	47	(nd)	—	6.9 (3.9)	31	(nd)	—
Acetaminophen	—	—	—	—	—	—	—	—
Naproxen	1.3	6	(nd)	6	1.0 (0.1)	6	1.3 (0.6)	3
Sulfasalazine	0.05	4	(nd)	4	—	—	0.04 (0.06)	2
Theophylline	0.2	11	(nd)	6	0.3 (0.1)	4	0.2 (0.2)	7
Ketoprofen	0.3 (0.1)	8	0.1 (0.1)	—	0.3 (0.1)	5	0.4 (0.1)	2
Hydrochlorothiazide	(nd)	5	(nd)	1	0.006 (0.005)	4	(nd)	3
Furosemide	(nd)	5	(nd)	4	0.01 (0.01)	4	0.09 (0.04)	2
Salicyclic acid	—	—	—	—	—	—	—	—
Piroxicam	2.1 (0.1)	8	2.2 (0.1)	6	2.0 (0.1)	6	2.2 (0.1)	4
Sulpiride	(nd)	9	(nd)	3	0.1 (0.1)	5	(nd)	3
Terbutaline	(nd)	5	(nd)	3	0.06 (0.01)	0	(nd)	2
Progesterone	5.2 (0.6)	80	42.3 (2.7)	31	4.0 (0.7)	88	37.9 (3.2)	33
Griseofulvin	9.7 (2.1)	46	21.4 (1.4)	25	5.1 (0.6)	41	21.7 (0.3)	21
Carbamazepine	9.1 (1.4)	20	13.8 (12.1)	20	5.1 (0.2)	23	15.7 (2.2)	19
Antipyrine	1.4 (0.1)	7	0.9 (0.2)	5	1.1 (0.2)	4	1.4 (0.3)	3
Caffeine	2.3 (0.4)	9	2.0 (0.1)	7	2.3 (0.1)	7	2.0 (0.2)	4

[a]All P_e and SD(P_e) are in units of 10^{-6} cm/s; (nd) = compound not detected in the acceptor compartment.

condition in the acceptor wells. Figure 7.30 shows permeability and membrane retention results for weak-base probes, using the Sigma-Aldrich source of lecithin, with and without sink and 0.5% wt/vol cholesterol. The presence of a sink dramatically increases permeabilities, as indicated in Figure 7.30a. In some cases, further significant increases in permeability were realized by the use of cholesterol, even though its amount was only 0.5%. Only in the diffusion-limited cases (right side of Fig. 7.30a) was there only minimal enhancement due to cholesterol.

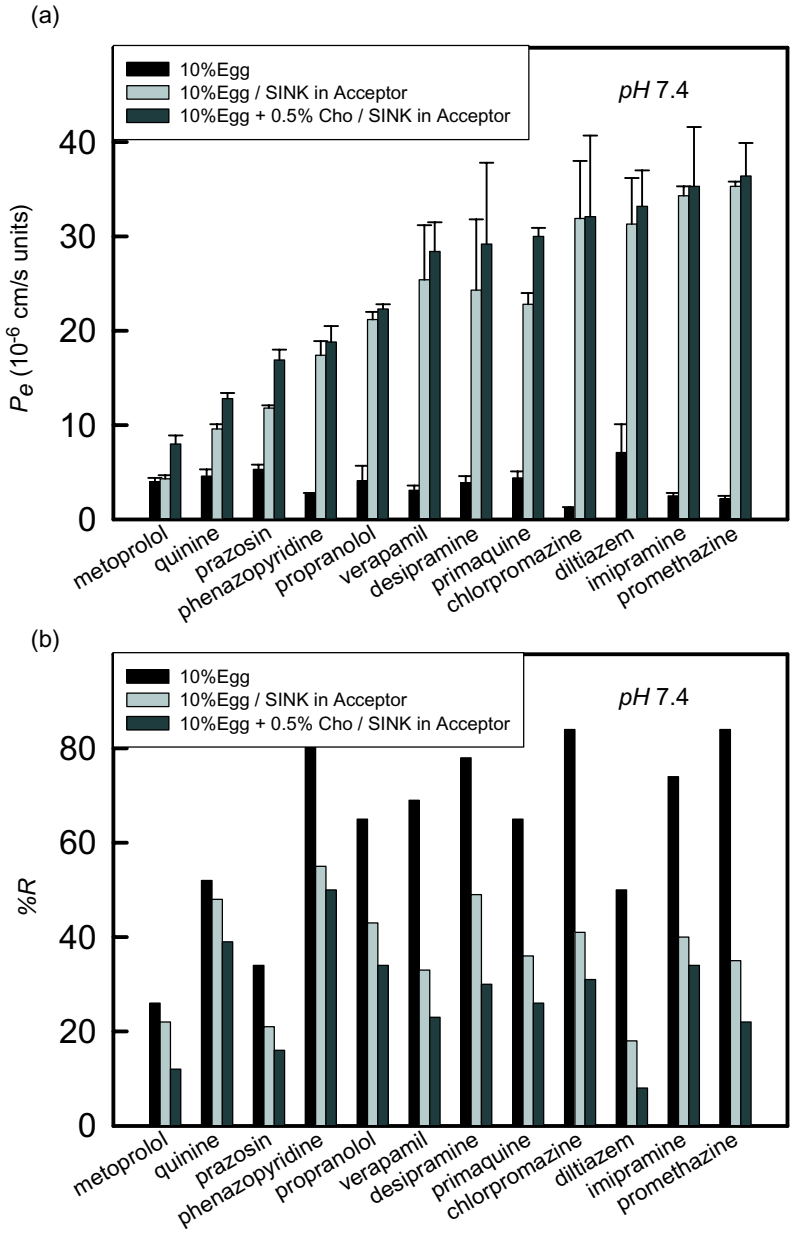

Figure 7.30 (a) Permeabilities [for egg lecithin (Sigma) in dodecane] and (b) membrane retentions for a series of weak bases in various egg lecithin PAMPA models.

Without an artificial sink, the membrane retentions are very high, with many basic probe molecules showing $R > 80\%$. With the imposed sink, many of the retentions dropped by as much as 50%. Furthermore, just 0.5% wt/vol cholesterol in dodecane (in addition to the sink) caused increased retention to drop by at least a further 10–30%. It was not possible to form stable cholesterol-containing lipid models under sink conditions with Avanti's egg lecithin; acceptor buffer solutions turned significantly turbid in the untenable model 13.1.

The peculiar depression of metoprolol and quinine permeabilities in 2% DOPC (model 1.0) was not seen in the egg lecithin models. Metoprolol and quinine were significantly more permeable in the lecithins, in line with expectations based on relative octanol–water lipophilicities and relative in vivo absorptions of β-blockers [593].

7.7.5.2 Soy Lecithin and the Effects of Phospholipid Concentrations

We explored the use of Avanti's "20% lecithin soy lipid extract," dissolved at various concentrations in dodecane. This is not a highly purified grade, and contains 37% unspecified neutral lipids, most likely asymmetric triglycerides. We chose this grade because it contained negatively charged phospholipids, having a charged : zwitterionic lipid ratio about half way between that of BBM and BBB compositions (Table 7.1). Soy-based PAMPA lipid models have been prepared with ("20% extract" grade) soy lecithin, 10–74% wt/vol in dodecane. These newly formulated lipids have net negative charge at pH 7.4, which further increases above pH 8, as the phosphatidic groups ionize (cf. ionization constants in Fig. 7.4). The inositol (predominant negatively charged lipid) content is 4 times higher in soy than in egg lecithin. However, when $\leq$74% phospholipid fractions are used, severe experimental problems arise. With lipophilic sample molecules, the use of concentrated phospholipid artificial membranes leads to two unwanted effects: (1) nearly complete membrane retention (90–100%) and (2) highly diminished permeability (indeterminate in some cases), both effects presumably due to excessive drug-membrane binding. These adverse effects are nearly eliminated by using an ionic surfactant to create a very strong sink condition in the acceptor compartment of the permeation cell. The negative charge on the micelles formed from the surfactant added to the acceptor compartment appears to play a stabilizing role.

Tables 7.12–7.14 list the pH 7.4 permeability and retention values of the probe series of drug substances, grouped as bases, acids, and neutral molecules. Figures 7.31a–c are graphs of the effective permeabilities with and without sink as a function of increasing soy content, beginning with 2% DOPC for a benchmark. Figures 7.32a–c are plots of the corresponding membrane retentions.

Most of the permeabilities of the bases decrease steadily as the phospholipid fraction increases. There are some significant exceptions. Metoprolol, which is only moderately permeable in the DOPC lipid, becomes appreciably permeable in 10% soy lecithin. But at the 68% soy level, this molecule also shows reduced transport.

The permeabilities of the acid examples rise with increasing phospholipid content, up to 20% lipid, with rank ordering preserved. Naproxen and ketoprofen

TABLE 7.12 Soy Lecithin in Dodecane PAMPA Models (No Sink), pH 7.4[a]

Sample	10% Soy (Model 16.0) P_e(SD)	%R	20% Soy (Model 17.0) P_e(SD)	%R	20% Soy +0.5% Cho (Model 18.0) P_e(SD)	%R	35% Soy (Model 19.0) P_e(SD)	%R	68% Soy (Model 21.0) P_e(SD)	%R
Phenazopyridine	5.8 0.4)	95	1.0 (0.3)	94	7.9 (2.4)	96	4.1 (1.2)	98	5.3 (0.5)	99
Verapamil	1.4 (1.3)	94	1.1 (0.1)	94	0.1 (0.2)	96	1.6 (1.5)	95	0.2 (0.3)	94
Promethazine	0.9 (0.8)	94	0.9 (1.0)	97	0.8 (0.7)	93	(nd)	96	0.1 (0.1)	97
Quinine	4.0 (0.1)	94	3.7 (2.6)	95	4.5 (1.4)	96	0.8 (1.4)	98	(nd)	98
Imipramine	0.001 (0.005)	98	0.2 (0.3)	93	1.9 (1.5)	91	3.2 (1.2)	95	1.8 (1.7)	96
Diltiazem	4.6 (1.2)	87	7.3 (0.8)	92	3.2 (2.5)	95	6.9 (2.0)	97	2.0 (1.7)	90
Prazosin	6.7 (0.1)	57	3.5 (0.1)	63	9.7 (0.8)	72	5.5 (0.6)	79	2.2 (0.1)	83
Propranolol	2.4 (1.3)	93	1.8 (0.5)	95	1.3 (0.9)	92	2.8 (1.4)	96	2.5 (0.8)	95
Desipramine	1.2 (1.2)	97	0.6 (0.7)	93	1.1 (1.6)	95	2.7 (4.6)	96	3.2 (3.3)	91
Alprenolol	2.5 (0.9)	92	0.01 (0.03)	90	4.8 (1.0)	93	5.6 (3.8)	95	4.8 (3.1)	95
Metoprolol	6.0 (0.7)	44	8.2 (1.2)	42	8.8 (2.1)	62	7.1 (1.7)	70	3.2 (0.1)	73
Ranitidine	0.41 (0.03)	8	0.36 (0.01)	13	—	—	0.43 (0.02)	22	0.13 (0.05)	16
Amiloride	0.004 (0.005)	14	0.003 (0.006)	13	(nd)	18	0.003 (0.005)	19	(nd)	0

Ibuprofen	4.0 (1.4)	63	5.0 (0.7)	21	5.7 (1.1)	18	6.3 (1.8)	18	1.6 (1.2)	30
Acetaminophen	0.7 (0.1)	4	1.1 (0.2)	14	—	—	0.8 (0.1)	15	(nd)	0
Naproxen	2.0 (0.2)	6	3.4 (0.1)	9	2.2 (0.1)	17	2.3 (0.1)	13	0.5 (0.1)	2
Sulfasalazine	0.001 (0.005)	1	0.01 (0.02)	8	—	—	0.002 (0.005)	6	0.002 (0.005)	3
Theophylline	0.65 (0.04)	6	0.79 (0.08)	8	0.85 (0.09)	12	0.60 (0.04)	3	0.10 (0.02)	7
Ketoprofen	1.0 (0.1)	4	1.5 (0.1)	9	1.1 (0.1)	16	1.0 (0.1)	16	0.2 (0.1)	10
Hydrochlorothiazide	0.02 (0.01)	6	0.01 (0.01)	9	(nd)	10	0.03 (0.01)	20	0.02 (0.04)	3
Furosemide	0.02 (0.01)	4	0.04 (0.02)	11	0.03 (0.02)	13	0.05 (0.03)	18	0.01 (0.01)	17
Salicyclic acid	0.13 (0.01)	2	0.24 (0.03)	10	—	—	0.26 (0.08)	14	0.03 (0.03)	9
Piroxicam	2.6 (0.1)	8	3.6 (0.1)	2	2.8 (0.1)	13	2.7 (0.2)	17	1.6 (0.1)	8
Sulpiride	0.19 (0.03)	12	0.25 (0.03)	14	0.20 (0.04)	14	0.18 (0.02)	21	0.10 (0.06)	16
Terbutaline	0.05 (0.09)	10	0.20 (0.14)	2	—	—	0.01 (0.01)	22	(nd)	12
Progesterone	5.8 (0.4)	91	4.6 (0.9)	90	—	—	1.6 (0.3)	92	2.6 (0.8)	93
Griseofulvin	7.2 (0.5)	44	6.6 (0.2)	54	13.8 (0.9)	56	6.4 (0.5)	62	5.4 (0.2)	73
Carbamazepine	6.1 (0.5)	29	10.8 (0.3)	37	12.7 (3.1)	39	6.4 (0.1)	44	5.3 (0.4)	55
Antipyrine	1.2 (0.1)	7	1.5 (0.1)	9	1.6 (0.2)	15	1.3 (0.5)	25	0.5 (0.1)	8
Caffeine	1.8 (0.1)	6	2.1 (0.1)	10	2.3 (0.1)	18	2.2 (0.1)	17	1.6 (0.1)	13

[a] All P_e and SD(P_e) are in units of 10^{-6} cm/s; (nd) = compound not detected in the acceptor compartment.

TABLE 7.13 Soy Lecithin in Dodecane PAMPA Models (with Sink), pH 7.4[a]

Sample	10% Soy (Model 16.1) P_e(SD)	%R	20% Soy (Model 17.1) P_e(SD)	%R	20% Soy +0.5% Cho (Model 18.1) P_e(SD)	%R
Chlorpromazine	—	—	—	—	30.9 (5.2)	40
Phenazopyridine	15.8 (1.4)	47	20.7 (2.0)	60	18.3 (1.7)	63
Verapamil	25.6 (1.5)	31	31.6 (2.8)	31	32.4 (1.4)	31
Promethazine	26.7 (3.2)	25	27.6 (0.9)	32	37.0 (0.9)	34
Quinine	24.6 (4.1)	44	17.6 (1.0)	49	20.5 (1.3)	46
Imipramine	30.1 (0.9)	38	22.9 (0.6)	40	28.5 (3.4)	37
Diltiazem	35.8 (1.3)	22	35.1 (1.9)	17	37.4 (3.8)	20
Prazosin	28.6 (1.3)	16	19.2 (0.3)	22	36.4 (3.7)	15
Propranolol	27.1 (3.4)	39	25.1 (1.7)	36	26.5 (2.0)	40
Desipramine	33.2 (2.8)	33	29.8 (0.2)	39	28.5 (3.2)	50
Primaquine	—	—	—	—	36.9 (2.6)	34
Alprenolol	30.6 (3.8)	30	26.3 (3.5)	40	—	—
Metoprolol	26.4 ((0.1)	27	26.5 (1.1)	23	29.0 (1.6)	29
Ranitidine	0.34 (0.01)	8	0.31 (0.03)	14	0.51 (0.13)	15
Amiloride	0.01 (0.02)	9	0.007 (0.005)	15	0.1 (0.1)	15
Ibuprofen	3.6 (1.4)	32	7.4 (1.1)	34	16.3 (2.3)	39
Acetaminophen	1.2 (0.2)	8	0.4 (0.1)	7	—	—
Naproxen	1.8 (0.1)	10	2.9 (0.1)	13	3.9 (0.5)	13
Sulphasalazine	0.001 (0.005)	2	0.002 (0.005)	10	0.7 (0.4)	11
Theophylline	0.5 (0.1)	7	0.8 (0.1)	8	1.2 (0.2)	16
Ketoprofen	0.8 (0.1)	9	1.2 (0.1)	12	1.5 (0.2)	19
Hydrochlorothiazide	0.004 (0.010)	11	0.004 (0.004)	12	(nd)	17
Furosemide	0.04 (0.02)	14	0.02 (0.01)	11	0.09 (0.08)	17
Salicyclic acid	0.2 (0.2)	13	0.1 (0.1)	7	—	—
Piroxicam	2.3 (0.1)	6	3.2 (0.2)	17	3.6 (0.1)	14
Sulpiride	0.2 (0.1)	6	0.1 (0.1)	14	(nd)	17
Terbutaline	0.2 (0.3)	14	0.1 (0.2)	13	(nd)	20
Progesterone	37.6 (1.3)	40	27.6 (1.1)	37	33.2 (3.2)	34
Griseofulvin	31.8 (1.5)	25	24.4 (1.2)	23	27.0 (3.3)	25
Carbamazepine	16.5 (1.7)	23	15.2 (0.7)	26	21.2 (0.8)	30
Antipyrine	1.6 (0.1)	6	1.6 (0.1)	13	2.5 (0.3)	19
Caffeine	1.5 (0.1)	8	2.0 (0.1)	14	3.0 (0.1)	19

[a]All P_e and SD(P_e) are in units of 10^{-6} cm/s; (nd) = compound not detected in the acceptor compartment.

TABLE 7.14 Soy Lecithin in Dodecane PAMPA Models (with Sink), pH 7.4[a]

Sample	35% Soy (Model 19.1) P_e(SD)	%R	50% Soy (Model 20.1) P_e(SD)	%R	74% Soy (Model 22.1) P_e(SD)	%R
Phenazopyridine	21.1 (3.5)	66	2.4 (0.2)	58	3.9 (1.1)	75
Verapamil	42.9 (4.0)	43	17.5 (0.1)	34	1.8 (2.2)	71
Promethazine	31.3 (3.0)	36	25.7 (2.9)	45	3.7 (0.3)	61
Quinine	27.6 (1.4)	55	9.6 (2.7)	54	2.6 (1.0)	67
Imipramine	42.9 (6.1)	46	5.2 (4.8)	63	5.0 (1.8)	63
Diltiazem	40.4 (7.1)	32	20.8 (1.0)	36	3.5 (5.3)	61
Prazosin	30.9 (2.4)	25	12.7 (0.7)	38	0.4 (0.4)	49
Propranolol	27.6 (4.0)	54	15.9 (5.0)	47	(nd)	62
Desipramine	37.1 (9.4)	48	18.4 (3.0)	39	1.7 (0.7)	59
Alprenolol	42.3 (5.2)	51	7.8 (2.2)	52	2.6 (2.6)	71
Metoprolol	31.4 (0.8)	42	11.6 (0.9)	43	4.0 (6.9)	52
Ranitidine	0.2 (0.1)	13	0.3 (0.4)	8	(nd)	3
Amiloride	0.02 (0.05)	11	0.05 (0.07)	0	(nd)	5
Ibuprofen	8.1 (4.2)	22	16.5 (3.6)	13	2.0 (3.4)	33
Acetaminophen	1.3 (1.1)	15	0.4 (0.5)	16	(nd)	0
Naproxen	2.5 (0.5)	9	1.4 (0.3)	11	0.2 (0.3)	1
Sulfasalazine	0.04 (0.02)	7	(nd)	—	(nd)	2
Theophylline	0.7 (0.1)	8	0.4 (0.3)	0	0.02 (0.03)	6
Ketoprofen	1.3 (0.6)	33	1.6 (1.4)	30	(nd)	4
Hydrochlorothiazide	0.03 (0.04)	10	0.09 (0.11)	1	0.01 (0.01)	5
Furosemide	0.01 (0.02)	16	(nd)	1	0.001 (0.005)	10
Salicyclic acid	1.1 (0.5)	11	0.3 (0.5)	5	0.2 (0.3)	0
Piroxicam	2.9 (0.2)	18	1.6 (0.1)	13	1.0 (0.2)	6
Sulpiride	0.5 (0.2)	17	0.3 (0.5)	2	0.1 (0.2)	3
Terbutaline	0.1 (0.1)	20	1.3 (1.8)	22	(nd)	1
Progesterone	36.2 (0.5)	36	23.2 (0.5)	65	31.8 (7.2)	39
Griseofulvin	22.1 (2.9)	27	14.6 (1.0)	37	13.4 (4.5)	44
Carbamazepine	15.3 (2.0)	27	9.9 (0.4)	36	2.1 (0.4)	38
Antipyrine	1.8 (1.0)	18	2.5 (1.4)	14	1.0 (0.3)	1
Caffeine	2.0 (0.1)	18	(nd)	9	1.2 (0.3)	8

[a]All P_e and SD(P_e) are in units of 10^{-6} cm/s; (nd) = compound not detected in the acceptor compartment.

show the most dramatic increases in going from 2% DOPC to 10% soy lipid membranes, somewhat higher in soy than in egg. Piroxicam shows less sensitivity to lipid changes. For higher phospholipid concentrations, all the acid permeabilities decrease.

The nonionizable molecules respond to the changes in the phospholipid content. Griseofulvin has the highest permeability in the lowest phospholipid-containing membranes. The most remarkable change of properties in going from 2% to 10%

phospholipid occurs with the membrane retention of the bases. Most of the bases are retained above 90% in all of the soy lecithin cases ($\leq$68% in dodecane). This is thought to be largely due to the added electrostatic attractions between positively charged sample molecules and the negatively-charged membrane constituents.

Acids show small, steady increases in membrane retention with increasing phospholipid content. Even though the acids are negatively charged at pH 7.4, as are a portion of the membrane constituents, the increasing phospholipid content draws the sample molecules in, due to increased hydrogen-bonding and any other lipophilic forces arising from the phospholipids (increased membrane-water partition coefficient). Decreased surface pH due to the membrane negative surface charge [457] may also play a role in increasing permeability of weak acids.

Neutral molecules show a range of retention properties between those of acids and bases. Progesterone membrane retention is very high in all cases. Griseofulvin and carbamazepine retention steeply increase with phospholipid content. The patterns of retention follow the lipophilicity properties of the molecules, as indicated by octanol–water apparent partition coefficients (Table 7.4).

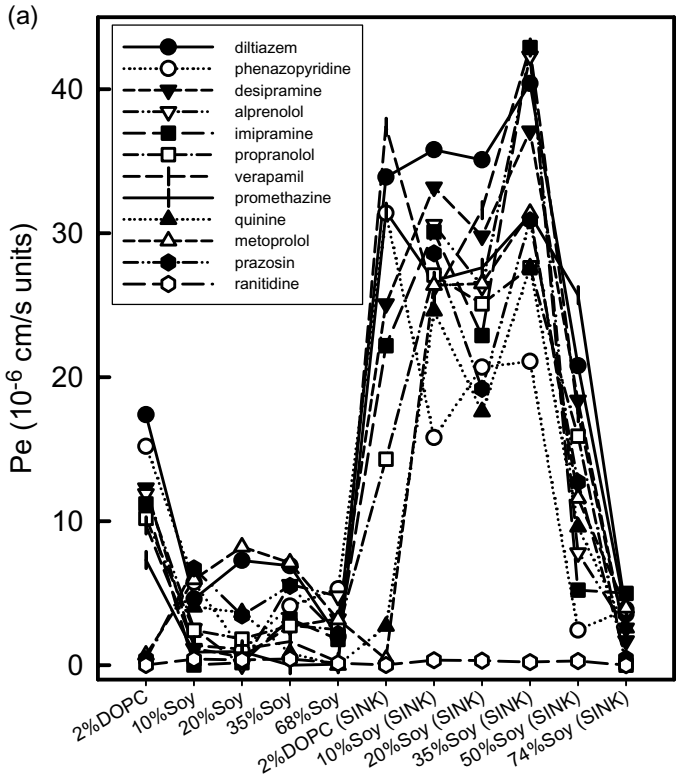

Figure 7.31 Soy lecithin permeabilities at various concentrations in dodecane, with and without sink: (a) bases; (b) acids; (c) neutrals.

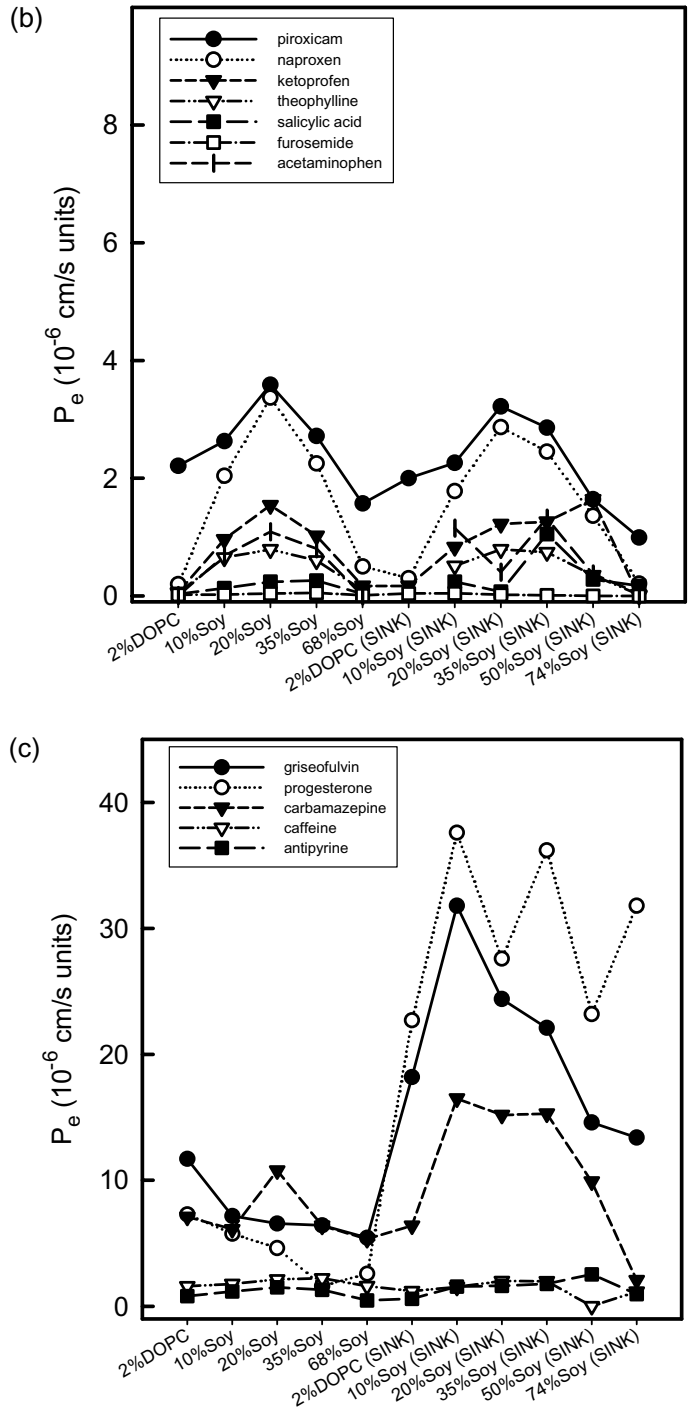

Figure 7.31 (*Continued*)

7.7.5.3 Lipophilicity and Decrease in Permeability with Increased Phospholipid Content in Dodecane

Figures 7.31a–c clearly show that after some critical soy content in dodecane, P_e values decrease with increasing soy, for both sink and sinkless conditions. [This is not due to a neglect of membrane retention, as partly may be the case in Fig. 7.23; permeabilities here have been calculated with Eq. (7.21).] Section 7.6 discusses the Kubinyi bilinear model (Fig. 7.19d) in terms of a three-compartment system: water, oil of moderate lipophilicity, and oil of high lipophilicity. Since liposome(phospholipid)–water partition coefficients (Chapter 5) are generally higher than alkane–water partition coefficients (Chapter 4) for drug-like molecules, soy lecithin may be assumed to be more lipophilic than dodecane. It appears that the increase in soy concentration in dodecane can be treated by the Kubinyi analysis. In the original analysis [23], two different lipid phases are selected at a fixed ratio (e.g., Fig. 7.20), and different molecules are picked over a range of lipophilicities.

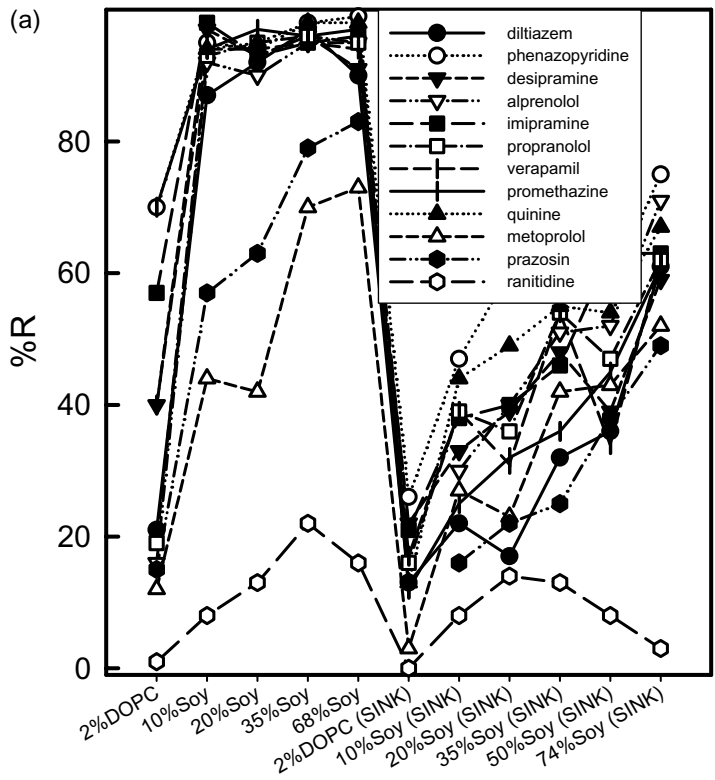

Figure 7.32 Soy lecithin membrane retentions at various concentrations in dodecane, with and without sink: (a) bases; (b) acids; (c) neutrals.

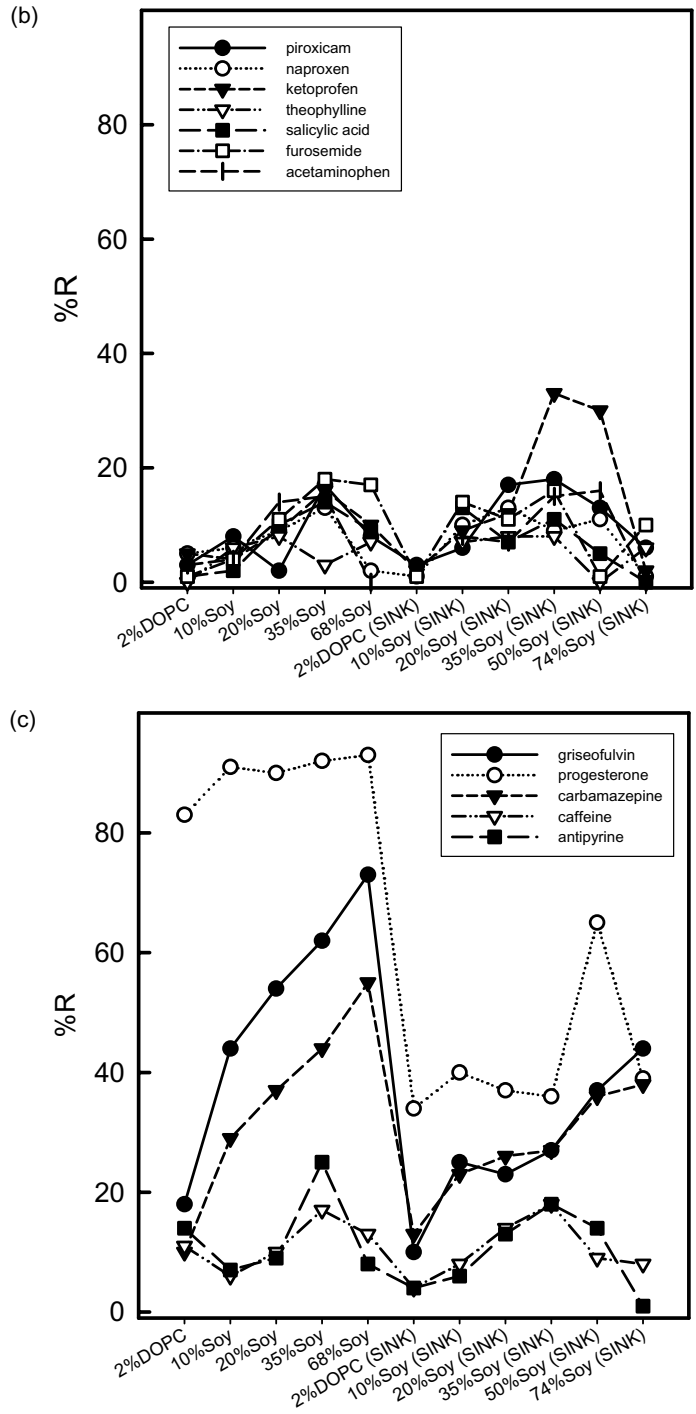

Figure 7.32 (*Continued*)

The more lipophilic molecules preferentially concentrate in the more lipophilic phase, leading to decreased permeabilities, according to the effect of the negative term in Eq. (7.44), as the concentration of solute in the lower-lipophilicity phase decreases. In the soy lecithin models, the lipid phases are systematically varied, with reference to a molecule of a particular lipophilicity. The plots in Figs. 7.31a–c are *orthogonally* equivalent to the Kubinyi model type plots (Fig. 7.19d), with each curve representing a particular molecule and the horizontal axis corresponding to varied lipid ratios. Eq. 7.44 applies and Figs. 7.31a–c may be interpreted as bilinear curves, for both sink and sinkless domains. For example, the maximum permeability for most molecules occurs at about 20% wt/vol lecithin in dodecane. For higher lecithin content, the negative term in Eq. (7.44) dominates, causing the P_e values to decrease.

7.7.5.4 Sink Condition to Offset the Attenuation of Permeability

The preceding section treats the decrease in permeabilities with increasing lecithin content in dodecane in terms of shifting concentration distributions between a weak lipophilic domain (dodecane) and a stronger lipophilic domain (lecithin). Another view of this may be that at the molecular level, as the amount of phospholipid increases, the effects of electrostatic and H-bonding play a more prominent role in the transport process. Generally, $\%R$ of the lipophilic molecules increases with increasing lecithin content, most dramatically in the case of lipophilic bases. Such losses of compound to the membrane pose a challenge to the analysis of concentrations, which can be significantly diminished (to undetectable levels at times) in the aqueous compartments. At the same time, the permeability drops to near vanishing values in 68% soy lecithin–dodecane membranes. Under these conditions, the permeabilities of the lipophilic bases and acids converge to similar low values, significantly departing from the expected values based on the octanol–water lipophilicity scale (Table 7.4) and the pH partition hypothesis. This excessive drug–membrane binding would not be expected under in vivo conditions in the small intestine, due to the naturally occurring sink state. There would be competing lipid environments in the receiving compartment (serum proteins, other membrane barriers, etc.), and the solute-binding membrane would release a portion of the retained lipophilic molecules, resulting in a concomitant higher effective permeability.

The transport properties of the molecules in concentrated soy lecithin, Tables 7.12–7.14, do not adequately model the in vivo permeabilities reported by Winiwarter et al. [56] (Table 7.4). The strategy to overcome this shortcoming of the model involves creating a model sink condition. However, the use of BSA or other serum proteins, although easily effected, is not practical in high-throughput screening, since the UV absorption due to the proteins would render determination of the compound concentrations in the acceptor compartments by direct UV spectrophotometry nearly impossible in most cases. Without knowledge of the concentration of sample in the acceptor compartment, the determination of $\%R$ would not be practical. Some PAMPA practitioners, using BSA to create sink conditions, make the simplifying assumption that membrane retention is zero. It is neither reason-

able nor warranted to expect that membrane retention is eliminated in the presence of serum proteins or other practical substitutes in the acceptor compartment. Figures 7.32a–c clearly show that retention under sink can be substantial.

Since lipophilic molecules have affinity for *both* the membrane lipid and the serum proteins, membrane retention is expected to decrease, by the extent of the relative lipophilicities of the drug molecules in membrane lipid versus serum proteins, and by the relative amounts of the two competitive-binding phases [see Eqs. (7.41)–(7.43)]. Generally, the serum proteins cannot extract all of the sample molecules from the phospholipid membrane phase at equilibrium. Thus, to measure permeability under sink conditions, it is still necessary to characterize the extent of membrane retention. Generally, this has been sidestepped in the reported literature.

We found that the negatively charged surfactant, sodium laurel sulfate, can be successfully substituted for the serum proteins used previously. In low ionic strength solutions, the cmc of the surfactant is 8.1 mM [577]. We explored the use of both sub-CMC (data not shown) and micelle-level concentrations. Saturated micelle solutions are most often used at *p*ION.

The addition of surfactant to the acceptor solution allows for the re-distribution of lipophilic permeants between the PAMPA membrane phase and the surfactant phase in the acceptor compartment, in the manner of Kubini's [23] analysis (Sec. 7.6), according to the relative lipophilicities of the two oil phases. This redistribution can be approximated. Garrone et al. [600] derived a Collander relationship for a series of substituted benzoic acids, relating their lipophilicities in 30–100 mM sodium laurel sulfate to the octanol-water system. The Collander equation comparing the drug partitioning in liposome–water to octanol–water systems (Fig. 5.6) can be combined with that of the above micellar relationship to get the approximate equation: $\log K_{p,\text{mic}} = 1.4 \log K_{p,\text{liposome}} - 1.6$. If it is assumed that the PAMPA membrane lipophilicity can be approximated by that of liposomes, then the strength of the surfactant-created acceptor sink can be compared to that of the PAMPA membrane, according to the latter expression. The most lipophilic molecules will favor the micellar phase when their liposome partition coefficients, $\log K_{p,\text{liposome}}$, are greater than 4. (The micellar and PAMPA lipid volumes are nearly the same.) Positively charged drug molecules will favor additional binding to the negatively charged micelles, unless the PAMPA membrane lipid composition also has negative charge.

The effect of the surfactant is most dramatic for the bases and neutral molecules studied, as shown in Tables 7.13 and 7.14. Permeabilities increased by up to fourfold for the lipophilic bases and neutral molecules, and membrane retentions were decreased by 50% in most cases of bases and neutral compounds (Figs. 7.31 and 7.32).

The transport properties of the acids did not respond significantly to the presence of the sink. This may be because at pH 7.4 the acids are negatively charged, as are the phospholipid membranes and also the surfactant micelles; electrostatic repulsions balanced out the attractive forces due to increased membrane lipophilicity. Lowered surface pH may also play a balancing role [457].

7.7.5.5 Comparing Egg and Soy Lecithin Models

The negative-charge lipid content in the egg lecithins is not as high as that found in BBM and especially BBB lipids (Table 7.1). Furthermore, the negative-charge content in the egg lecithin is about one-fourth that in the soy lecithin. This is clearly evident in the membrane retention parameters for the bases at the 10% lecithin levels (models 12.0 or 14.0 in Table 7.8 vs. model 16.0 in Table 7.12), as they are ~20–30% lower for the lipophilic bases in egg, compared to soy.

For acids, the membrane retention actually *increases* in the case of egg lecithin, compared to soy lecithin. This may be due to decreased repulsions between the negatively charged sample and negatively charged phospholipid, allowing H-bonding and hydrophobic forces to more fully realize in the less negatively charged egg lecithin membranes. The neutral molecules display about the same transport properties in soy and egg lecithin, in line with the absence of direct electrostatic effects. These differences between egg and soy lecithins make soy lecithin the preferred basis for further model development.

7.7.5.6 Titrating a Suspension of Soy Lecithin

Since soy lecithin (''20% extract'' from Avanti) was selected as a basis for absorption modeling, and since 37% of its content is unspecified, it is important to at least establish that there are no titratable substituents near physiological pH. Asymmetric triglycerides, the suspected unspecified components, are not expected to ionize. Suspensions of multilamellar vesicles of soy lecithin were prepared and titrated across the physiological pH range, in both directions. The versatile Bjerrum plots (Chapter 3) were used to display the titration data in Fig. 7.33. (Please note the extremely expanded scale for $\bar{n}_H$.) It is clear that there are no ionizable groups

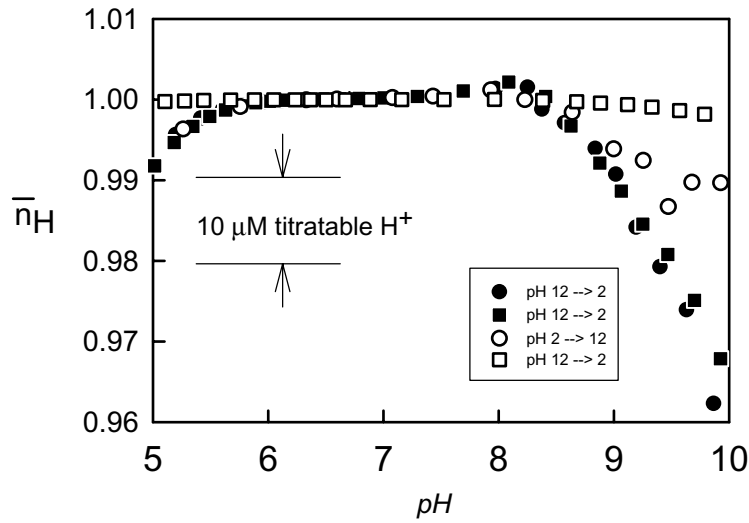

Figure 7.33 Bjerrum plot for titration of a suspension of 1 mM soy lecithin.

between pH 5.5 and 8.0 with concentrations in excess of 1 μM. For pH > 8, phosphatidic and possibly free fatty acids start to ionize, approximately to the extent of 1% of the total soy content by pH 9.

7.7.6 Intrinsic Permeability, Permeability–pH Profiles, Unstirred Water Layers (UWL), and the pH Partition Hypothesis

Up to now we have focused on measurement of permeability and membrane retention at pH 7.4. Since the GIT covers a range of pH values, with pH 5–8 characterizing the small intestine, it is necessary to address the pH dependence of the transport of drug molecules. Even nonionizable molecules may be affected by pH dependence, since several biological membrane components themselves are ionizable (pK_a values listed in Fig. 7.4). For example, with PS, PA, and DA (free fatty acid) undergoing changes in charge state in the pH 5–8 interval. In this section, we examine the consequences of pH dependence.

7.7.6.1 Unstirred Water Layer Effect (Transport across Barriers in Series and in Parallel)

Passive transport across a membrane barrier is a combination of diffusion through the membrane and also diffusion through the stagnant water layers at the two sides of the membrane. Stirring the bulk aqueous solution does not appreciably disturb the water layers in contact with the membrane. When the solute is introduced into the bulk aqueous phase, convective mixing resulting from applied stirring, quickly positions the drug molecule next to the so-called unstirred water layer (UWL). At that point, the passage through the UWL is governed by the laws of diffusion, and is independent of stirring. In simple hydrodynamic models [534–538] the UWL is postulated to have a distinct boundary with the rest of the bulk water. The UWL can be made thinner with more vigorous stirring, but it cannot be made to vanish. Extensions of the simple UWL models have been discussed in the literature [539,540], but such models are not often used in practice.

The actual thickness of the unstirred water layer depends somewhat on the transport model system. The in vivo UWL is significantly different from the in vitro assay measuring cell UWL. Because of the efficient mixing near the surface of the epithelium, the in vivo UWL is estimated to be 30–100 μm thick. The UWL in the endothelial microcapillaries of the brain is nil, given that the diameter of the capillaries is ~7 μm and the efficiency of the mixing due to the passage of erythrocytes [612]. However, in unstirred in vitro permeation cells, the UWL values can be 1500–2500 μm thick, depending on cell geometry and dimensions.

It may be assumed that the total resistance to passive transport across the trilamellar (UWL–membrane–UWL) barrier is the sum of the resistances of the membrane and the UWL on each side of it. Resistance is the inverse of permeability. So

$$\frac{1}{P_e} = \frac{1}{P_m} + \frac{1}{P_u} \tag{7.46}$$

where P_e refers to the measured *effective* permeability, P_u refers to the total UWL permeability, P_m is the permeability of the *membrane* (which would be measured if the UWL were made vanishingly thin). If it is possible to separate the donor and acceptor contributions to the UWL, then the total P_u can be allocated between its parts according to $1/P_u = 1/P_u^{(D)} + 1/P_u^{(A)}$. In Caco-2 literature, equations like Eq. (7.46) often have a fitter, P_f, component, to account for resistance of the water-filled pores of the fitter. In PAMPA, all pores are filled with lipid, and no consideration of filter contributions are needed.

The UWL permeability is nearly the same for drugs of comparable size, and is characterized by the water diffusivity (D_{aq}) of the drug divided by twice the thickness of the layer (h_{aq}), $P_u = D_{aq} / (2\ h_{aq})$, in a symmetric permeation cell [40]. The unstirred water layer permeability can be determined experimentally in a number of ways: based on pH dependency of effective permeability [25,509,535–538], stirring rate dependence [511–514,552,578], and transport across lipid-free microfilters [25,546].

7.7.6.2 Determination of UWL Permeability using pH Dependence (pK_a^{flux}) Method

The membrane permeabilities P_m may be converted to *intrinsic* permeabilities P_0, when the pK_a is taken into consideration. An ionizable molecule exhibits its intrinsic permeability when it is in its uncharged form and there is no water layer resistance. The relationship between P_m and P_0 is like that between the pH-dependent apparent partition coefficient (log K_d) and the true partition coefficient (log K_p), respectively. This relationship can be rationalized by the mass balance. Take, for example, the case of a monoprotic acid, HA. The total substance concentration is

$$C_{HA} = [HA] + [A^-] \tag{7.47}$$

Using the ionization quotient expression [Eq. (3.1)], $[A^-]$ may be expressed in terms of [HA]:

$$\begin{aligned} C_{HA} &= [HA] + \frac{[HA]K_a}{[H^+]} \\ &= [HA]\left(1 + \frac{K_a}{[H^+]}\right) \\ &= [HA](1 + 10^{-pK_a + pH}) \end{aligned} \tag{7.48}$$

In the UWL, HA and A^- diffuse in parallel; the total UWL flux, J_u, is the sum of the two individual flux components. If it is assumed that the transport is under steady

state and that the aqueous diffusivities of HA and A^- are the same, the UWL flux becomes

$$\begin{aligned} J_u &= J_u^{\mathrm{HA}} + J_u^{\mathrm{A}} \\ &= P_u^{\mathrm{HA}}\Delta[\mathrm{HA}] + P_u^{\mathrm{A}}\Delta[\mathrm{A}^-] \\ &= P_u\Delta C_{\mathrm{HA}} \end{aligned} \tag{7.49}$$

where ΔC_{HA} represents the drop in total concentration across the entire trilamellar barrier. If the pH partition hypothesis holds, then the flux in the membrane is related to the concentration gradient of the uncharged solute

$$J_m = P_0\Delta[\mathrm{HA}] \tag{7.50}$$

where $\Delta[\mathrm{HA}]$ represents the drop in concentration of the uncharged species in the membrane. Since the membrane and the UWL are in series, the total flux J may be expressed as

$$\begin{aligned} \frac{1}{J} &= \frac{1}{J_u} + \frac{1}{J_m} \\ &= \frac{1}{P_e\Delta C_{\mathrm{HA}}} \end{aligned} \tag{7.51}$$

Multiplying this expression by the total sample concentration change, we obtain

$$\begin{aligned} \frac{1}{P_e} &= \frac{1}{P_u} + \frac{\Delta C_{\mathrm{HA}}}{\Delta[\mathrm{HA}]P_0} \\ &= \frac{1}{P_u} + \frac{1 + K_a/[\mathrm{H}^+]}{P_0} \\ &= \frac{1}{P_u} + \frac{(1 + 10^{-\mathrm{p}K_a + \mathrm{pH}})}{P_0} \end{aligned} \tag{7.52}$$

Equating Eqs. (7.52) and (7.46) reveals the relationship between intrinsic and membrane permeabilities, Eq. (7.53), for the case of weak acids. Similar steps lead to expressions for weak bases and ampholytes, Eqs. (7.54) and (7.55):

$$P_0 = P_m(1 + 10^{-\mathrm{p}K_a + \mathrm{pH}}) \qquad \text{(weak acid)} \tag{7.53}$$

$$P_0 = P_m(1 + 10^{\mathrm{p}K_a - \mathrm{pH}} \qquad \text{(weak base)} \tag{7.54}$$

$$P_0 = P_m(1 + 10^{\mathrm{p}K_{a1} - \mathrm{pH}} + 10^{-\mathrm{p}K_{a2} + \mathrm{pH}}) \qquad \text{(ampholyte)} \tag{7.55}$$

For ionizable molecules, the intrinsic P_0 and the UWL P_u can be deduced from the pH dependence of P_e, as shown by Gutknecht and co-workers [535–537].

As can be seen from the second line of Eq. (7.52), a plot of $1/P_e$ versus $1/[H^+]$ is expected to be linear (for a weak acid), with the intercept: $1/P_u + 1/P_0$ and the slope K_a/P_0. When the pK_a of the molecule is known, then both P_0 and P_u can be determined. If P_u can be independently determined, then, in principle, the ionization constant may be determined from the pH dependence of the effective permeability.

Figure 7.34 shows the pH dependence of the effective permeability of ketoprofen (measured using *p*ION's PAMPA system with 2% DOPC in dodecane membrane lipid) [558], a weak acid with pK_a 4.12 (0.01 M ionic strength, 25°C). Figure 7.34a shows that the log P_e curve has a flat region for pH < pK_a and a region with a slope of -1 for pH > pK_a. At pH 7.4, ketoprofen has a very low permeability, since it is almost entirely in a charged form. The molecule shows increasing permeabilities with decreasing pH, approaching 18×10^{-6} cm/s (thick curve, Fig. 7.34b inset). This is close to the value of the UWL permeability, 21×10^{-6} cm/s (log $P_e - 4.68$). The small difference vanishes for very lipophilic molecules, such as imipramine. For lipophilic acids, when pH < pK_a, the transport is said to be ''diffusion-limited.'' For pH > pK_a, the P_e curve coincides with the P_m curve, where transport is ''membrane-limited.'' In general, highly permeable molecules all show nearly the same maximum effective permeability when measured in the same apparatus. In order to deduce the uncharged molecule membrane permeability (top of the dashed curve in Fig. 7.34a), it is necessary to analyze the P_e–pH curve by the Gutknecht method [535–537]; thus, Eq. (7.52) is solved for P_u and P_0, when pK_a is known. Such analysis produces the dashed curve in Figs. 7.34a,b.

The P_m curve (dashed line) is not shifted to the right of the ''fraction neutral substance'' curve f_u, (see inset in Fig. 7.34b). It just looks that way when unmatched scaling is used [554]. The two curves are exactly superimposed when the vertical coordinates of the P_m and f_u are normalized to a common value. The P_e curve, in contrast, is shifted to the right for weak acids and to the left for weak bases. In the log–log plot (log P_e vs. pH), the pH value at the intersection of the slope 0 and slope -1 curve segments indicates an *apparent* pK_a (Fig. 7.34a).

We have seen many instances of slope–(0, ±1) log–log plots (e.g., Figs. 2.2, 4.2–4.4, 4.6, 5.7, 5.11, 6.1–6.4, 6.12). Behind each tetrad equilibrium (e.g., Figs. 4.1, 5.1, 6.5) there is such a log–log plot, and associated with each such log–log plot is an apparent pK_a. We have called these pK_a^{oct}, pK_a^{mem}, pK_a^{gibbs}. In permeability, there is yet another one: pK_a^{flux} (Fig. 7.34a). If we take the difference between pK_a and pK_a^{flux}, we can deduce the difference between log P_0 and log P_u:

$$\log P_0 = \log P_u + |pK_a - pK_a^{flux}| \tag{7.56}$$

The shapes of permeability–pH profiles mirror those of solubility–pH (see, Figs. 6.1a, 6.2a, and 6.3a), with slopes of *opposite* signs. In solutions *saturated* with an insoluble compound, the product of solubility and permeability (''flux,'' as described in Chapter 2) is pH-independent! This is indicated in Fig. 2.2 as the maximum flux portions of the curves.

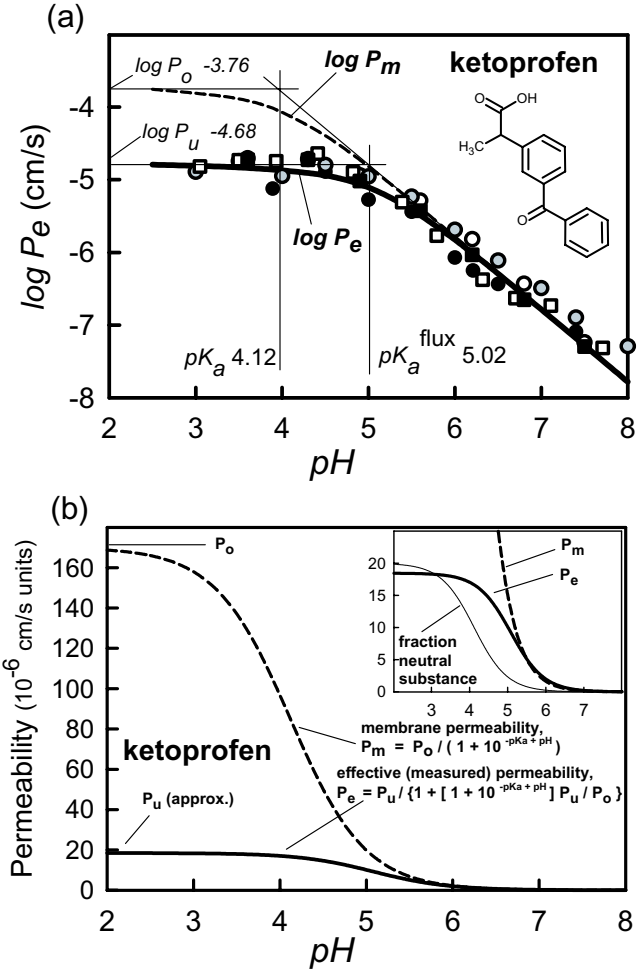

Figure 7.34 Permeability–pH profiles of ketoprofen: (a) log–log plot; solid curve represents effective permeability, and the dashed curve is the membrane permeability, calculated by Eq. (7.53). The latter curve levels off at the intrinsic permeability, P_0. The effective curve levels off to approximately the unstirred water layer permeability, P_u. (b) Direct plot; the inset curve for the fraction neutral substance levels of at 100% (scale not shown). [Avdeef, A., *Curr. Topics Med. Chem.*, **1**, 277–351 (2001). Reproduced with permission from Bentham Science Publishers, Ltd.]

Figure 7.35 shows the characteristic log P_e–pH curve for a weak base, phenazopyridine (pK_a 5.15). With bases, the maximum permeability is realized at high pH values. As in Fig. 7.34, the PAMPA assays were performed under iso-pH conditions (same pH in donor and acceptor wells), using the 2% DOPC in dodecane lipid system.

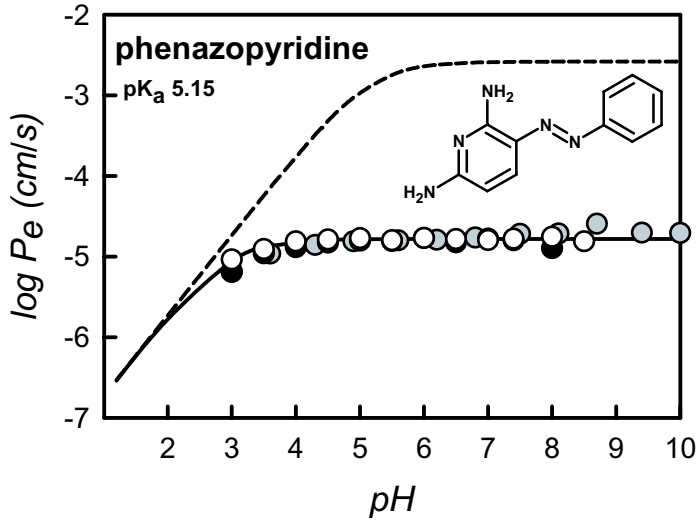

Figure 7.35 Permeability–pH profile of phenazopyridine under iso-pH conditions. [Based on data in Ref. 558.]

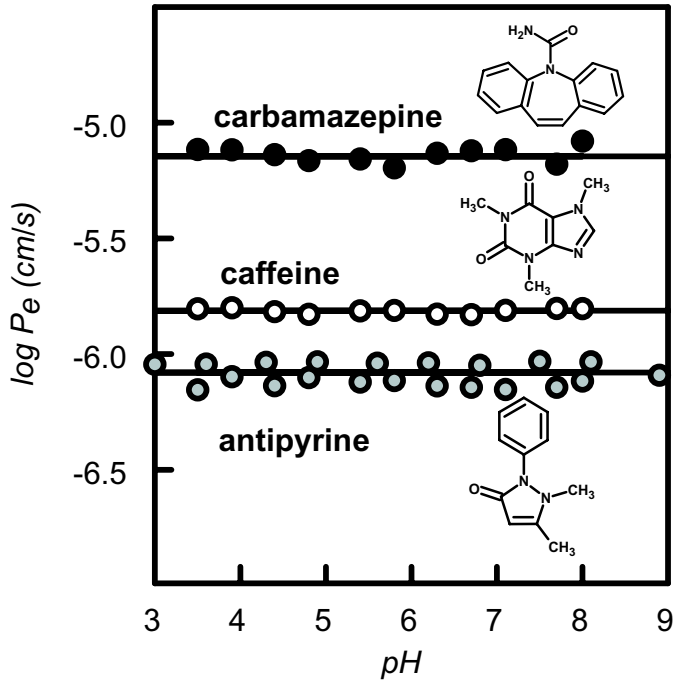

Figure 7.36 Permeability–pH profile of three neutral molecules under iso-pH conditions.

Figure 7.36 shows the log P_e–pH plots for three nonionizable molecules: carbamazepine, caffeine, and antipyrine. As is expected, there is no pH dependence shown; neither the molecules, nor the 2% DOPC/dodecane membrane show charge-state changes in the pH interval from pH 3 to 9.

Table 7.15 lists the intrinsic permeabilities and the unstirred water permeabilities of 16 drugs, determined by the Gutknecht method. The average unstirred water layer permeability is 16×10^{-6} cm/s. Since the aqueous diffusivity (D_{aq}) of most of the drugs in Table 7.15 is near 8×10^{-6} cm^2/s, the average thickness of the unstirred water layer on each side of the membrane is $\sim$2500 μm in the unagitated 96-well microtiter plates, used by *p*ION's PAMPA system. The permeation cell dimensions in typical Caco-2 assays indicate UWL of about 1500 μm (when the plates are unstirred) [554]. The thickness of the unstirred water layer can be driven down to values as low as 300–500 μm if the plate is vigorously stirred during permeation [546,554,556].

The intrinsic membrane permeabilities in Table 7.15 span about eight orders of magnitude, whereas the effective (measured in the in vitro assay) permeabilities are confined to a much narrower range, limited by the UWL. Since the in vivo UWL in the gut is estimated to be about 50 μm [541], it is more appropriate to use P_m than P_e values in oral absorption prediction strategies.

7.7.6.3 Determination of UWL Permeabilities using Stirring Speed Dependence

Caco-2 assay permeabilities corrected for the UWL usually include P_u determined as a function of the stirring speed (since the cells are not stable over a wide pH range), as in Eq. (7.57) [511–514,552,578]

$$P_u = \kappa \nu^x \tag{7.57}$$

where κ is a constant descriptive of the diffusivity of the solute and ν is the stirring speed (rpm). If the thickness of the UWL is different on the two sides of the membrane, then there are two different values of κ [514]. Equation (7.57) may be substituted into Eq. (7.46) to obtain

$$\frac{1}{P_e} = \frac{1}{P_m} + \frac{1}{\kappa \nu^x} \tag{7.58}$$

Measurements of P_e in fixed-pH solutions but at various different stirring speeds need to be made. The double-reciprocal analysis, $1/P_e$ versus $1/\nu^x$, for Caco-2 permeability measurements in the Transwell (Corning Costar) system produced a linear plot for $x = 0.8$ [514]. The intercept yields the membrane permeability for the particular pH value in the study; the slope determines the κ constant. From the analysis of testosterone transport, for the stirring speed of 25 rpm (planar rotating shaker), the thickness of each UWL (assuming symmetric geometry) was calculated to be 465 μm; at 150 rpm, $h_{aq} = 110$ μm [514]. Karlsson and Artursson [512] found $x = 1.0$ to best represent their stirring-based analysis of the UWL permeability.

TABLE 7.15 Intrinsic Permeabilities and Unstirred Water Layer Permeabilities Determined from Iso-pH Dependence of Effective Permeabilities: 2% DOPC in Dodecane

Compound	P_0 (cm/s) (SD)[a]	$\log P_0$ (SD)	$P_u 10^{-6}$ cm/s (SD)[b]	$\log P_u$ (SD)	MW	pK_a ($I = 0.01$ M, 25° C)	pK_a^{FLUX}	pH Range[c]	n[d]	GOF[e]
Imipramine	3.8 (0.3)	+0.58 (0.04)	17.0 (0.8)	−4.77 (0.02)	280.4	9.51	4.2	3.0–7.6	11	0.8
Verapamil	$1.5\ (0.1) \times 10^{-1}$	−0.82 (0.03)	13.2 (0.3)	−4.88 (0.01)	454.6	9.07	5.6	4.7–8.1	36	0.6
Propranolol	$5.7\ (0.3) \times 10^{-3}$	−2.24 (0.03)	13.3 (0.7)	−4.88 (0.02)	259.3	9.53	7.1	5.5–8.1	95	1.3
Ibuprofen	$3.0\ (0.3) \times 10^{-3}$	−2.52 (0.04)	12.3 (0.6)	−4.91(0.02)	206.3	4.59	6.9	4.0–9.0	9	0.6
Phenazopyridine	$2.6\ (0.5) \times 10^{-3}$	−2.58 (0.08)	16.7 (0.5)	−4.78 (0.01)	213.2	5.15	3.4	2.9–10.1	35	1.1
Piroxicam	$1.1\ (0.1) \times 10^{-3}$	−2.96 (0.04)	16.9 (0.8)	−4.77 (0.02)	331.4	2.3, 5.22	6.8	2.9–9.8	33	1.4
Naproxen	$4.9\ (0.4) \times 10^{-4}$	−3.31 (0.04)	18.2 (1.2)	−4.74 (0.03)	230.3	4.32	5.7	3.5–9.8	43	1.5
Ketoprofen	$1.7\ (0.1) \times 10^{-4}$	−3.76 (0.04)	20.7 (1.5)	−4.68 (0.03)	254.3	4.12	5.0	2.9–8.8	54	1.5
Metoprolol	$7.5\ (0.4) \times 10^{-5}$	−5.13 (0.02)	6.3 (0.3)	−5.20 (0.05)	267.4	9.56	8.4	6.8–10.1	56	0.7
Quinine	$6.0\ (0.4) \times 10^{-5}$	−4.22 (0.03)	12.8 (0.7)	−4.89 (0.02)	324.4	4.09, 8.55	7.8, 4.0	6.6–10.1	24	0.6
Salicylic acid	$2.9\ (0.1) \times 10^{-5}$	−4.53 (0.02)	33.0 (6.0)	−4.48 (0.01)	138.1	3.02	3.3	2.9–6.1	12	0.4
Carbamazepine	$1.6\ (0.3) \times 10^{-5}$	−4.8 (0.1)	—	—	236.3	—[f]	—	3.5–8.0	11	0.5
Caffeine	$1.8\ (0.1) \times 10^{-6}$	−5.7 (0.2)	—	—	194.2	—[f]	—	3.5–8.0	11	0.2
Antipyrine	$8.7\ (0.3) \times 10^{-7}$	−6.1 (0.1)	—	—	188.2	—[f]	—	3.0–9.0	21	0.5
Acetaminophen	$5\ (1) \times 10^{-8}$	−7.3 (0.1)	—	—	151.2	9.78	—	3.5–8.5	8	1.3
Hydrochlorothiazide	$7\ (3) \times 10^{-9}$	−8.2(0.1)	—	—	297.7	8.76, 9.95	—	3.5–8.5	10	0.7

Source: Based on data in Ref. 558.

[a] P_0 = intrinsic permeability, SD = estimated standard deviation.

[b] P_u = unstirred water permeability.

[c] Data range actually used in the regression analysis.

[d] Number of P_e measurements.

[e] GOF = goodness of fit in the weighted nonlinear regression analysis.

[f] Carbamazepine, caffeine, and antipyrine are neutral molecules. Their effective permeabilities were corrected for the unstirred water layer using the average unstirred water layer permeability of 1.6×10^{-5} cm/s, determined by the other molecules.

Similar analysis can be applied to side-by-side diffusion cell systems, where stirring is effected by bubbling an O_2/CO_2 gas mixture. For a bubbling rate of 40 mL gas/min, each UWL was estimated to be 282 μm [515].

7.7.6.4 Determination of UWL Permeabilities from Transport across Lipid-Free Microfilters

An infrequently used method (in pharmaceutical research) for determining the UWL permeability involves measuring transport of molecules across a high-porosity microfilter that is not coated by a lipid. The molecules are able to diffuse freely in the water channels of the microfilter. The filter barrier prevents convective mixing between the donor and acceptor sides, and an UWL forms on each sides of the microfilter. Camenisch et al. [546] measured the effective permeabilities of a series of drug molecules in 96-well microtiter plate–filterplate (Millipore GVHP mixed cellulose ester, 0.22 μm pore) ''sandwich'' where the filters were not coated by a lipid. The permeabilities were nearly the same for all the molecules, as shown in Fig. 7.8a. Our analysis of their data, Fig. 7.8b, indicates $h_{aq} = 460$ μm (sandwich stirred at 150 rpm). We have been able to confirm similar results in our laboratory with different microfilters, using the lipid-free method.

7.7.6.5 Estimation of UWL Thickness from pH Measurements Near the Membrane Surface

Antonenko and Bulychev [84] measured local pH changes near BLM surfaces using a variably positioned 10 μm antimony-tip pH microelectrode. Shifts in pH near the membrane surface were induced by the addition of $(NH_4)_2SO_4$. As the neutral NH_3 permeated, the surface on the donor side of the BLM accumulated excess H^+ and the surface on the acceptor side of the membrane was depleted of H^+ as the permeated NH_3 reacted with water. These effects took place in the UWL. From measurement of the pH profile as a function of distance from the membrane surface, it was possible to estimate h_{aq} as 290 μm in the stirred solution.

7.7.6.6 Prediction of Aqueous Diffusivities D_{aq}

The method preferred in our laboratory for determining the UWL permeability is based on the pH dependence of effective permeabilities of ionizable molecules [Eq. (7.52)]. Nonionizable molecules cannot be directly analyzed this way. However, an approximate method may be devised, based on the assumption that the UWL depends on the aqueous diffusivity of the molecule, and furthermore, that the diffusivity depends on the molecular weight of the molecule. The thickness of the unstirred water layer can be determined from ionizable molecules, and applied to nonionizable substances, using the (symmetric) relationship $P_u = D_{aq}/2h_{aq}$. Fortunately, empirical methods for estimating values of D_{aq} exist. From the Stokes–Einstein equation, applied to spherical molecules, diffusivity is expected to depend on the inverse square root of the molecular weight. A plot of log D_{aq} versus log MW should be linear, with a slope of -0.5. Figure 7.37 shows such a log–log plot for 55 molecules, with measured diffusivities taken from several

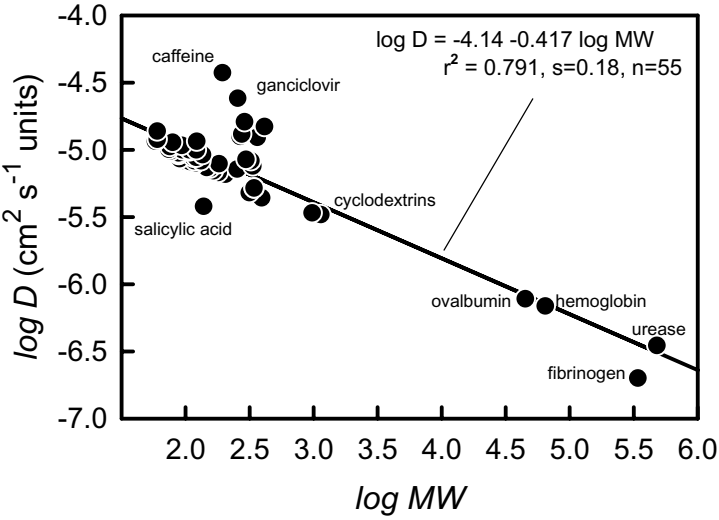

Figure 7.37 Log aqueous diffusivities versus log molecular weights.

sources [40,553,594]. Molecular weights spanned from ~100 to 500,000 Da. The linear regression equation from the analysis is

$$\log D_{\text{aq}} = -4.14 - 0.417 \ \log \text{MW} \tag{7.59}$$

with $r^2 = 0.79$, $s = 0.2$, $n = 55$. The slope is close to the theoretically expected value of -0.5.

The P_u values in Table 7.15 can be combined with Eq. (7.59) to determine approximate h_{aq}. The plot of log P_u versus log MW for 11 molecules is shown in Fig. 7.38. The solid line in the plot was determined from the equation (based on $P_u = D_{\text{aq}}/h$)

$$\begin{aligned} \log P_u &= \log D_{\text{aq}} - \log h \\ &= -4.14 - 0.417 \ \log \text{MW} - \log h \end{aligned} \tag{7.60}$$

where h is the sum UWL thickness. The best-fit value of h was determined by regression to be 4.5 mm. Thus each UWL thickness is ~2300 μm. Note that this represents approximately the thickness of the water layer in the unagitated microtiter plate sandwich configuration of the *p*ION system. The two highest deviation points in Fig. 7.38 correspond to metoprolol and salicylic acid. These deviations are due mainly to the weak UV spectra of these molecules in the acceptor wells in the PAMPA iso-pH assay.

7.7.6.7 Intrinsic Permeability–log K_p Octanol–Water Relationship

Once the 2% DOPC/dodecane permeability data have been corrected for pH and UWL effects, the resulting intrinsic permeabilities P_0 should be linearly related

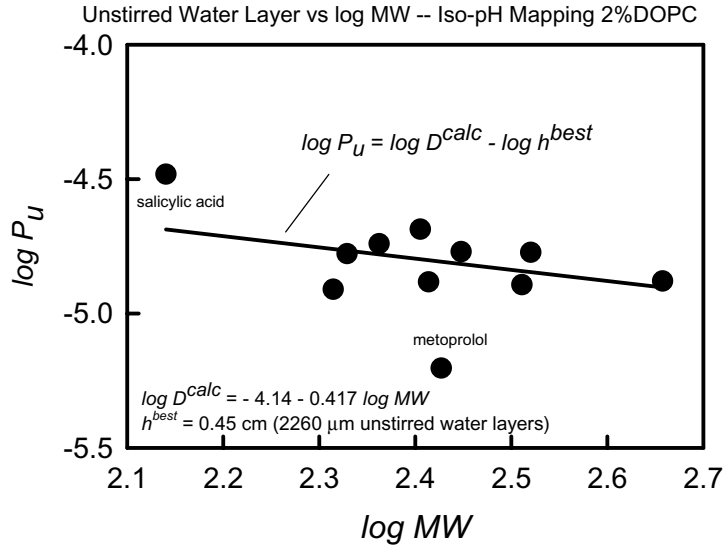

Figure 7.38 Log unstirred water permeabilities versus log molecular weights, based on analysis of iso-pH data.

to the partition coefficients, octanol–water K_p, provided the octanol–water system is a suitable model for the phospholipid system. Ideally, a plot of $\log P_0$ versus $\log K_p$ would represent case (a) in Fig. 7.19. For permeability data uncorrected for UWL effects, a case (b) relationship would be expected. The case (c) pattern in Fig. 7.19 would be expected if water pore transport were an available mechanism in PAMPA. Figure 7.39, showing $\log P_0$ (Table 7.10) versus $\log K_p$ (Table 7.4), indicates that the relationship is approximately linear (r^2 0.79) over eight orders of magnitude of permeability, suggesting the absence of water pores.

7.7.6.8 Iso-pH Permeability Measurements using Soy Lecithin–Dodecane–Impregnated Filters

The above iso-pH measurements are based on the 2% DOPC/dodecane system (model 1.0 over pH 3–10 range). Another membrane model was also explored by us. Table 7.16 lists iso-pH effective permeability measurements using the soy lecithin (20% wt/vol in dodecane) membrane PAMPA (models 17.1, 24.1, and 25.1) The negative membrane charge, the multicomponent phospholipid mixture, and the acceptor sink condition (Table 7.1) result in different intrinsic permeabilities for the probe molecules. Figure 7.40 shows the relationship between the 2% DOPC and the 20% soy iso-pH PAMPA systems for ketoprofen. Since the intrinsic permeability of ketoprofen in the soy lecithin membrane is about 20 times greater than in DOPC membrane, the flat diffusion-limited transport region of the $\log P_e$

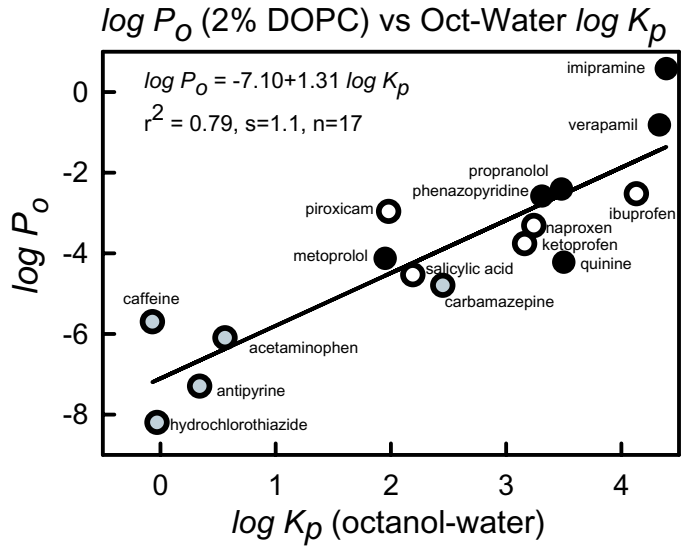

Figure 7.39 Intrinsic permeabilities (iso-pH data analysis) versus octanol–water partition coefficients.

curve is extended to higher pH values. Thus less evidence of membrane-limited transport is visible in the physiological pH range when the soy lecithin system is used. For this reason, correction for the UWL effect is all the more important when devising oral absorption prediction models, which reflect the pH gradient found in the small intestine.

TABLE 7.16 Permeability (10^{-6} cm/s units) and Retention in 20% wt/vol Soy Lecithin, at Iso-pH 5.0, 6.5, 7.4 with Sink in Acceptor Wells

Sample	pH 5.0	*%R*	pH 6.5	*%R*	pH 7.4	*%R*
Desipramine	10.4	35	19.4	35	29.7	39
Propranolol	37.4	31	26.0	37	25.8	40
Verapamil	9.1	30	20.7	20	31.6	31
Metoprolol	2.9	17	16.1	25	28.6	26
Ranitidine	0.00	4	0.03	2	0.31	14
Piroxicam	10.2	24	8.9	12	3.2	17
Naproxen	11.8	50	6.6	12	2.3	13
Ketoprofen	9.5	37	6.5	12	1.2	12
Furosemide	0.8	25	0.0	2	0.0	11
Carbamazepine	19.5	27	17.9	18	15.3	26
Antipyrine	0.9	17	3.0	11	1.7	14

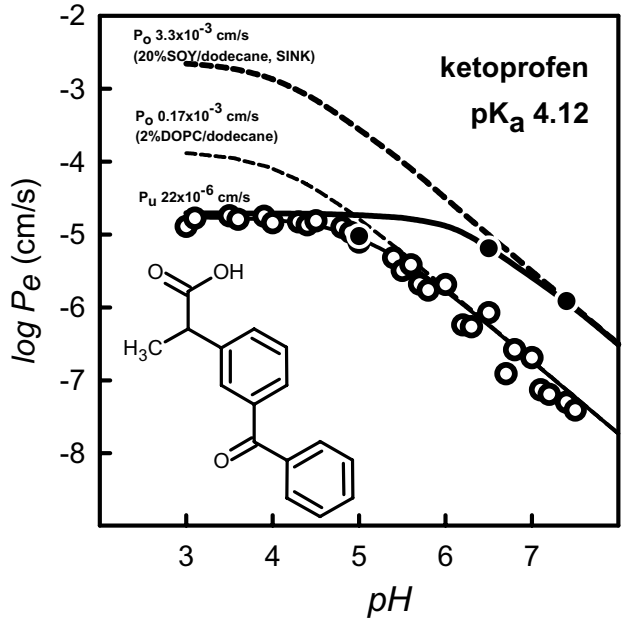

Figure 7.40 Permeability–pH profiles for ketoprofen under iso-pH conditions for two different PAMPA models: unfilled circles = 2% DOPC/dodecane, filled circles = 20% soy lecithin/dodecane. [Reprinted from Avdeef, A., in van de Waterbeemd, H.; Lennernäs, H.; Artursson, P. (Eds.). *Drug Bioavailability. Estimation of Solubility, Permeability, Absorption and Bioavailability.* Wiley-VCH: Weinheim, 2003 (in press), with permission from Wiley-VCH Verlag GmbH.]

7.7.6.9 Gradient pH Effects

The gradient pH soy lecithin, acceptor sink systems (models 26.1–30.1 in Table 7.3) were explored in the search for the best GIT PAMPA model [559]. Figures 41a–c show examples of three bases: verapamil, propranolol, and metoprolol (in order of decreasing lipophilicities; see Table 7.4). In each case, the acceptor pH was 7.4, but the donor pH values ranged from 3 to 10. Figures 42a–c show examples of three acids: naproxen, ketoprofen, and piroxicam (decreasing lipophilicity order). In all of the examples above, the diffusion-controlled zone spans a much wider pH range, compared to the DOPC system (Figs. 7.34 and 7.35). This is the consequence of increased intrinsic permeabilities in the soy-based system. Figure 7.43 shows examples of two neutral molecules: carbamazepine and antipyrine. It was possible to approximate the membrane permeability curve for carbamazepine (dashed line in Fig. 7.43), based on the analysis of the UWL permeabilities of the ionizable molecules. Antipyrine is hydrophilic and has equivalent P_m and P_e curves.

Table 7.17 summarizes the analysis of the gradient pH experiments. The range of intrinsic permeabilities spans 11 orders of magnitude! The UWL permeabilities ranged from 16 to 52×10^{-6} cm/s. Those molecules that appeared to bind strongly to the sink-forming acceptor surfactant showed UWL P_u values that were about

twice those calculated from the iso-pH nonsink assays (Table 7.15). The strong binding between the solute and the surfactant in the acceptor wells drives the unbound fraction of the solute molecules to near zero. According to the pH partition hypothesis, it is the unbound neutral species which crosses the membrane. Since its

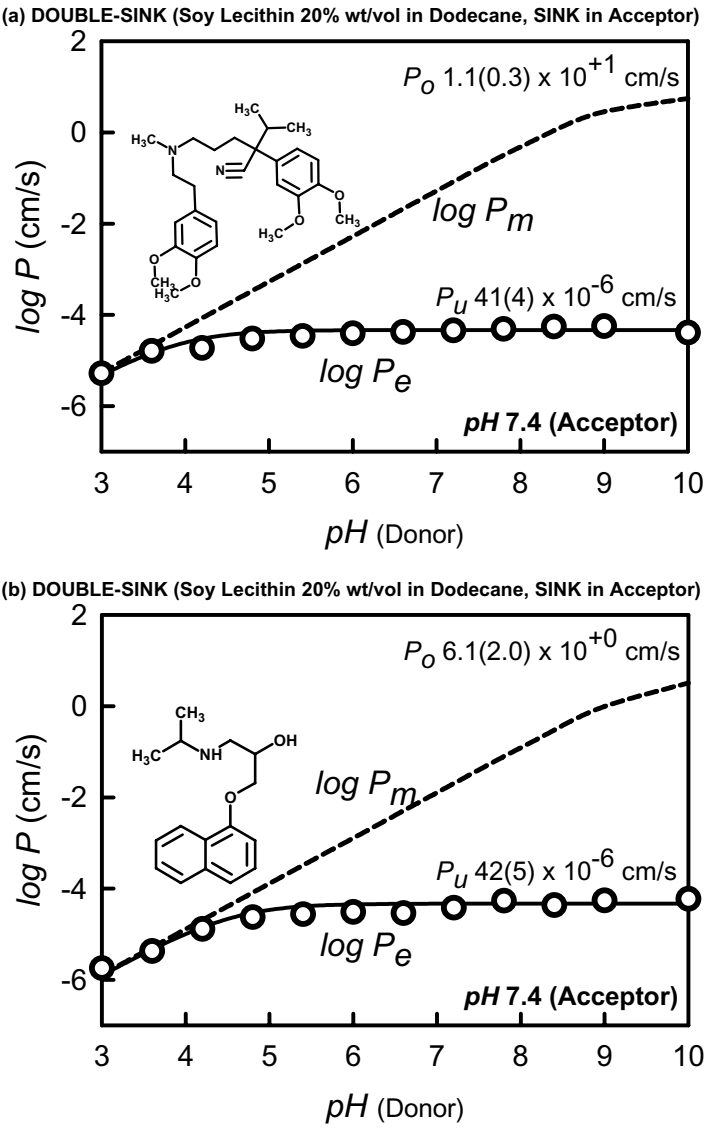

Figure 7.41 Gradient pH profiles for three weak bases with double-sink conditions, 20% wt/vol soy lecithin in dodecane: (a) verapamil (pK_a 9.07); (b) propranolol (pK_a 9.53); (c) metoprolol (pK_a 9.56).

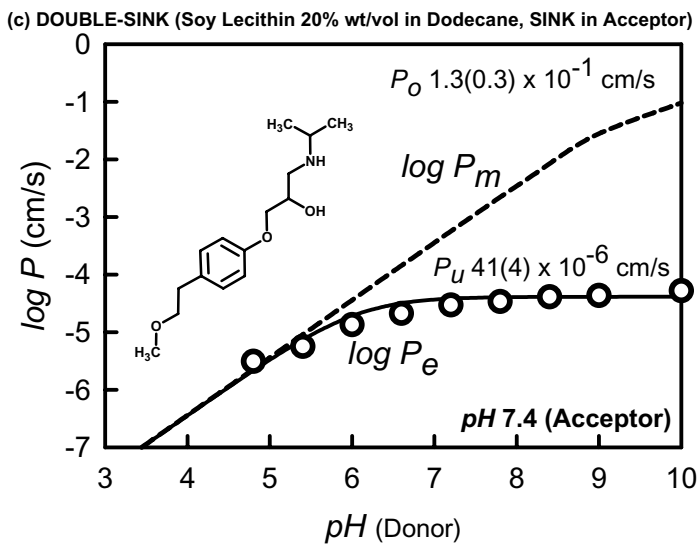

Figure 7.41 (*Continued*)

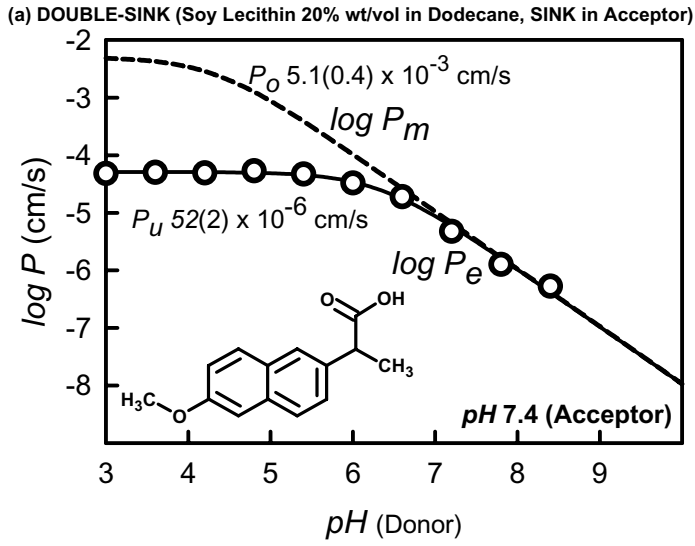

Figure 7.42 Gradient pH profiles for three weak acids with double-sink conditions, 20% wt/vol soy lecithin in dodecane: (a) naproxen (pK_a 4.32); (b) ketoprofen (pK_a 4.12); (c) piroxicam (pK_a 5.22, 2.3).

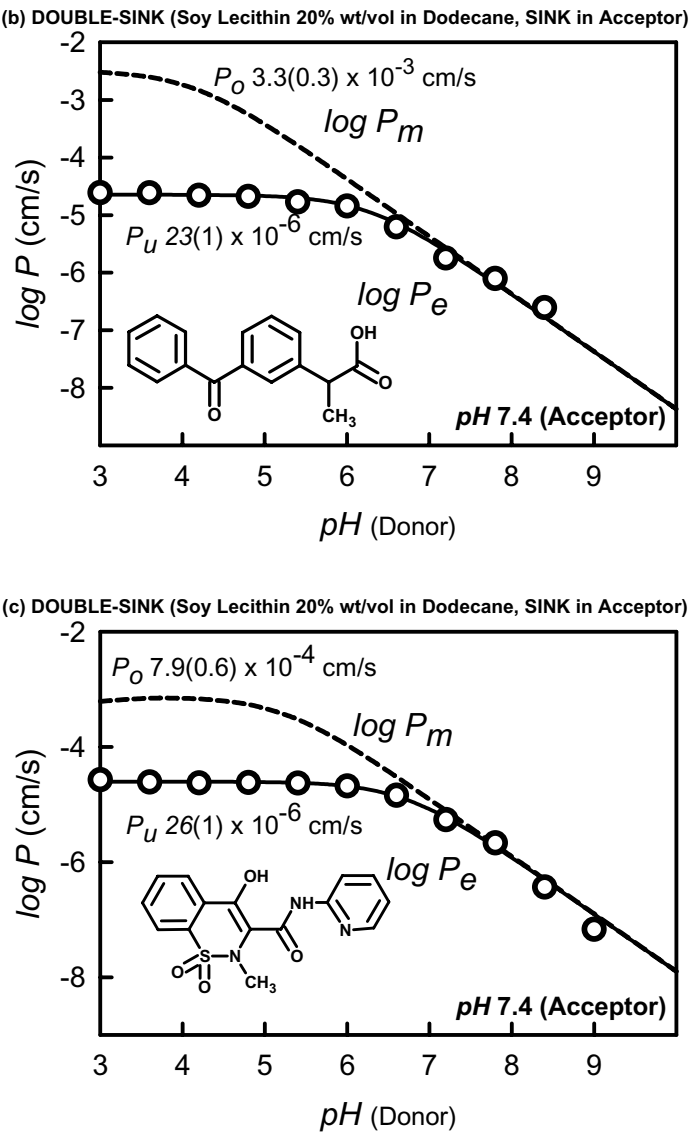

Figure 7.42 (*Continued*)

concentration is near zero, the acceptor-to-donor backflux is nil [see Eq. (7.26)]. So the UWL resistance on the acceptor side is of little consequence in the transport process. When strong binding takes place under the simulated sink condition, only the UWL on the donor side directly contributes to the overall resistance. Hence, P_u values are calculated to be about twice as large as in the case of no-sink iso-pH (Table 7.15).

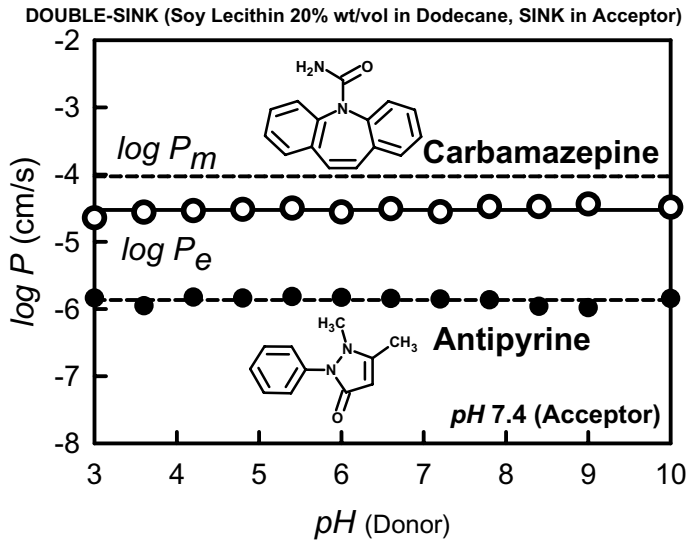

Figure 7.43 Gradient pH profiles for two nonionizable molecules: double-sink conditions, 20% wt/vol soy lecithin in dodecane.

Table 7.18 lists the interpolated apparent and membrane permeabilities, along with the membrane retentions, of the probe molecules used in the gradient pH study, at pH values 5.0, 5.5, 6.0, 6.5, and 7.4.

7.7.6.10 Collander Relationship between 2% DOPC and 20% Soy Intrinsic Permeabilities

The 20% soy lecithin (Table 7.17) and the 2% DOPC (Table 7.15) intrinsic permeabilities may be compared in a Collander equation, as shown in Fig. 7.44. The slope of the regression line, soy versus DOPC, is greater than unity. This indicates that the soy membrane is more lipophilic than the DOPC membrane. Intrinsic permeabilities are generally higher in the soy system. Three molecules were significant outliers in the regression: metoprolol, quinine, and piroxicam. Metoprolol and quinine are less permeable in the DOPC system than expected, based on their apparent relative lipophilicities and in vivo absorptions [593]. In contrast, piroxicam is more permeable in DOPC than expected based on its relative lipophilicity. With these outliers removed from the regression calculation, the statistics were impressive at r^2 0.97.

7.7.7 Evidence of Transport of Charged Species

In Section 4.8 the topic of charged-species absorption (''fact or fiction'') was first considered. The partitioning properties of some lipophilic charged molecules in the

TABLE 7.17 Intrinsic Permeabilities and the Unstirred Water Layer Permeabilities Determined from Gradient–pH Dependence of Effective Permeabilities: 20% Soy Lecithin in Dodecane, Sink in Acceptor

Compound	P_0 (cm/s) (SD)[a]	$\log P_0$ (SD)	$P_u(10^{-6}$ cm/s) (SD)[b]	$\log P_u$ (SD)	MW	pK_a ($I = 0.01$ M, 25° C)	pK_a^{FLUX}	pH Range[c]	n[d]	GOF[e]
Desipramine	$1.9\ (0.8) \times 10^{+2}$	+2.27 (0.19)	42.1 (4.1)	−4.38 (0.04)	302.8	10.16	3.7	3.0–10.0	12	2.4
Verapamil	$1.1\ (0.3) \times 10^{+1}$	+1.03 (0.14)	41.2 (3.5)	−4.39 (0.04)	454.6	9.07	3.9	3.0–9.0	11	2.0
Propranolol	6 (2)	+0.79 (0.15)	41.8 (4.7)	−4.38 (0.05)	259.3	9.53	4.5	3.0–10.0	12	2.6
Metoprolol	$1.3\ (0.3) \times 10^{-1}$	−0.88 (0.10)	41.2 (3.5)	−4.39 (0.04)	267.4	9.56	6.0	4.8–10.0	9	1.7
Quinine	$5.0(0.7) \times 10^{-2}$	−1.30 (0.06)	15.6 (0.6)	−4.81 (0.02)	324.4	4.09, 8.55	5.1	3.6–10.0	11	0.7
Naproxen	$5.1\ (0.4) \times 10^{-3}$	−2.30 (0.04)	51.8 (1.6)	−4.29 (0.01)	230.3	4.32	6.2	3.0–8.4	8	0.7
Ketoprofen	$3.3\ (0.3) \times 10^{-3}$	−2.49 (0.05)	22.8 (1.0)	−4.64 (0.02)	254.3	4.12	6.2	3.0–8.4	8	0.7
Piroxicam	$7.9\ (0.6) \times 10^{-4}$	−3.11 (0.03)	26.3 (0.8)	−4.58 (0.01)	331.4	2.33, 5.22	6.7	3.0–9.0	11	0.5
Furosemide	$1.3\ (0.1) \times 10^{-4}$	−3.90 (0.03)	17.0 (1.0)	−4.77(0.03)	330.8	3.67, 10.93	4.6	3.0–6.6	7	0.4
Carbamazepine	$9.4\ (0.6) \times 10^{-5}$	−4.03 (0.03)	44[f]	−4.36	236.3	—	—	3.0–10.0	12	1.0
Ranitidine	$5.6\ (0.6) \times 10^{-6}$	−5.25 (0.04)	19.8 (10.2)	−4.70 (0.22)	350.9	8.31	8.2	6.0–10.0	7	0.4
Antipyrine	$1.4\ (0.2) \times 10^{-6}$	−5.86 (0.06)	17[f]	−4.77	188.2	—	—	3.0–10.0	12	0.5
Terbutaline	$1.2\ (0.2) \times 10^{-7}$	−6.91 (0.08)	17[f]	−4.77	274.3	8.67, 10.12	—	3.0–10.0	12	1.0
Hydrochlorothiazide	$5\ (6) \times 10^{-9}$	−8.30 (0.49)	17[f]	−4.77	297.7	9.81, 10.25	—	3.0–10.0	5	0.8

[a] P_0 = intrinsic permeability, SD = estimated standard deviation.
[b] P_u = unstirred water permeability.
[c] Data range actually used in the regression analysis.
[d] Number of P_e measurements.
[e] GOF = goodness of fit in the weighted nonlinear regression analysis.
[f] Carbamazepine, antipyrine, terbutaline, and hydrochlorothiazide were treated as neutral molecules. Their effective permeabilities were corrected for the unstirred water layer using estimated unstirred water layer permeabilities, determined by the other molecules of similar lipophilicities and size.

TABLE 7.18 Interpolated Apparent and Membrane Permeabilities Determined from Double-Sink Conditions: 20% Soy Lecithin in Dodecane

	pH 5.0			pH 5.5			pH 6.0			pH 6.5			pH 7.4		
Compound	P_a (10^{-6} cm/s)	P_m (cm/s)	%R	P_a (10^{-6} cm/s)	P_a (cm/s)	%R	P_a (10^{-6} cm/s)	P_m (cm/s)	%R	P_a (10^{-6} cm/s)	P_m (cm/s)	%R	P_a (10^{-6} cm/s)	P_m (cm/s)	%R
Verapamil	39	9.2×10^{-4}	28	41	2.9×10^{-3}	30	41	9.2×10^{-3}	29	41	0.029	32	41	0.23	34
Quinine	7	1.4×10^{-5}	55	12	4.5×10^{-5}	56	14	1.4×10^{-4}	58	15	4.4×10^{-4}	58	16	3.3×10^{-3}	59
Propranolol	34	1.8×10^{-4}	35	39	5.7×10^{-4}	38	41	1.8×10^{-3}	39	42	5.7×10^{-3}	39	42	0.045	39
Desipramine	41	1.3×10^{-3}	34	42	4.0×10^{-3}	35	42	0.013	36	42	0.040	37	42	0.32	39
Metoprolol	3	3.6×10^{-6}	19	9	1.1×10^{-5}	20	19	3.6×10^{-5}	24	30	1.1×10^{-4}	24	39	9.0×10^{-4}	25
Ranitidine	0.003	2.7×10^{-9}	16	0.009	8.7×10^{-9}	16	0.03	2.7×10^{-8}	17	0.09	8.6×10^{-8}	17	0.6	6.1×10^{-7}	19
Naproxen	49	2.7×10^{-4}	22	44	3.1×10^{-4}	22	35	1.0×10^{-4}	21	20	3.3×10^{-5}	20	4	4.2×10^{-6}	13
Ketoprofen	22	3.8×10^{-4}	21	19	1.3×10^{-4}	21	15	4.2×10^{-5}	20	9	1.3×10^{-5}	19	2	1.7×10^{-6}	16
Hydrochlorothiazide	0.005	5.0×10^{-9}	16	0.005	5.0×10^{-9}	16	0.005	5.0×10^{-9}	16	0.005	5.0×10^{-9}	14	0.005	5.0×10^{-9}	14
Furosemide	4.2	5.6×10^{-6}	42	1.7	1.8×10^{-6}	34	0.6	5.9×10^{-7}	32	0.2	1.9×10^{-7}	24	0.02	2.3×10^{-8}	19
Piroxicam	25	4.9×10^{-4}	28	24	2.7×10^{-4}	25	21	1.1×10^{-4}	23	16	3.9×10^{-5}	17	4	5.1×10^{-6}	16
Terbutaline	0.1	1.2×10^{-7}	18	0.1	1.2×10^{-7}	18	0.1	1.2×10^{-7}	18	0.1	1.2×10^{-7}	19	0.1	1.2×10^{-7}	19
Carbamazepine	30	9.4×10^{-5}	29	30	9.4×10^{-5}	29	30	9.4×10^{-5}	29	30	9.4×10^{-5}	29	30	9.4×10^{-5}	29
Antipyrine	1.3	1.4×10^{-6}	14	1.3	1.4×10^{-6}	14	1.3	1.4×10^{-6}	14	1.3	1.4×10^{-6}	14	1.3	1.4×10^{-6}	14

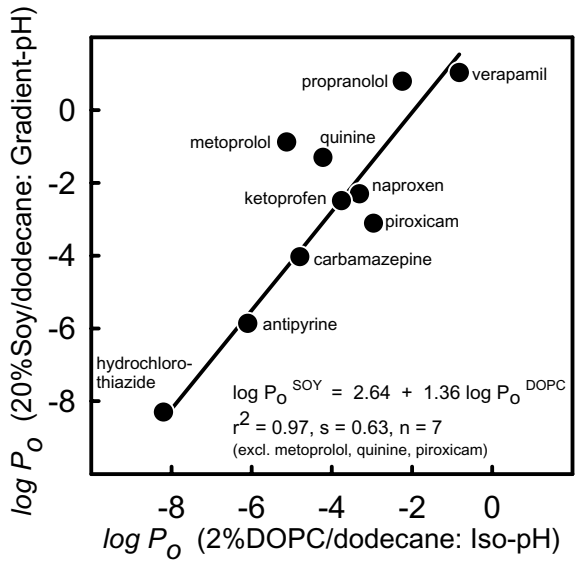

Figure 7.44 Collander relationship between intrinsic permeabilities of 20% soy lecithin versus 2% DOPC PAMPA models.

octanol–water system might suggest that, given a background solution of a lipophilic counterion, ion pair transmembrane transport takes place (e.g., Section 4.5). Such hypotheses can be tested in a direct way in the PAMPA assay. If the charged species, especially quaternary ammonium drugs, appear in the acceptor compartment, the case for charged species transport could be further advanced. It is very difficult to make the case for charged-species transmembrane transport using the in vitro cultured cell model, because of the simultaneous presence of several possible transport mechanisms [1].

7.7.7.1 The Case for Charged-Species Transport from Cellular and Liposomal Models

Trimethylaminodiphenylhexatriene chloride (TMADPH; Fig. 7.45) is a fluorescent quaternary ammonium molecule that appears to permeate cell membranes [595]. TMADPH fluoresces only when it is in the bilayer, and not when it is dissolved in water. Therefore, its location in cells can be readily followed with an imaging fluorescence microscope. One second after TMADPH is added to the extracellular solution bathing HeLa cell types, the charged molecule fully equilibrates between the external buffer and the extracellular (outer) leaflet bilayer. Washing the cells for one minute removes >95% of the TMADPH from the outer leaflet. If the cells are equilibrated with TMADPH for 10 min at 37°C, followed by a one-minute wash that removed the TMADPH from the outer leaflet, the fluorescent molecule is

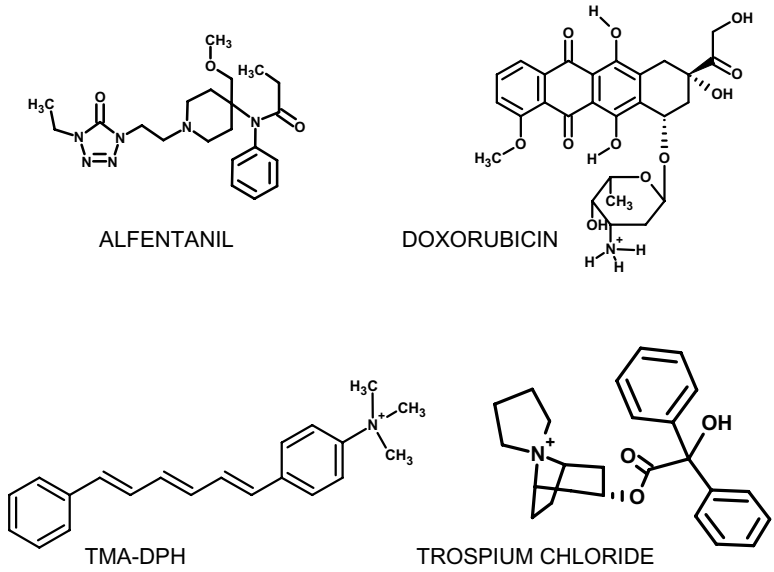

Figure 7.45 Molecules that may violate the pH partition hypothesis.

seen concentrated in the perinuclear and the mitochondrial membranes inside the cytoplasm. This indicates that the charged molecule somehow crossed the cell wall. Endocytosis is not likely to be the influx mechanism, because the charged molecule would not have been able to interact with the perinuclear and mitochondrial membranes. P-gp transfected HeLa cells showed decreased intracellular fluorescence, but the concentration of the fluorescent molecule in the outer leaflet was not affected by P-gp presence. When cyclosporin A, a known P-gp inhibitor, was added, TMADPH intracellular accumulation was reestablished. Since P-gp is postulated to interact with its substrates brought to the active site at the inner leaflet position of the bilayer [596], TMADPH must be somehow crossing the bilayer to get into the inner leaflet. These observations led Chen et al. [595] to propose a flip-flop mechanism, since active transporters for TMADPH were not seen. However, the possibility of a surface protein assisted transport could not be ruled out. Since several transport mechanisms are possible, the unequivocal route is not established with certainty. An ideal follow-up experiment would have utilized ''ghost'' vesicles formed from protein-free reconstituted HeLa cell lipids. Such an experiment has not been reported.

Regev and Eytan [597] studied the transport properties of doxorubicin (Fig. 7.45) across bilayers, using model liposomes formed from anionic phosphatidylserine and ''ghost'' erythrocytes. Doxorubicin, unlike TMADPH, can undergo charge-state changes. At neutral pH, the amine on the daunosamine moiety is expected to be positively charged ($pK_a \sim 8.6$). The phenolic protons are expected to have

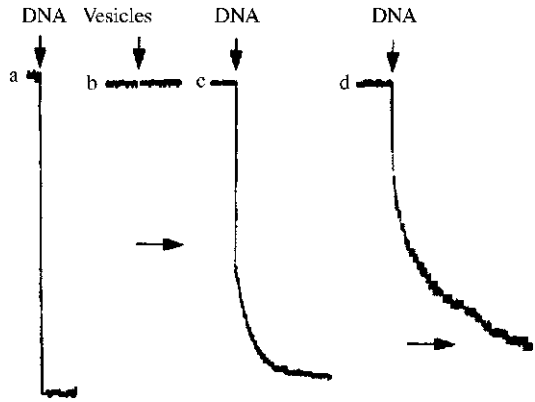

Figure 7.46 Fluorescence quenching of doxorubicin by DNA [597]: (a) doxorubicin in aqueous solution, quenched immediately on addition of DNA; (b) doxorubicin fluorescence not affected by vesicles; (c) Doxorubicin preequilibrated with vesicles, and then subjected to DNA. The fraction bound to the outer membrane leaflet is immediately quenched by the DNA. (d) Same as (c), but multilamellar vesicles used. The left arrow represents a 5-min interval and applies to the first three cases; the right arrow represents 30-min interval and applies to (d) only. [Reprinted from Ronit Regev and Gera D. Eylan, *Biochemical Pharmacology*, vol. 54, 1997, pp. 1151–1158. With permission from Elsevier Science.]

p$K_a > 11$, due to the likely formation of six-membered ring intramolecular H bonds. Doxorubicin is mildly lipophilic, with an octanol–water log K_p 0.65 (slightly less than morphine) and log K_d of -0.33. It is not very permeable across 2% DOPC/dodecane PAMPA membranes ($P_e \sim 4 \times 10^{-9}$ cm/s). About 90% of doxorubicin is surface-bound in PS liposomes [597]. Doxorubicin is fluorescent in water. Its fluorescence is quickly quenched by interactions with DNA; an aqueous solution of doxorubicin is immediately quenched by the addition of DNA, as shown in curve (a) of Fig. 7.46, where the left arrow represents 5 min and applies to curves (a)–(c) in Fig. 7.46. Vesicles don't affect the fluorescence [Fig. 7.46, curve (b)]. However, a solution equilibrated with doxorubicin and unilamellar liposomes, is 50% quenched instantly, and 100% quenched after about 5 min (1.1–1.3 min half-life at 23°C), as shown in curve (c) of Fig. 7.46 [597]. This indicates that the outer leaflet doxorubicin (50% of the total) is immediately quenched, and the intravesicular doxorubicin takes $\sim$1 min to permeate out, by crossing the bilayer, presumably as a charged species at neutral pH. Curve (d) of Fig. 7.46 represents a multilamellar liposome extraction quenching, where the right arrow is $\sim$30 min long. About 20% of the doxorubicin is quickly quenched, but the rest of the drug takes about 2 h to quench, since many bilayers need to be crossed by the positively charged molecule. Still, these observations do not prove that the actual permeating molecule is charged. The molecule (charged in the aqueous phase) may be permeating as the neutral species (in the membrane phase). The only clue that perhaps some degree of charged species permeation is taking place comes from the observation

that at pH 9.7, the transcellular transport is increased only twofold. If the pH partition hypothesis were valid, and the pK_a were 8.6, then changing pH from 7.4 to 9.7 should have increased transport by much more than a factor of 2. It would have been interesting to perform the experiments of Regev and Eytan using TMADPH, to unequivocally demonstrate the violation of the pH partition hypothesis.

Trospium chloride, a quaternary ammonium drug (Fig. 7.45), appears to be a substrate of P-gp, and it can be taken up by cells quicky [597]. The evidence for transmembrane diffusion appears substantial. The molecule is very soluble in water (>50 mg/mL), but not in lipids (9.2 μg/mL in mineral oil); the octanol-water log K_p is −1.22 [598]. The human intestinal absorption (HIA) is 11%; the molecule is not metabolized. In cell intestinal patch uptake studies, trospium is absorbed from a 7.5 mM solution at the rate of 7 μg/h, after a slow 60-min buildup to an approximate steady state flux. At donor concentration of 0.5 mM, rat Caco-2 P_e is 8×10^{-7} cm s^{-1}. At the higher concentration of 45 mM, the permeability increases to 2.2×10^{-6} cm s. This suggests that an efflux transporter is saturable. At 5 mM trospium concentration, the apical-to-basolateral permeability is 7 times lower than the basolateral-to-apical permeability. Verapamil (P-gp inhibitor) equalizes the above two permeabilities. Since the mechanism of P-gp efflux involves the interaction of the substrate from the inner leaflet of the bilayer [596], trospium is somehow crossing lipid bilayers. But since cells were used, it is difficult to rule out a carrier-mediated transport. More light could be shed with simpler models, perhaps using ''ghost'' erythrocytes or PAMPA.

Palm et al. [578] studied the Caco-2 permeabilities of two molecules, alfentanil (Fig. 7.45) and cimetidine, whose pK_a values were near neutral (6.5 and 6.8, respectively), but whose octanol–water partition coefficients, log K_p, were more than an order of magnitude different (2.2 and 0.4, respectively). The group studied the permeabilities over a range of pH values, from 4 to 8, something that is very rarely done in Caco-2 assays. The viability of the cells was demonstrated for pH 4.8–8.0. The analysis of the pH-dependent permeability data indicated that the positive-charge form of alfentanyl had a permeability coefficient $(1.5 \times 10^{-6}\,\text{cm/s})$ that was substantially greater than that of cimetidine $(5 \times 10^{-8}\,\text{cm/s})$. Since alfentanyl has a molecular weight of 416 (cimetidine has 252), it is not expected to transport by the paracellular route. The authors proposed that the charged form of the drug can permeate membrane by passive transcellular diffusion.

7.7.7.2 PAMPA Evidence for the Transport of Charged Drugs

It is difficult to prove that quaternary ammonium compounds can cross lipid bilayers using cell uptake experiments, since several mechanisms may be operative, and separating contributions from each may be very difficult [1]. It may be an advantage to use PAMPA to investigate transport properties of permanently ionized molecules. Of all the molecules whose permeabilities were measured under iso-pH conditions in 2% DOPC/dodecane, verapamil, propranolol, and especially quinine seem to partially violate the pH partition hypothesis, as shown in Figs. 7.47a–c. In Fig. 7.47c, the solid line with slope of +1 indicates the expected effective permeability if the pH partition hypothesis were strictly adhered to. As can be seen at pH 4

in the figure, quinine is about 100 times more permeable than predicted from the pH partition hypothesis. Instances of acids violating the pH partition hypothesis have not been reported.

When negatively charged membranes are used, the weak bases no longer appear to violate the pH partition hypothesis, as indicated in Fig. 7.48 for quinine. It appears that the negative membrane surface charge and the positive drug charge leads to electrostatic interactions that inhibit the passage of charged drugs through the membranes. These observations will be further explored in our laboratory.

7.7.8 $\Delta \log P_e$–Hydrogen Bonding and Ionic Equilibrium Effects

Most drug-like molecules dissolved in water form hydrogen bonds with the solvent. When such a molecule transfers from water into a phospholipid bilayer, the solute–water hydrogen bonds are broken (desolvation), as new solute–lipid H bonds form in the lipid phase. The free-energy difference between the two states of solvation has direct impact on the ability of the molecules to cross biological barriers.

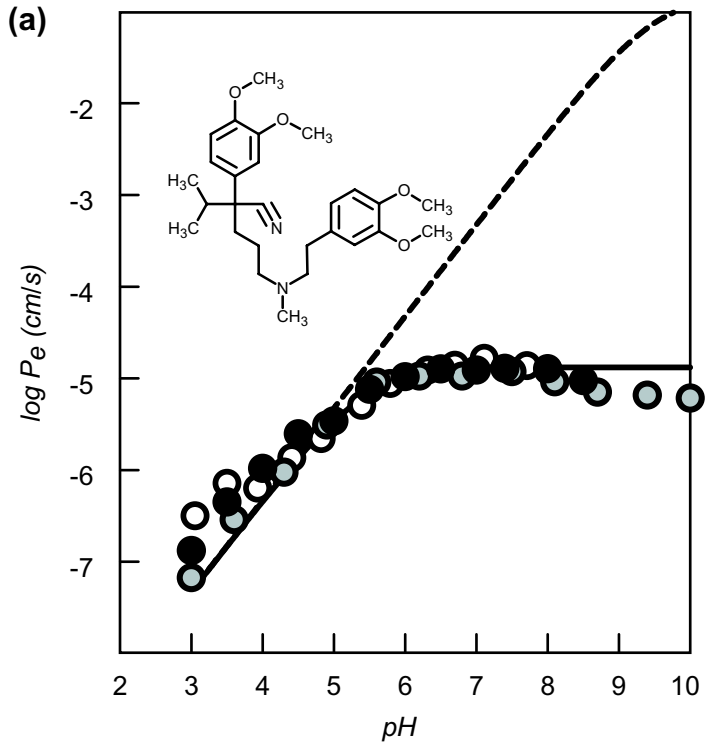

Figure 7.47 Examples of three bases that appear to violate the pH partition hypothesis in 2% DOPC/dodecane PAMPA models: (a) verapamil (pK_a 9.07); (b) propranolol; (c) guinine (pK_a 8.55, 4.24).

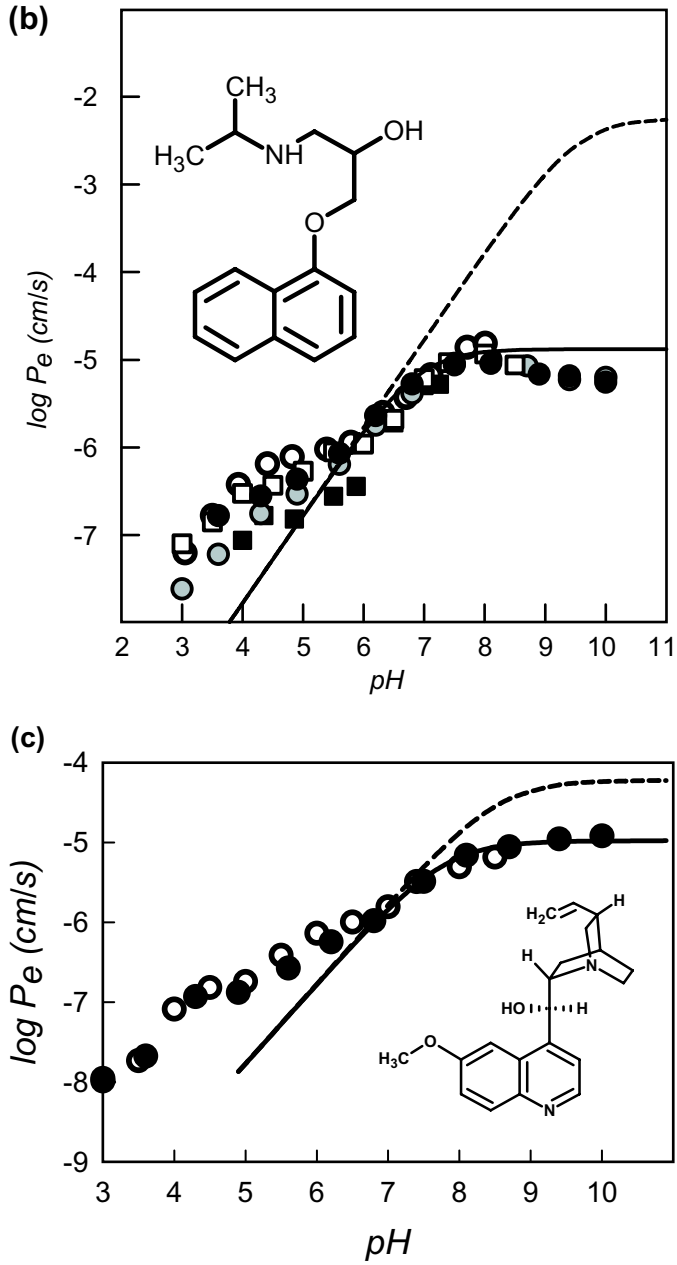

Figure 7.47 (*Continued*)

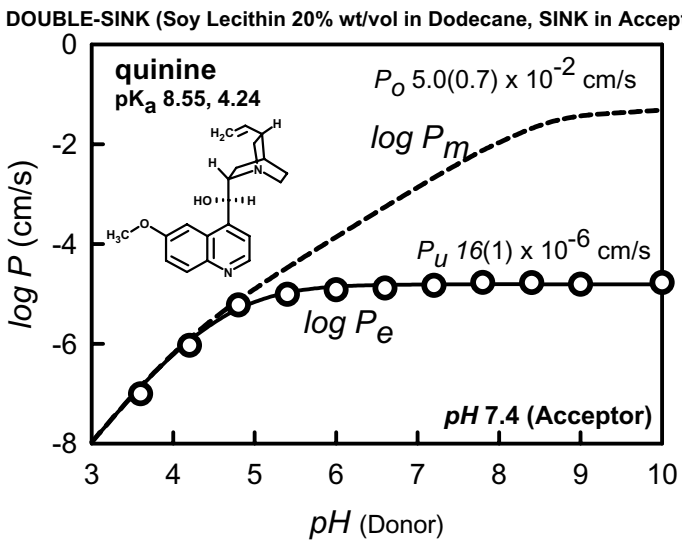

Figure 7.48 Negatively charged PAMPA models showing no evidence for violation of the pH partition hypothesis.

Seiler [250] proposed a way of estimating the extent of hydrogen bonding in solute partitioning between water and a lipid phase by measuring the so-called $\Delta \log P$ parameter. The latter parameter is usually defined as the difference between the partition coefficient of a solute measured in the octanol–water system and that measured in an inert alkane–water suspension: $\Delta \log P = \log K_{p,\,\mathrm{oct}} - \log K_{p,\,\mathrm{alk}}$.

Young et al. [599] demonstrated the usefulness of the $\Delta \log P$ parameter in the prediction of brain penetration of a series of H_2-receptor histamine antagonists. Neither $\log K_{p,\,\mathrm{oct}}$ nor $\log K_{p,\,\mathrm{alk}}$ was found to correlate with brain penetration, log BB (where BB is defined as the ratio of the compound concentration in the brain and the compound concentration in plasma). However, the difference between the two partition coefficients correlated well, as shown in Fig. 7.49. When the difference is large, so is the H bonding expressed by the solute, and less brain penetration is expected. It was suggested that the $\Delta \log P$ parameter accounts for H-bonding ability and reflects two distinct processes—alkane encodes the partitioning into nonpolar regions of the brain and octanol encodes protein binding in the peripheral blood. El Tayar et al. [255] elaborated that the parameter contains information on the capacity of a solute to donate H bonds; the rate-limiting step in brain penetration was proposed to be the donation of H bonds of solute to hydrophilic parts of lipids in the blood–brain barrier (BBB). Van de Waterbeemd and Kansy [251] re-examined Young et al. [599] data with solvatochromic equations for identifying physicochemical properties governing solubility and partitioning. They suggested that the combination of calculated molar volumes and just the log $\log K_{p,\mathrm{alk}}$ could

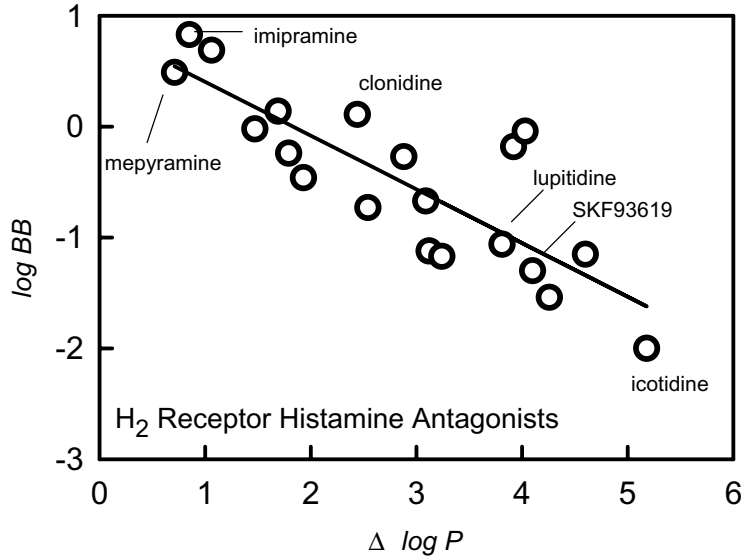

Figure 7.49 Brain penetration and Δ log P (from Young et al. [599]).

substitute for two-lipid partition measurements, thus reducing the amount of measurement needed. Also, they introduced the use of polar surface areas as an interesting alternative to the use of $\Delta \log P$. Abraham et al. [257] analyzed the $\Delta \log P$ parameter in terms of the Abraham descriptors to broaden the understanding of the concept. Von Geldern et al. [252] used the $\Delta \log P$ parameter to optimize structural modifications to a series of endothelin A-receptor antagonists to improve gut absorption. A urea fragment in their series of molecules had NH residues systematically replaced with NCH_3, O, and CH_2, and correlations between $\Delta \log P$ and antagonist selectivity effectively guided the optimization procedure.

Avdeef et al. [556] measured the PAMPA permeabilities of a series of drug molecules and natural products using both dodecane- and (dodecane + 2%DOPC)-coated filters. It was proposed that a new H-bonding scale could be explored, based not on partition coefficients but on permeabilities.

$$\Delta \log P_e = \log P_e^{2\%\text{DOPC}} - \log P_e^{\text{dodecane}} \tag{7.61}$$

Figure 7.50 shows $\Delta \log P_e$ (difference permeability) versus $\log P_e$ (dodecane-treated filters) for a series of common drugs and research compounds at pH 7.4. Some of the differences are positive, and some are negative. For example, phenazopyridine is attenuated by the presence of DOPC in the dodecane, but diltiazem is accelerated by the DOPC [556]. The effects are most pronounced where the permeability in pure dodecane is less than about 3×10^{-6} cm/s. That is, molecules that are very permeable in dodecane are unaffected by the presence of DOPC, as

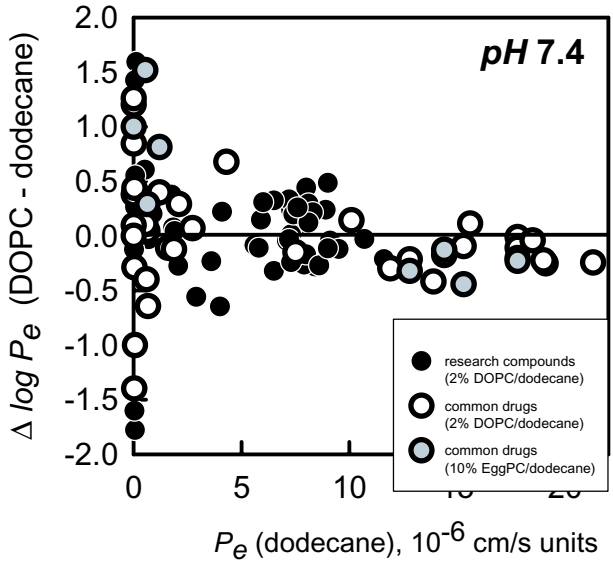

Figure 7.50 Hydrogen bonding/electrostatics scale based on phospholipid–alkane permeability differences: Δ log P_e versus P_e (dodecane).

indicated in Fig. 7.50. Both H-bonding and ionic interactions may be encoded in the $\Delta \log P_e$ parameter. This topic is the subject of further investigation at *p*ION, with the aim of developing BBB PAMPA models.

7.7.9 Effects of Cosolvent in Donor Wells

Many research compounds are poorly soluble in water. When very lipophilic molecules precipitate in the donor wells, it is possible to filter the donor solution before the PAMPA sandwich is prepared. On occasion, the filtered donor solution contains such small amounts of the compound that determination of concentrations by UV spectrophotometry becomes impractical. One strategy to overcome the precipitation of the sample molecules in the donor wells is to add a cosolvent to the solutions (Section 7.4.4). It is a strategy of compromise and practicality. Although the cosolvent may solubilize the lipophilic solute molecule, the effect on transport may be subtle and not easy to predict. At least three mechanisms may cause P_e and membrane retention (%*R*) values to alter as a result of the cosolvent addition. To a varying extent, all three mechanisms may simultaneously contribute to the observed transport:

1. The cosolvent will lower the dielectric constant of the mixed solvent, independent of the properties of the solute molecule. The ionization constant of acids will increase and that of bases will decrease (see Sections 3.3.3 and 3.3.4), the result of which is to increase the fraction of uncharged substance in

solution (f_u in Table 7.4). With an increased concentration of the uncharged species in the donor solution, both P_e and $\%R$ are expected to *increase*. Generally, this effect is minimal for cosolvent amounts less than 10% vol/vol [119,172].

2. The cosolvent may increase the aqueous solubility of the sparingly soluble molecules, which would lower the membrane–donor solution partition coefficient. According to Eq. (2.3), P_e will *decrease*. Since $\%R$ is related to lipophilicity (Section 7.7.2), the retention is also expected to *decrease*.
3. Sparingly soluble surface-active molecules, such as chlorpromazine, may form water-soluble high-molecular-weight (HMW) aggregates (Sections 6.2, 6.5.2, 6.5.3). Their diffusion in the unstirred water layer will decrease according to Eq. (7.60). Cosolvent may break up these aggregates, resulting in *increased* P_e, and to a lesser extent, an *increased* $\%R$.

Table 7.19 summarizes the PAMPA (2% DOPC in dodecane) transport properties of several molecules, with and without 10% 1-propanol in the donor wells. This particular cosolvent was selected for its low UV absorbance and low volatility.

The most dramatic effects are with the bases. The first seven bases in Table 7.19 are the most lipophilic. Cosolvent causes their $\%R$ to decrease, consistent with effect (2) listed above. For the three least-lipophilic bases, $\%R$ increases with cosolvent, consistent with effect (1). Chlorpromazine and verapamil experience

TABLE 7.19 Effect of 10% 1-Propanol, pH 7.4[a]

Sample	2% DOPC (Model 1.0) P_e(SD)	$\%R$	2% DOPC (Cosolvent) P_e(SD)	$\%R$
Chlorpromazine	5.5 (0.4)	85	18.0 (8.9)	71
Phenazopyridine	8.4 (1.1)	70	6.5 (0.3)	50
Verapamil	9.7 (1.0)	39	19.4 (3.1)	25
Promethazine	7.3 (0.7)	70	3.1 (0.2)	34
Propranolol	10.0 (0.5)	18	8.3 (1.7)	12
Desipramine	12.3 (0.4)	40	5.3 (0.4)	22
Primaquine	1.4 (0.1)	70	2.6 (0.4)	26
Alprenolol	11.8 (0.3)	16	10.2 (2.5)	28
Metoprolol	0.69 (0.04)	11	1.5 (0.1)	27
Amiloride	0.002 (0.005)	0	0.03 (0.04)	19
Naproxen	0.33 (0.03)	4	1.6 (0.2)	25
Sulfasalazine	0.007 (0.004)	1	0.04 (0.01)	26
Theophylline	0.04 (0.01)	1	0.33 (0.05)	15
Salicyclic acid	0.006 (0.004)	1	0.13 (0.05)	19
Sulpiride	0.01 (0.01)	1	(nd)	10
Terbutaline	0.04 (0.01)	6	(nd)	12

[a]All P_e and SD(P_e) are in units of 10^{-6} cm/s; (nd) = compound not detected in the acceptor compartment.

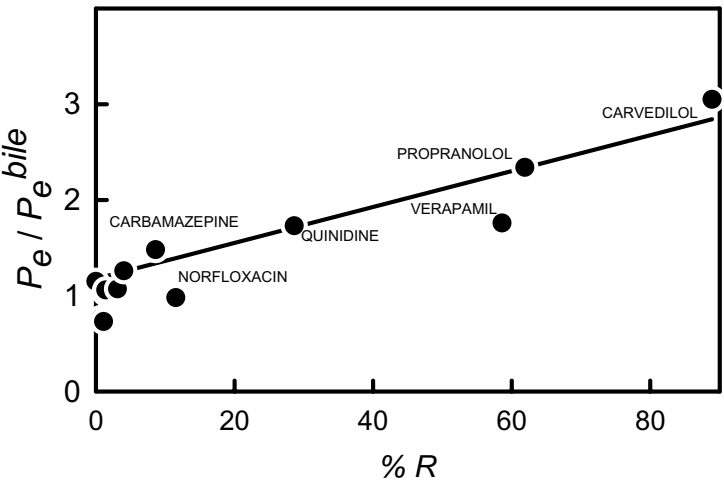

Figure 7.51 Effect of bile salt on permeability in donor well at pH 6.5.

significantly elevated P_e, consistent with effects (1) and (3). The four acids in the Table 7.19 behave according to effect (1) listed above; both P_e and $\%R$ are elevated. The two ampholytes may also be affected this way, judging by the increased $\%R$.

7.7.10 Effects of Bile Salts in Donor Wells

An alternative method to overcome the solubility problem mentioned in the last section is to use bile salts to solubilize lipophilic molecules in the donor wells. Figure 7.51 shows a plot of relative permeability (P_e without bile/P_e with bile) versus membrane retention, which is related to lipophilicity (Section 7.7.2). As the plot shows, the most lipophilic molecules (carvedilol, propranolol, and verapamil) have attenuated permeabilities (by a factor of 3 in the case of carvedilol). The effective partition coefficient between the PAMPA membrane phase and the aqueous phase containing bile salt micelles [577] is expected to be lower for lipophilic molecules, which should result in lower P_e values. This is evident in the figure.

7.7.11 Effects of Cyclodextrin in Acceptor Wells

The method for creating acceptor sink condition discussed so far is based on the use of a surfactant solution. In such solutions, anionic micelles act to accelerate the transport of lipophilic molecules. We also explored the use of other sink-forming reagents, including serum proteins and uncharged cyclodextrins. Table 7.20 compares the sink effect of 100 mM β-cyclodextrin added to the pH 7.4 buffer in the acceptor wells to that of the anionic surfactant. Cyclodextrin creates a weaker sink for the cationic bases, compared to the anionic surfactant. The electrostatic binding force between charged lipophilic bases and the anionic surfactant micelles

TABLE 7.20 Effect of 100 mM β-Cyclodextrin in Acceptor Wells, pH 7.4[a]

Sample	20% Soy (Model 17.0) P_e(SD)	%R	20% Soy (Cyclodextrin) P_e(SD)	%R	20% Soy (Model 17.1) P_e(SD)	%R
Verapamil	1.1 (0.1)	94	3.5 (0.4)	53	31.6 (2.8)	31
Propranolol	1.8 (0.5)	95	3.4 (0.4)	61	25.1 (1.7)	36
Desipramine	0.6 (0.7)	93	9.3 (5.7)	56	29.8 (0.2)	39
Metoprolol	8.2 (1.2)	42	21.0 (0.7)	26	26.5 (1.1)	23
Ranitidine	0.36 (0.01)	13	0.20 (0.04)	8	0.31 (0.03)	14
Naproxen	3.4 (0.1)	9	3.6 (0.2)	9	2.9 (0.1)	13
Ketoprofen	1.5 (0.1)	9	1.2 (0.1)	11	1.2 (0.1)	12
Hydrochlorothiazide	0.01 (0.01)	9	0.01 (0.03)	9	0.004 (0.004)	12
Furosemide	0.04 (0.02)	11	0.05 (0.01)	0	0.02 (0.01)	11
Piroxicam	3.6 (0.1)	2	3.2 (0.2)	9	3.2 (0.2)	17
Terbutaline	0.20 (0.14)	2	(nd)	7	0.1 (0.2)	13
Carbamazepine	10.8 (0.3)	37	22.9 (0.9)	25	15.2 (0.7)	26
Antipyrine	1.5 (0.1)	9	2.1 (0.3)	9	1.6 (0.1)	13

[a]All P_e and SD(P_e) are in units of 10^{-6} cm/s; (nd) = compound not detected in the acceptor compartment.

is missing in the cyclodextrin system. Some molecules (e.g., metoprolol, carbamazepine) may have the suitable shape to take advantage of strong cyclodextrin binding, and thus indicate substantially increased permeabilities.

7.7.12 Effects of Buffer

Gutknecht and Tosteson [535] considered the effect of buffer on the transport of salicylic acid across a single bilayer (BLM). Buffers affect the magnitude of the pH gradient formed in the unstirred water layer as the result of the diffusion of ionizable permeants. (This is in addition to bulk solution pH gradient conditions formed by the added buffers.) In turn, the pH at the membrane–water interface affects the concentration of the uncharged (membrane-permeant) species, and thus contributes to the magnitude of the permeant concentration gradient in the membrane phase. The gradient pH permeation cell considered in the abovementioned study [535] (unbuffered in Fig. 7.52a or buffered in Fig. 7.52b) consisted of a pH 3.9 donor solution, a membrane, and a phosphate buffered acceptor solution. The flux (10^{-8} mol cm^{-2} s^{-1} units) was measured to be 0.09 in the unbuffered solution and 3.9 in the buffered solution. The buffer attenuates the pH gradient in the donor-side unstirred water layer and causes the pH at the donor-side surface of the membrane to be 4.81, (Fig. 7.52a) compared to pH 7.44 (Fig. 7.52b) in the unbuffered donor solution. With the lower pH, the fraction of uncharged salicylic acid at the membrane–water interface is higher, and so transport is increased (43 times), over the condition of the unbuffered solution.

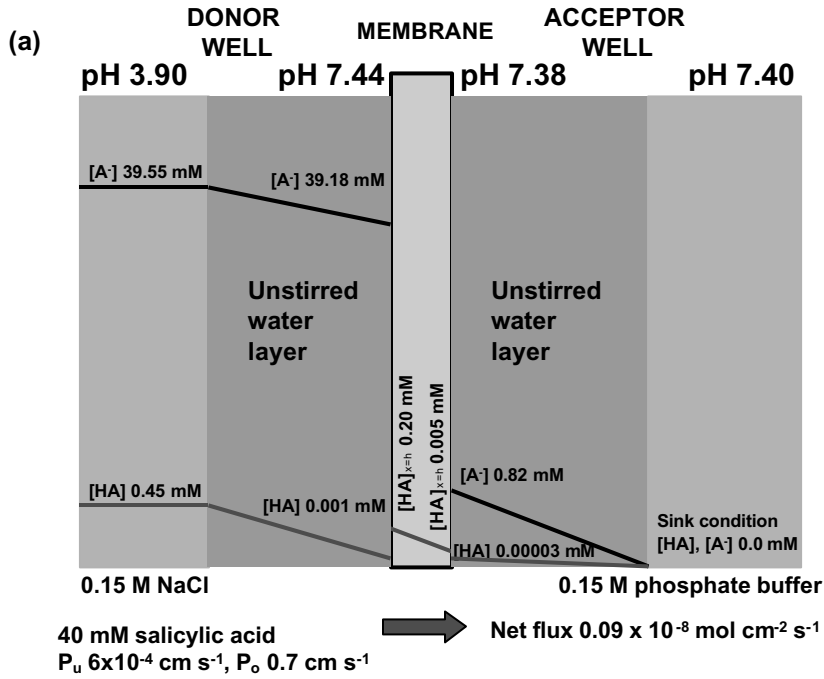

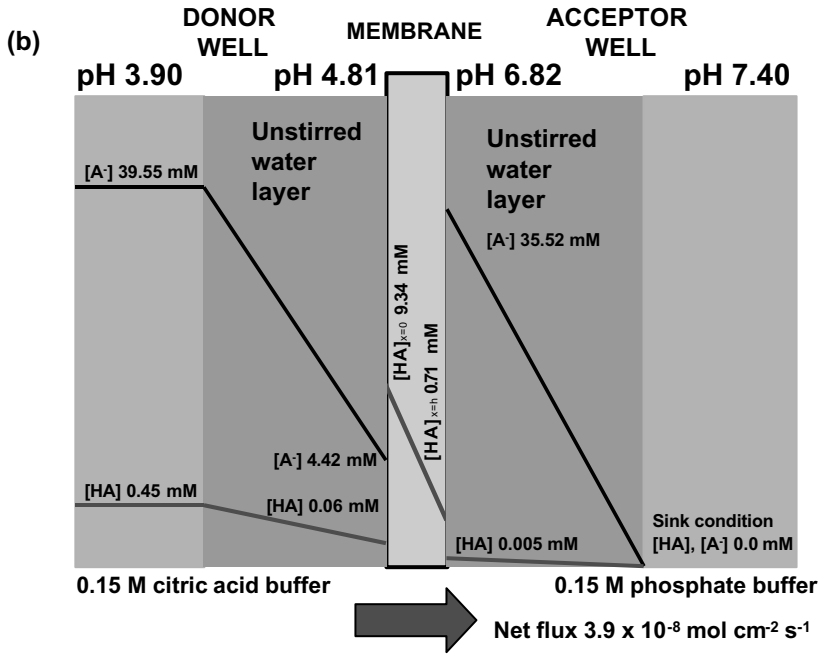

Figure 7.52 Effect of buffer on flux.

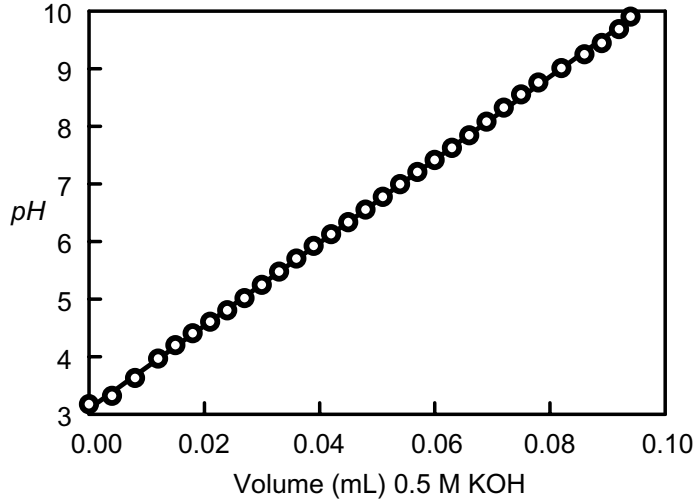

Figure 7.53 Universal buffer for robotic pH adjustment.

Antonenko et al. [540] considered pH gradients forming in the UWL under bulk solution iso-pH conditions. They elegantly expanded on the buffer effect model and made it more general by considering multicomponent buffer mixtures. Direct measurements of the pH gradients (using wire-coated micro-pH electrodes) near the membrane-water interface were described.

A 10 mM ionic strength universal buffer mixture, consisting of Good zwitterionic buffers, [174] and other components (but free of phosphate and boric acid), is used in the *p*ION apparatus [116,556]. The 5-pK_a mixture produces a linear response to the addition of base titrant in the pH 3–10 interval, as indicated in Fig. 7.53. The robotic system uses the universal buffer solution for all applications, automatically adjusting the pH with the addition of a standardized KOH solution. The robotic system uses a built-in titrator to standardize the *pH mapping* operation.

7.7.13 Effects of Stirring

Stirring the permeation cell solution increases the effective permeability, by decreasing the thickness of the UWL (Section 7.7.6.3). Since the PAMPA sandwich (Fig. 7.9) has no airgaps in the bottom wells, and since the solution volumes are small (200–400 μL), the use of rotary-motion platforms to stir the plate is not very effective. Avdeef et al. [556] described the effects of stirring up to speeds of 600 rpm, and noted that the stirring efficiency is about 4 times greater along the periphery of the plate compared to the center locations. This is demonstrated in Fig. 7.54 by 96-replicate verapamil permeability measurements in a plate stirred at 500 rpm. The use of individual magnetic stir bars in each bottom well is a more effective way to stir the solutions. This is currently being developed at *p*ION.

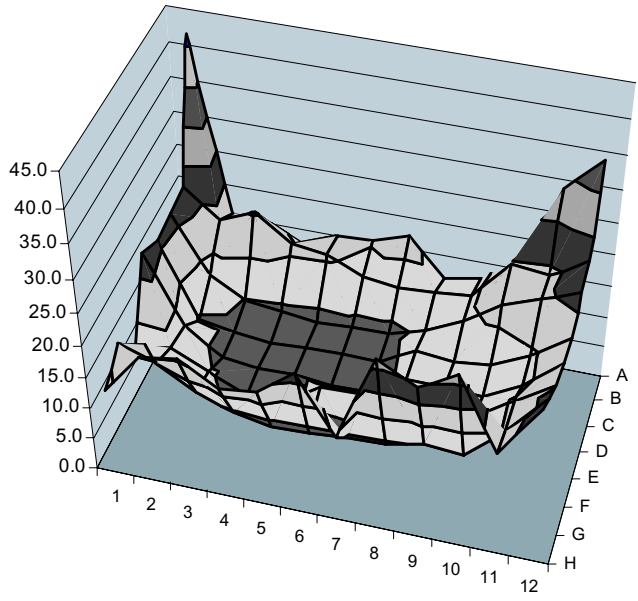

Figure 7.54 Effect of stirring: verapamil permeabilities (in units of $10^{-}6$ cm/s) in 96 replicates, orbital shaker at 500 rpm.

7.7.14 Errors in PAMPA: Intraplate and Interplate Reproducibility

Figure 7.55 shows a plot of over 2000 2%DOPC/dodecane P_e measurements (10^{-6} cm/s units), each representing at least three intra-plate replicates, vs. the estimated standard deviations, $\sigma(P_e)$. Over 200 different drug-like compounds were measured. The %CV (coefficient of variation $100 \times \sigma(P_e)/P_e$) is about 10% near $P_e 10 \times 10^{-6}$ cm/s, and slightly increases for higher values of permeability, but rapidly increases for $P_e < 0.1 \times 10^{-6}$ cm/s, as shown in Table 7.21. These statistics accurately reflect the errors that should be expected in general. For some molecules, such as caffeine and metoprolol, %CV has been typically about 3–6%.

The errors mentioned above represent the reproducibility obtained on the same microtiter plate when the sample molecule is assayed in several different wells. When the reproducibility of P_e measurement is assessed on the basis of assays performed at different times over a long period of time, more systematic sources of errors show up, and the reproducibility can be about 2–3 times worse. Figure 7.56 shows reproducibility of standard compounds taken over a period of about 12 months. Carbamazepine show a long-term reproducibility error of $\sim$15%. The other compounds show somewhat higher errors.

Considering that PAMPA is a high-throughput screening method, the errors are low enough to encourage the use of the method to study mechanistic properties, as our group at *p*ION has done since 1997.

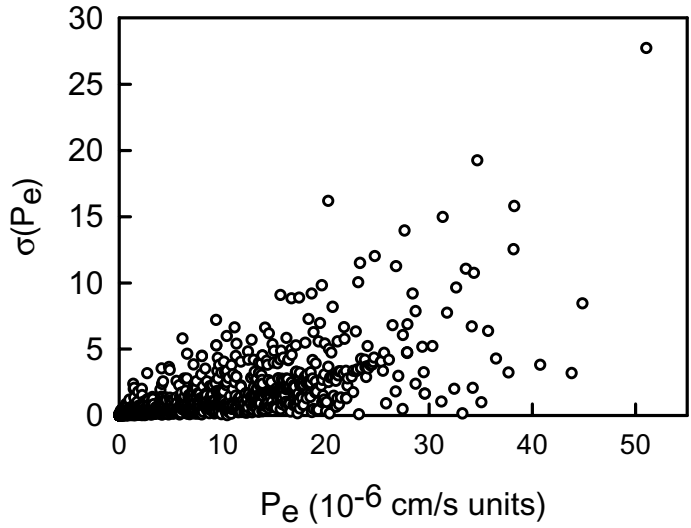

Figure 7.55 Intraplate errors in PAMPA measurement in 2% DOPC model.

7.7.15 UV Spectral Data

The use of direct UV spectrophotometry to measure sample concentrations in pharmaceutical research is uncommon, presumably because of the prevalence and attractiveness of HPLC and LC/MS methods. Consequently, most researchers are unfamiliar with how useful direct UV can be. The UV method is much faster than the other methods, and this is very important in high-throughput screening.

If samples are highly impure or decompose readily, the UV method is inappropriate to use. LC/MS has been demonstrated to be a suitable detection system

TABLE 7.21 Approximate Intraplate Errors in PAMPA Measurement[a]

$P_e(10^{-6}\,\mathrm{cm/s})$	%CV
<0.01	>100%
0.1	60%
0.5	25%
1	15%
5	10%
10	10%
20	15%
30	20%
50	25%

[a]Based on ~6000 measurements of >200 different compounds using the 2% DOPC/dodecane (model 1.0) PAMPA system.

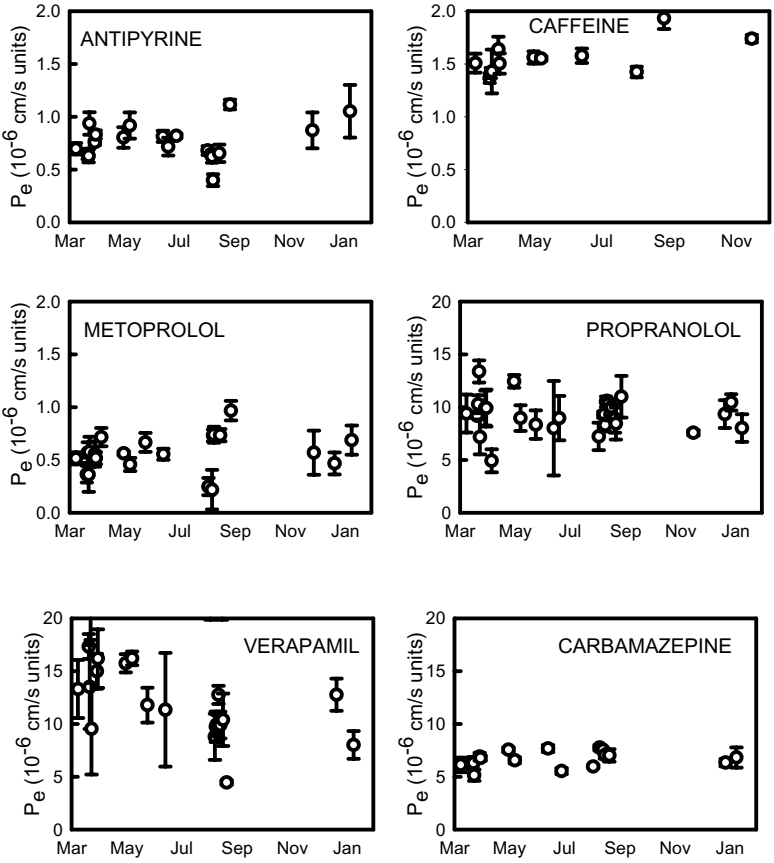

Figure 7.56 Interplate errors in 2% DOPC model (pH 7.4) over 12 months.

under those conditions [556]. When used carefully, LC/MS produces excellent results. However, when LC/MS data-taking is driven very rapidly (e.g., 20 min/plate), disappointing results have been noted in collaborative studies [data not shown].

Figures 7.57a–c show the acceptor, donor, and reference spectra of 48 μM propranolol at the end of 15 h PAMPA assay using 20% wt/vol soy lecithin in dodecane. The sum of the donor (3 μM) and the acceptor (<1 μM) well concentrations indicates that 45 μM is lost to the membrane. In the absence of sink-creating surfactant, only a trace of propranolol reached the acceptor wells at the end of 15 h, with 94% of the compound trapped in the membrane, compared to 19% in the 2% wt/vol DOPC case (Table 7.5). The effective permeability in 20% soy dropped to 1.8×10^{-6} cm/s, compared to the DOPC value of 10.2×10^{-6} cm/s.

With surfactant-created sink condition in the acceptor compartment, the amount of propranolol reaching the acceptor wells is dramatically increased (Fig. 7.57d),

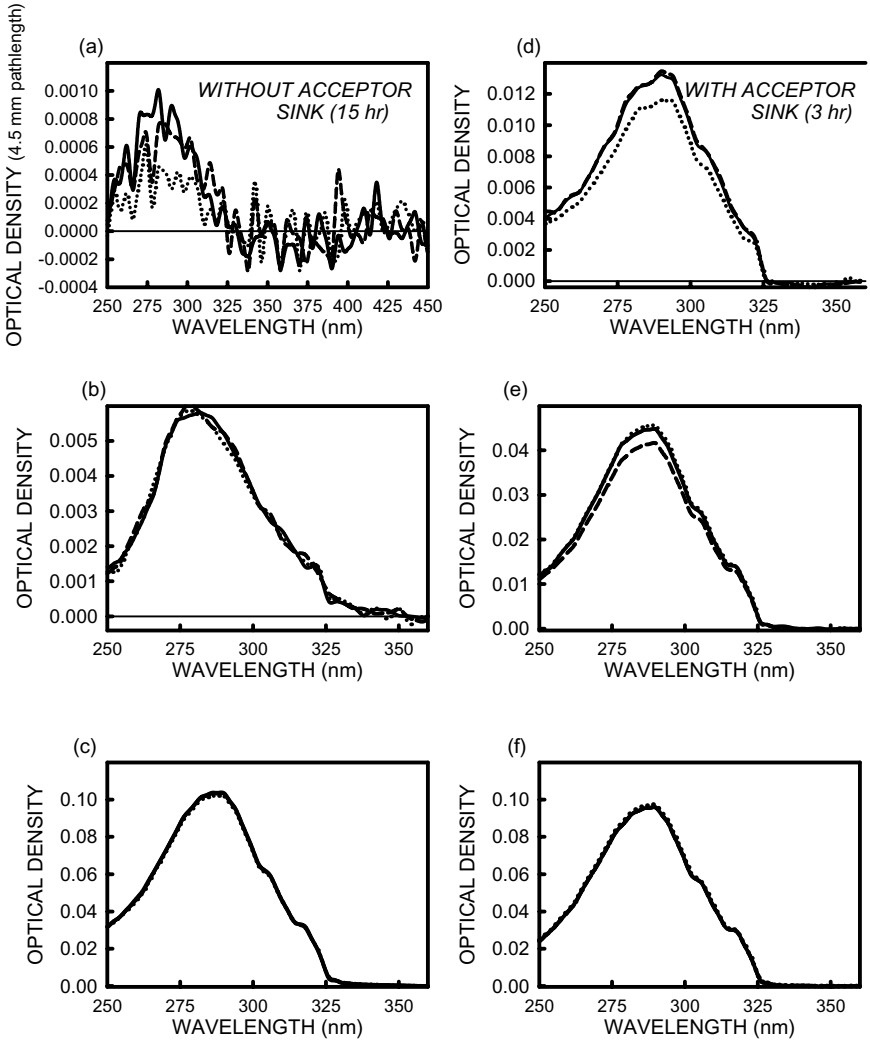

Figure 7.57 UV spectra of propranolol: (a,d) acceptor wells; (b,e) donor wells; (c,f) reference wells (pH 7.4, 47 μm).

with the concomitant decrease in membrane retention from 94% to 41%. Furthermore, the effective permeability rises to 25.1×10^{-6} cm/s, more than a 10-fold increase, presumably due to the desorption effect of the surfactant. Only 3 h permeation time was used in the case (Figs. 7.57d–f). With such a sink at work, one can lower the permeation time to less than 2 h and still obtain very useful UV spectra. This is good for high-throughput requirements.

Figure 7.57a shows that reproducible absorbances can be measured with optical density (OD) values as low as 0.0008, based on a spectrophotometric pathlength

of 0.45 cm. The baseline noise (OD in the range 350–500 nm in Fig. 7.57a) is estimated to be about ±0.0002 OD units.

7.8 THE OPTIMIZED PAMPA MODEL FOR THE GUT

7.8.1 Components of the Ideal GIT Model

The examination of over 50 PAMPA lipid models has led to an optimized model for gastrointestinal tract (GIT) absorption. Table 7.22 shows six properties of the GIT, which distinguish it from the blood–brain barrier (BBB) environment.

1. The in vitro measurements of permeability by the cultured-cell or PAMPA model underestimate true membrane permeability, because of the UWL, which ranges in thickness from 1500 to 2500 μm. The corresponding in vivo value is 30–100 μm in the GIT and nil in the BBB (Table 7.22). The consequence of this is that highly permeable molecules are (aqueous) diffusion limited in the in vitro assays, whereas the membrane-limited permeation is operative in the in vivo case. Correcting the in vitro data for the UWL effect is important for both GIT and BBB absorption modeling.
2. The in vivo environment of the GIT is characterized by a pH gradient; the pH value is constant at 7.4 in the receiving compartment (blood), and varying in the donor compartment (lumen) from ~5 to ~8 from the start to the end of the small intestine. In contrast, the BBB has a constant iso-pH 7.4. Modeling the two environments requires proper pH adjustment in the in vitro model, as indicated in Table 7.22.
3. The receiver compartment in the GIT has a strong sink condition, effected by serum proteins. In contrast, the BBB does not have a strong sink condition. In the GIT, lipophilic molecules are swept away from the site of absorption; in

TABLE 7.22 In Vitro Double-Sink PAMPA Models for GIT and BBB Targets

	In Vivo GIT	In Vivo BBB	In Vitro Double-Sink GIT Model (20% Soy Lecithin)	In Vitro Double-Sink BBB Model (20% Soy Lecithin)
Unstirred water layer (μm)	30–100	0	2300→30 (corr.)	2300→0 (corr.)
pH donor/receiver	5–8 /7.4	7.4/7.4	5.0/7.4, 6.2/7.4, 7.4/7.4	7.4/7.4
Receiver sink	Yes	No	Yes	No
Mixed micelles in lumen[a]	Yes	No	Yes	No
Negative-charge lipids (% wt/wt)	13	27	16	16
Cholesterol + triglycerides + cholesterol ester (% wt/wt)	37	27	37	37

[a]Proposed simulated intestinal fluid containing fasted-state mixed micelle, 3 mM sodium taurocholate + 0.75 mM lecithin, or fed-state mixed micelle, 15 mM sodium taurocholate +3.75 mM lecithin [61].

the brain, lipophilic molecules accumulate in the endothelial cells. Consequently, the in vitro GIT model calls for a sink condition; the BBB model does not.

4. Highly insoluble molecules are in part transported in the GIT by partitioning into the mixed micelles injected into the lumen from the biliary duct in the duodenum (Fig. 2.3). Mixed micelles consist of a 4 : 1 mixture of bile salts and phospholipids (Fig. 7.13). In contrast, at the point of absorption in the BBB, highly insoluble molecules are transported by serum proteins. This distinction is expected to be important in in vitro assay modeling. The use of simulated intestinal fluids is appealing.
5. The GIT has about 13% wt/wt negatively charged lipid-to-zwitterionic phospholipid ratio. It is about twice as large in the BBB. Factoring this into the in vitro model is expected to be important.
6. The white fat content of the GIT is higher than that of the BBB. The use of triglycerides and cholesterol in in vitro modeling seems important.

The strategy for the development of the oral absorption model at *p*ION is illustrated in Fig. 7.58. The human jejunal permeabilities reported by Winiwarter et al. [56] were selected as the *in vivo* target to simulate by the in vitro model. In particular, three acids, three bases and two nonionized molecules studied by the University of Uppsala group were selected as probes, as shown in Fig. 7.58. They are listed in the descending order of permeabilities in Fig. 7.58. Most peculiar in the ordering is that naproxen, ketoprofen, and piroxicam are at the top of the list, yet these three acids are ionized under *in vivo* pH conditions and have lipophilicity $(\log K_d)$ values near or below zero. The most lipophilic molecules tested, verapamil and carbamazepine

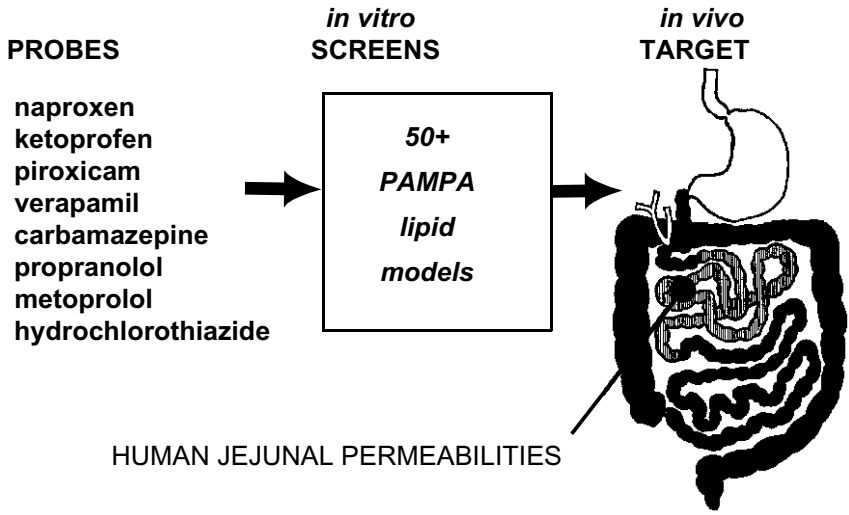

Figure 7.58 Strategy for oral absorption model (from Winiwarter et al. [56]).

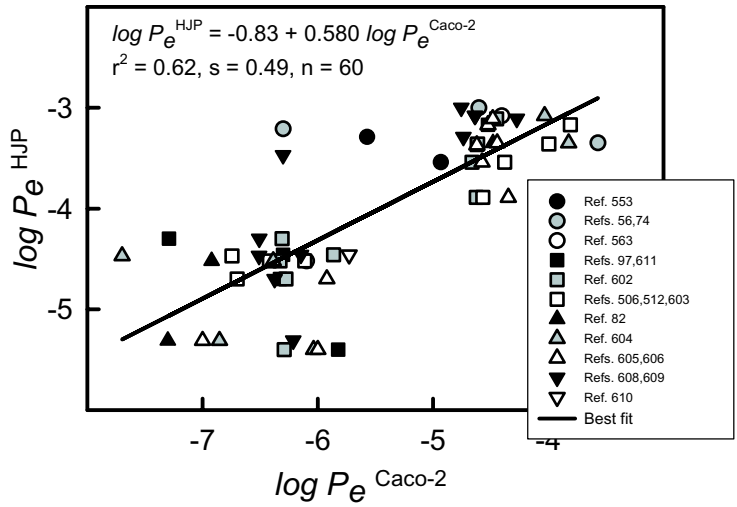

Figure 7.59 Human jejunal permeabilities compared to Caco-2 permeabilities from several groups.

(log $K_d \sim 2.5$; cf. Table 7.4), are in second rank ordering. We took it as a challenge to explain these anomalies in our optimized in vitro GIT model.

As Fig. 7.58 indicates, our task was to explain the ordering of the eight probe molecules in the human in vivo target, but subjecting the eight probe molecules to each of the 50 PAMPA lipid models. For each PAMPA model, the regression correlation coefficient, r^2, was used to assess the appropriateness of the model.

7.8.2 How Well Do Caco-2 Permeability Measurements Predict Human Jejunal Permeabilities?

Since the widely accepted in vitro permeability model in the pharmaceutical industry is based on the use of cultured cells, such as Caco-2 or MDCK, it was appropriate to analyze the regression correlation coefficients based on the comparisons of Caco-2 log P_e and the log P_e values based on the human jejunal measurements [56].

Figure 7.59 shows a plot of log P_e^{HJP} (human jejunal permeabilities) vs. log $P_e^{\text{Caco-2}}$ taken from the literature, based on the work of more than 11 laboratories. The r^2 for the correlation is 0.62. It is clear from the plot that some laboratories better predicted the HJP than other laboratories. Figure 7.60 shows the plot of the results published by Artursson's group [506,512,603], where r^2 was calculated as 0.95, the most impressive value of all the comparisons. It is noteworthy that naproxen, ketoprofen, and piroxicam were not available for the comparison in the Fig. 7.60 plot.

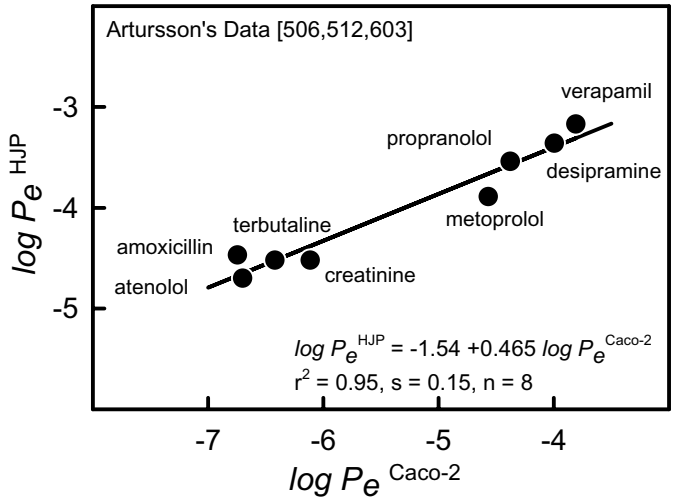

Figure 7.60 Human jejunal permeabilities compared to Caco-2 permeabilities from Artursson's group.

7.8.3 How Well Do PAMPA Measurements Predict the Human Jejunal Permeabilities?

Table 7.23 shows the results for 47 specific PAMPA models tested at *p*ION, according the the scheme in Fig. 7.58. The two columns on the right are the r^2 values in the comparisons. The neutral-lipid models (1.0, 1A.0, 2.0, 3.0, and 4.0) at pH 7.4 do not explain the permeability trend indicated in the human jejunal permeabilities [56]. Octanol was least effective, with r^2 0.01. This should not be too surprising, since we did note that the appearance of naproxen, ketoprofen, and piroxicam at the top of the HJP ordering was unexpected. Our ''expectations'' were based on the octanol–water lipophilicity scale, which clearly does not correlate with the HJP trend. Adding a sink condition to the 2% DOPC model (model 1.1) improves correlation (r^2 increases from 0.33 to 0.53). The addition of cholesterol to the 2% DOPC/dodecane system made the model unstable to the surfactant-created sink condition.

Introducing negative-charge phospholipids to the 2% DOPC at pH 7.4 improved the correlations significantly (models 5.0, 6.0, 7.0, 8.0, 9.0, 10.0). Sink conditions only marginally improved the correlations for the dodecylcarboxylic acid (1.1% DA) and phosphatidic acid (0.6% PA) models (models 6.1 and 7.1). The phosphatidylglycerol (PG) models (models 9.1 and 10.1) did not correlate well under sink conditions. The modified Chugai model at pH 7.4 performed well (r^2 0.60), but was unstable under sink conditions.

Several egg lecithin models were tested at pH 7.4. The Avanti egg lecithin behaved differently from the Sigma-Aldrich egg lecithin, and was unstable under sink conditions when cholesterol was added. The correlation coefficients were

TABLE 7.23 Correlation (r^2) between Human Jejunal and PAMPA Permeabilities

No.	Type	Composition	pH_{DON}/pH_{ACC}	No Sink	With Sink
1	Neutral	2% DOPC	7.4	0.33	0.53
1A		2% DOPC + 0.5% Cho	7.4	0.61	(Turbid)
2		100% olive oil	7.4	0.36	—
3		100% octanol	7.4	0.01	—
4		100% dodecane	7.4	0.32	—
5	2-Component anionic	2% DOPC + 0.6% DA	7.4	0.58	0.53
6		2% DOPC + 1.1% DA	7.4	0.53	0.61
7		2% DOPC + 0.6% PA	7.4	0.60	0.61
8		2% DOPC + 1.1% PA	7.4	0.52	0.33
9		2% DOPC + 0.6% PG	7.4	0.55	0.10
10		2% DOPC + 1.1% PG	7.4	0.79	0.25
11	5-Component anionic	0.8% PC + 0.8% PE + 0.2% PS + 0.2% PI + 1% Cho	7.4	0.60	(Turbid)
12	Lecithin extracts anionic	10% eggPC (Avanti)	7.4	0.47	0.22
13		10% eggPC (Avanti) + 0.5% Cho	7.4	0.60	(Turbid)
14		10% eggPC (Sigma)	7.4	0.65	0.17
15		10% eggPC (Sigma) + 0.5% Cho	7.4	0.58	0.57
16		10% soyPC	7.4	0.62	0.48
17		20% soyPC	7.4	0.65	0.55
18		20% soyPC + 0.5% Cho	7.4	0.56	0.63
19		35% soyPC	7.4	0.58	0.42
20		50% soyPC	7.4	—	0.36
21		68% soyPC	7.4	0.29	—
22		74% soyPC	7.4	—	0.04
24	Iso-pH	20% soyPC	6.5 / 6.5	—	0.77
25		20% soyPC	5.0 / 5.0	—	0.86
26	Gradient–pH	20% soyPC	6.5 / 7.4	—	0.52
27	(Corrected UWL)	20% soyPC	6.0 / 7.4	—	0.72
28		20% soyPC	5.5 / 7.4	—	0.89
29		20% soyPC	5.0 / 7.4	—	0.97
30		20% soyPC	4.5 / 7.4	—	0.95

slightly better with the Sigma-Aldrich source of egg lecithin. In all cases, the sink condition caused the correlation coefficients to be lower at pH 7.4.

The soy lecithin models (Avanti) were tested most thoroughly at pH 7.4. Figure 7.61 shows the plot of r^2 versus the amount of soy lecithin dissolved in dodecane, from 10% to 74% wt/vol, with and without acceptor sink condition. In the plot, the maximum r^2 was achieved at about 20% wt/vol. The sink condition depressed the (dashed) curve by about 0.15 in r^2 at pH 7.4. The 20% soy lecithin formulation was selected for all subsequent testing.

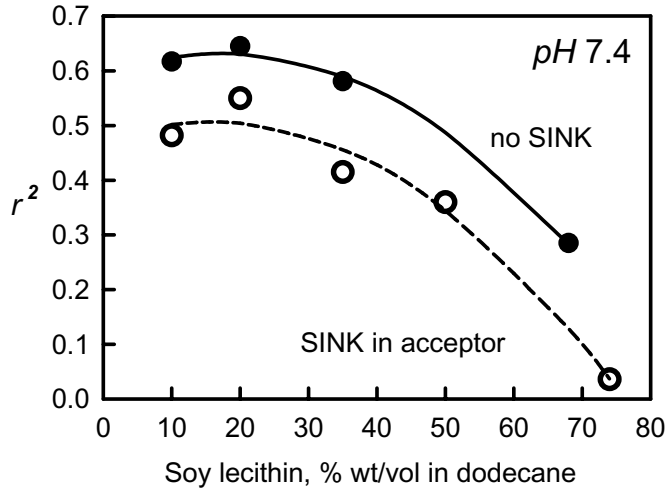

Figure 7.61 Correlation between human jejunal permeabilities and soy lecithin models (in dodecane) at pH 7.4.

Considerable improvements were achieved when iso-pH solutions were tested, at pH 6.5 and 5.0 (Table 7.23). At pH 5, r^2 reached 0.86.

The best correlations were observed under gradient pH and sink conditions (''double-sink'' set at the bottom of Table 7.23), with the donor pH 5 and acceptor pH 7.4 producing r^2 0.97. The r^2/donor pH plot is shown in Fig. 7.62. The data represented by the solid line corresponds to P_m values (P_e corrected for the

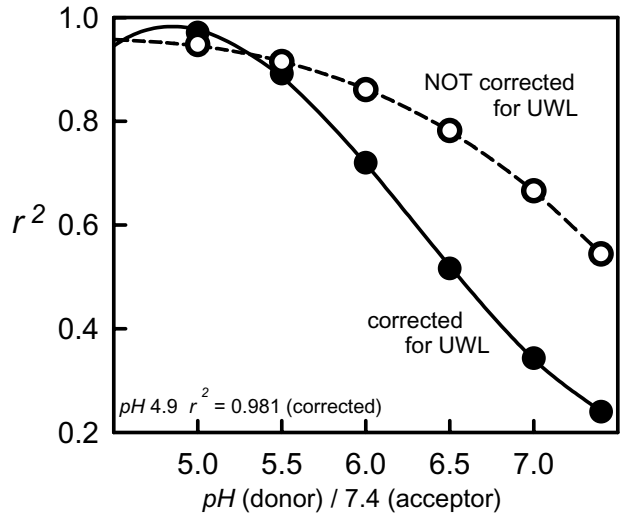

Figure 7.62 Correlation between human jejunal permeabilities [vs. PAMPA (double-sink)] and soy lecithin models under gradient–pH conditions.

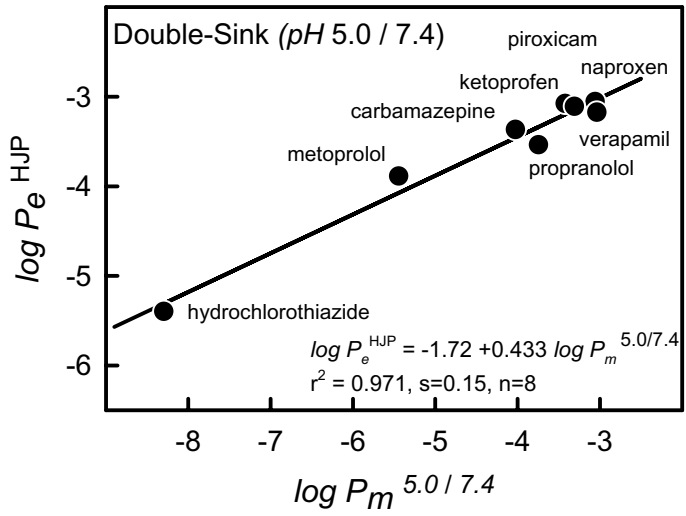

Figure 7.63 Human jejunal permeabilities compared to *p*ION's double-sink sum-P_e PAMPA GIT model.

UWL), and the data represented by the dashed line corresponds to P_e values (uncorrected for the UWL, r^2 data not shown in Table 7.23).

The *p*ION double-sink GIT model, with donor pH 5, predicts the human jejunal permeabilities as well as the best reported Caco-2 model (Artursson's), and a lot better than the rest of the reported Caco-2 models, as shown in Fig. 7.63.

7.8.4 Caco-2 Models for Prediction of Human Intestinal Absorption (HIA)

The strategy of the preceding sections was based on predicting the permeabilities of drug compounds in the human jejunum. The rest of the intestinal tract has higher pH, and this needs to be factored in when considering models to predict *not* human permeabilities, but human *absorption* (see Fig. 2.3 and Table 7.2).

Caco-2 permeabilities have been used to predict human intestinal absorption (HIA) in the literature. Figure 7.64 is a plot of %HIA versus log $P_e^{\text{Caco-2}}$, drawing on the published work of about a dozen laboratories. The plot in Fig. 7.64 resembles "rain," and perhaps very little can be learned from such a plot. This may be an example of what Lipinski [1] pointed out as the consequences of using multimechanistic ADME measurements—the more data points are brought in, the worse the plot looks. Another way of looking at this is that each laboratory has a somewhat differently expressed Caco-2 line, and interlaboratory comparisons can only be done in a rank-order sense. When individual-laboratory data are examined, some groups have better correlations than others. Figure 7.65 shows the results from

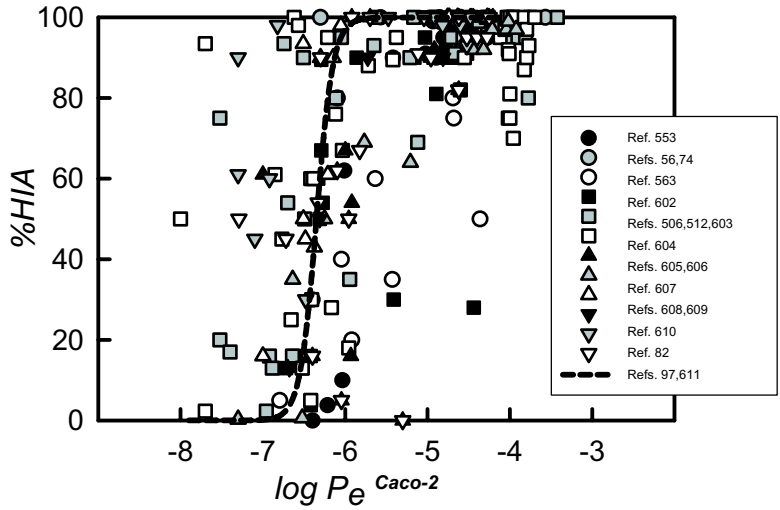

Figure 7.64 Human intestinal absorption compared to Caco-2 permeabilities from several groups.

Yazdanian's group [602], which seem to be marginally better than those of most of the other groups. Griseofulvin is a false positive outlier, which can be rationalized by recognizing that very low solubility of the molecule may be responsible for the low HIA value. The other outlier is nadolol, which has good aqueous

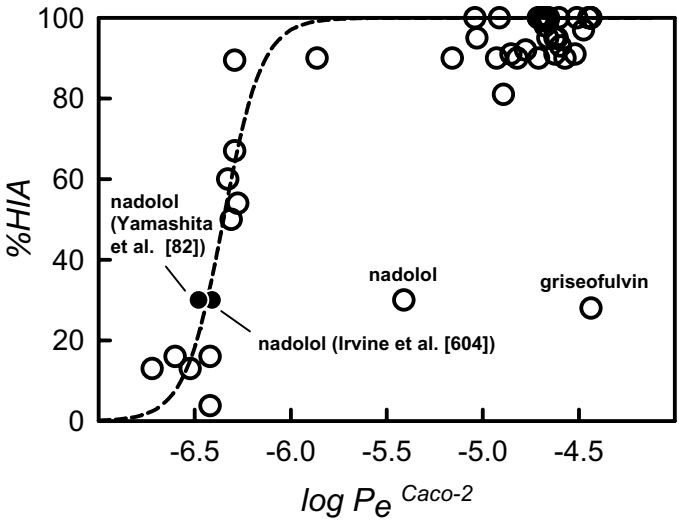

Figure 7.65 Human intestinal absorption compared to Caco-2 permeabilities from Yazdanian's group [602].

solubility. The results from Irvine et al. [604] and Yamashita et al. [82] place nadolol on the best-fit curve (dashed line). The pharmacokinetic data indicates low HIA for nadolol, possibly due to P-gp efflux attenuating absorption. The Caco-2 result from Yazdanian's group may be high because of the use of high drug concentrations, enough to saturate the P-gp transport in Caco-2. There appears to be no consensus on what sample concentrations to use in Caco-2 assays, and every laboratory appears to have slightly different protocols, when it comes to Caco-2 measurements.

7.8.5 Novartis max-P_e PAMPA Model for Prediction of Human Intestinal Absorption (HIA)

The PAMPA strategy to predict HIA is based on recognizing that gradient pH conditions need to be incorporated into the in vitro models, and that the donor pH values must reflect the properties of the entire GIT (Table 7.2 and Fig. 2.3). Weak acids ought to be better absorbed in the jejunum, where the pH is well below 7.4. However, at the low pH, weak bases may not be well absorbed, since they are positively charged. In the ileum, where the pH may be as high as 8, the absorption of weak bases should be higher than that of weak acids, since the fraction of uncharged form of the bases will be higher at pH 8, compared to pH 5.

In a screening application, where the acid–base properties of discovery molecules may not be certain, it is necessary to screen at least at two pH values, to reflect the conditions of the small intestine. The higher of the two measured permeabilities can then be used to predict HIA. For example, if pH 5 and 7.4 were the two pH values in the PAMPA assay, a weak acid may show very high P_e at pH 5 but a very low P_e at pH 7.4. A single-pH assay at pH 7.4 may have classed the weak acid as a negative, whereas its absorption may have been excellent in the jejunum (pH 5), but this would not have been recognized in the single-pH assay. If a two-pH PAMPA assay is used, then the selection of the maximum P_e of the two measured values would avoid the case of false negatives. This strategy was recognized by Avdeef [26], Faller and Wohnsland [509,554], and Zhu et al. [549]. Figure 7.66 shows the plot of percent absorption versus PAMPA %flux [509]. Figure 7.66a shows the values were taken from just a single pH 6.8; Fig. 7.66b shows the correlation when the max-P_e value is selected from the range pH 5–8. The 50–70% absorption region, shows improvement in the max-P_e model (Fig. 7.66b).

7.8.6 *p*ION Sum-P_e PAMPA Model for Prediction of Human Intestinal Absorption (HIA)

The preceding section can be further generalized, to properly account for absorption of nonionized molecules. The selection of the maximum P_e for HIA prediction implicitly recognized that only a fraction of the small intestine is available for the maximum absorption of acids (with pK_a near 4) and bases (with pK_a near 9). But when this approach is applied to nonionizable molecules, then the absorption may be underestimated, since absorption should be uniform across the whole intestinal tract. The remedy is to sum the two P_e values. This is roughly equivalent to

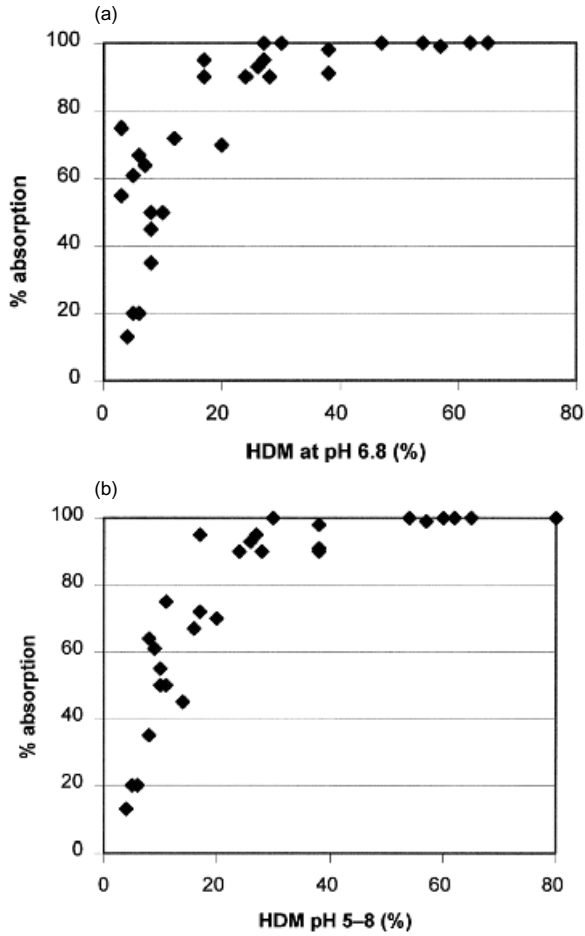

Figure 7.66 Novartis' max-P_e PAMPA model [509]. [Reprinted from Faller, B.; Wohnsland, F., in Testa, B.; van de Waterbeemd, H.; Folkers, G.; Guy, R. (Eds.). *Pharmacokinetic Optimization in Drug Research*, Verlag Helvetica Chimica Acta: Zürich and Wiley-VCH: Weinheim, 2001, pp. 257–274. With permission from Verlag Helvetica Chimica Acta AG.]

integrating a system with parallel absorption taking place in different parts of the intestine. Our preference is to perform PAMPA assay at three gradient pH conditions, with acceptor sink included (double-sink method): donor pH 5, 6.2, and 7.4, with acceptor pH always at 7.4. Figure 7.67a shows such a double-sink sum-P_m (P_e data corrected for the UWL) plot. Figure 7.67b shows the plot of $\log P_e^{\mathrm{HJP}}$ versus %HIA—human permeability data attempting to predict human absorption. As can be seen, the PAMPA data and the HJP data perform equally and tolerably well. One is a lot cheaper to do than the other! Of particular note is that the PAMPA scale covers nearly eight orders of magnitude, compared to

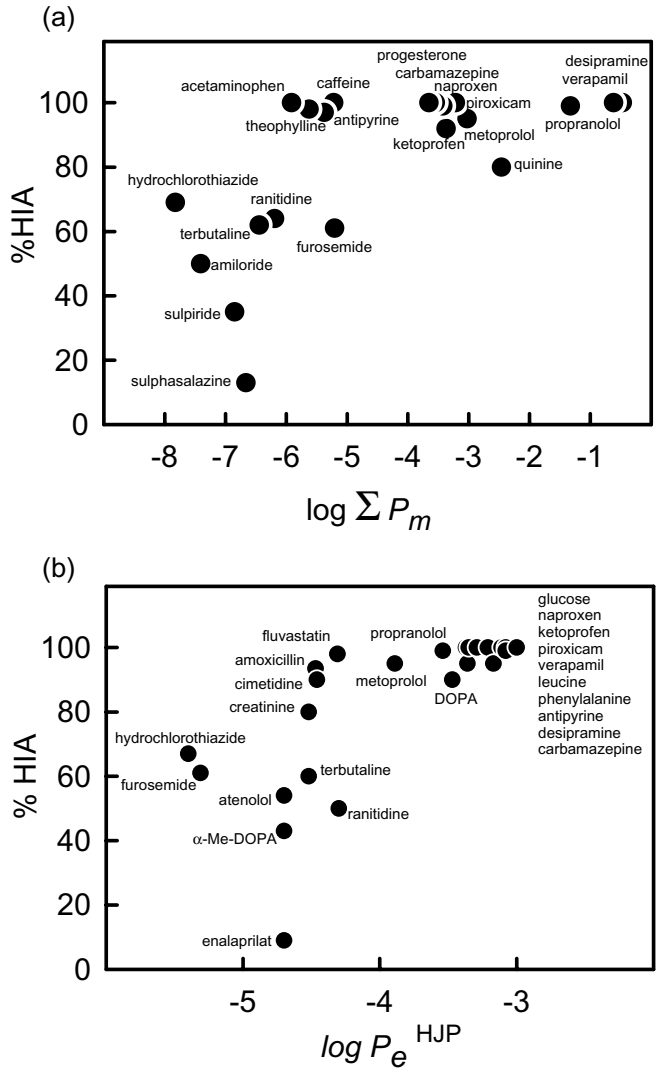

Figure 7.67 Human intestinal absorption compared to (a) *p*ION's double-sink sum-P_e PAMPA GIT model and (b) human jejunal permeabilities [56].

about two and a half orders for the HJP data. Such a spread in the PAMPA data could facilitate the selection of well-absorbed molecules from those poorly absorbed.

In conclusion, the double-sink sum-P_e PAMPA in vitro GIT assay seems to predict human absorption as well as in vivo human permeability measurements (see Figs. 7.66a,b) and in vitro Caco-2 permeability measurements (see Figs. 7.60 and 7.63), but at a lower cost and higher speed.